

# **Tryptophan scanning of barttin identifies molecular determinants of its function on ClC-K chloride channels**

Der Naturwissenschaftlichen Fakultät  
der Gottfried Wilhelm Leibniz Universität Hannover  
zur Erlangung des Grades

Doktor der Naturwissenschaften

- Dr.rer.nat. -

genehmigte Dissertation  
von

Dipl.-Biol. Daniel Wojciechowski  
geboren am 21.04.1977  
in Augsburg

2013



Betreuer: Prof. Dr. Christoph Fahlke  
Referent: Prof. Dr. Rita Gerardy-Schahn  
Co-Referent: Prof. Dr. Anaclet Ngezahayo  
Tag der Promotion: 19.11.2013

Keywords: Barttin  
Mutagenesis scan  
ClC-K chloride channels

Stichwörter: Barttin  
Mutagenese Scan  
ClC-K Chlorid Kanäle

Der Spaß fängt erst dann an, wenn man die Regeln kennt.  
Im Universum aber sind wir momentan noch dabei,  
die Spielanleitung zu lesen.  
*Richard P. Feynman*



LIST OF FIGURES .....	III
LIST OF TABLES .....	V
ABBREVIATIONS .....	VI
ABSTRACT .....	VII
ZUSAMMENFASSUNG .....	IX

## 1 INTRODUCTION ..... 1

1.1 CLC CHLORIDE CHANNEL/TRANSPORTER FAMILY .....	2
1.1.1 Structure of CLC proteins .....	3
1.1.2 The family members of CLC chloride channels and transporters .....	6
1.1.2.1 hCLC-Ka/rCLC-K1 and hCLC-Kb/rCLC-K2 .....	6
1.1.2.1.1 Role of CLC-K channels in the kidney and the inner ear .....	6
1.1.2.1.2 Bartter Syndrome .....	8
1.1.2.2 CLC-1 and CLC-2 .....	9
1.1.2.3 CLC chloride/proton antiporter .....	10
1.1.2.3.1 CLC-3, CLC-4, CLC-5 .....	10
1.1.2.3.2 CLC-6 and CLC-7 .....	10
1.1.3 Interacting proteins of CLC channels and transporters .....	11
1.1.3.1 Adaptor proteins .....	11
1.1.3.2 $\beta$ -subunit barttin .....	12
1.2 AIM OF THIS STUDY .....	14

## 2 MATERIAL AND METHODS ..... 15

2.1 MATERIAL .....	15
2.2 METHODS .....	16
2.2.1 Molecular Biology – Vectors used .....	16
2.2.2 PCR strategies .....	17
2.2.2.1 Substitution of single amino acids to tryptophan: QuikChange® site directed mutagenesis .....	18
2.2.2.1.1 Quikchange® PCR .....	19
2.2.2.1.2 DpnI digestion .....	21
2.2.2.1.3 Agarose gel electrophoresis .....	21
2.2.2.1.4 DNA purification – gel extraction .....	21
2.2.2.1.5 Competent cells .....	21
2.2.2.1.6 Growth of transformed bacteria in LB-medium/ on LB-Agar plates .....	22
2.2.2.1.7 Transformation .....	22
2.2.2.1.8 Vector recovery .....	23
2.2.2.1.9 Glycerol stock .....	23
2.2.2.1.10 Control restriction .....	23
2.2.2.1.11 Sequencing .....	24
2.2.2.1.12 Subcloning .....	24
2.2.2.1.13 Ligation .....	24
2.2.2.2 Side overlap extension PCR (SOE-PCR) .....	25
2.2.2.2.1 Covalent link of barttin to rCLC-K1 and V166E rCLC-K1 .....	25
2.2.2.2.2 N-terminal link of the concatamers with mYFP (Quikchange) .....	26
2.2.2.2.3 Generation of CLC-2 and V166E rCLC-K1 chimera (SOE-PCR) .....	27
2.2.3 Cell culture .....	29
2.2.3.1 Cell lines .....	29
2.2.3.1.1 MDCKII for confocal microscopy and biotinylation assay .....	29
2.2.3.1.2 HEK293T for electrophysiology .....	29
2.2.3.1.3 Flp-in™ T-REx for stable cell lines .....	30
2.2.3.2 Splitting .....	30
2.2.3.3 Transfection .....	30
2.2.3.3.1 $\text{Ca}_2\text{PO}_3$ -precipitation .....	31
2.2.3.3.2 Lipofectamin™ 2000 .....	31
2.2.3.4 Freezing cells .....	31
2.2.3.5 Thawing cells .....	32
2.2.4 Electrophysiology .....	32
2.2.4.1 Setup .....	32
2.2.4.2 Pipettes and electrodes .....	32
2.2.4.3 Preparation of cells .....	33

2.2.4.4	Solutions.....	33
2.2.4.5	Determination of relative open probabilities and times constants of activation.....	34
2.2.4.6	Noise analysis.....	35
2.2.5	<i>Confocal imaging</i> .....	37
2.2.6	<i>Protein biochemistry</i> .....	37
2.2.6.1	Biotinylation assay.....	37
2.2.6.1.1	Labeling with biotin.....	38
2.2.6.1.2	Whole cell lysate.....	39
2.2.6.1.3	Surface membrane fraction.....	39
2.2.6.2	SDS-PAGE gel.....	41
2.2.6.3	Typhoon laser scanning.....	41
2.2.6.4	SDS-PAGE gel analysis.....	42
2.2.6.5	Densitometric analysis.....	43
2.2.6.6	Western blot.....	43
2.2.6.6.1	Qualitative control for surface membrane proteins.....	43
2.2.6.6.2	Qualitative check for built concatamers.....	44
<b>3</b>	<b>RESULTS.....</b>	<b>45</b>
3.1	<b>hClC-Ka AND THE EFFECTS OF BARTTIN AND MUTANT BARTTINS.....</b>	<b>45</b>
3.1.1	<i>hClC-Ka is activated by WT barttin – and only by four helix 1-mutants.....</i>	<i>45</i>
3.1.2	<i>Functional barttin mutants leave single channel properties of hClC-Ka/barttin unaffected.....</i>	<i>47</i>
3.1.3	<i>Expression level of mutant barttin and hClC-Ka.....</i>	<i>49</i>
3.1.4	<i>F24W and M26W barttin are misfolded or degraded.....</i>	<i>52</i>
3.1.5	<i>Surface membrane insertion of ClC-K/barttin channels is impaired for some barttin mutants....</i>	<i>52</i>
3.1.6	<i>Investigation of subcellular barttin and hClC-Ka distribution by confocal imaging.....</i>	<i>56</i>
3.2	<b>V166E rClC-K1 AND THE EFFECTS OF BARTTIN AND BARTTIN MUTANTS.....</b>	<b>61</b>
3.2.1	<i>Barttin modifies gating of V166E rClC-K1.....</i>	<i>61</i>
3.2.2	<i>Mutant barttins interact with V166E rClC-K1 - and many alter the gating.....</i>	<i>63</i>
3.2.3	<i>Helix 1 is necessary for channel activation.....</i>	<i>66</i>
3.2.4	<i>Functional determinants important for slow gating of V166E rClC-K1.....</i>	<i>67</i>
3.2.5	<i>Many mutant barttins lower minimal fast gate open probability.....</i>	<i>69</i>
3.2.6	<i>Many mutations of barttin vary the voltage dependence of the fast, but not of the slow gate of V166E rClC-K1.....</i>	<i>71</i>
3.2.7	<i>Summary: Topology models of the effects of substitution on V166E rClC-K1 and hClC-Ka.....</i>	<i>72</i>
<b>4</b>	<b>DISCUSSION.....</b>	<b>76</b>
4.1	EFFECTS OF POINT MUTATIONS.....	76
4.2	HYPOTHESIS OF BINDING.....	83
4.3	CONCLUSIONS.....	90
4.4	OUTLOOK.....	91
<b>5</b>	<b>REFERENCES.....</b>	<b>94</b>
<b>6</b>	<b>SUPPLEMENTAL DATA.....</b>	<b>104</b>
6.1	TIME COURSE OF ACTIVATION - MANY MUTATIONS SLOW DOWN THE FAST GATE KINETIC.....	104
6.2	CONCATENATED BARTTIN/V166E rClC-K1 SUGGESTS A STOICHIOMETRY OF BARTTIN:PROTOPORE HIGHER THAN 1:1.....	105
6.3	CHIMERIC CHANNELS REVEAL THE B-HELIX TO BE ESSENTIAL FOR FAST GATING.....	111
6.4	POINT MUTATIONS T36W OR M44W DO NOT IMPAIR BINDING OF BARTTIN TO V166E rClC-K1 ....	113
<b>7</b>	<b>ACKNOWLEDGEMENTS.....</b>	<b>114</b>
<b>8</b>	<b>CURRICULUM VITAE.....</b>	<b>115</b>
<b>9</b>	<b>LIST OF PUBLICATIONS.....</b>	<b>116</b>



## List of Figures

Fig.1 Dendrogram of the ClC protein family.....	2
Fig.2 Crystal structure of homodimeric <i>CmClC</i> .....	3
Fig.3 Topology model of ClC proteins.....	3
Fig.4 Scheme of the open and closed pore conformation of <i>EcClC</i> and an alignment of the highly conserved chloride binding sites of ClC family members.....	4
Fig.5 Localization and physiological function of ClC-K channels in the nephron and the inner ear.....	7
Fig.6 Topology model of barttin.....	12
Fig.7 Scheme of SOE-PCR.....	25
Fig.8 Scheme of PCR reaction needed for helix substitution between rClC-K1 and ClC-2.....	27
Fig.9 Molecular structure of EZ-linked NHS-sulfo-SS-biotin.....	38
Fig. 10 Scheme of biotinylation assay procedure.....	40
Fig. 11 Fluorescence scan of SDS-PAGE gel of MDCKII cells expressing YFP hClC-Ka alone or with WT barttin mCFP.....	42
Fig.12 Representative recordings of HEK293T cells expressing hClC-Ka or hClC-Ka with WT barttin.....	46
Fig.13 Stationary noise analysis of currents of HEK293T cells coexpressing hClC-Ka and barttin.....	48
Fig.14 Fluorescent SDS-PAGE gel of whole cell lysates of MDCKII cells expressing hClC-Ka without or with barttin.....	49
Fig.15 SDS-PAGE gel analysis; quantification of fluorescent band intensities of (A) barttin, normalized to WT barttin and (B) hClC-Ka, normalized to hClC-Ka in presence of WT barttin.....	49
Fig.16 Fluorescent SDS-PAGE gel to illustrate the lower expression level of hClC-Ka with raising concentration of co-transfected plasmids coding for barttin.....	50
Fig.17 Plot of macroscopic hClC-Ka current amplitudes at 105 mV versus barttin expression levels.....	51
Fig.18 Excerpt of a fluorescence scan of SDS-PAGE gel of mutant barttins coexpressed with hClC-Ka....	52
Fig.19 Fluorescence scan of SDS-PAGE gels of hClC-Ka coexpressed with mutant or WT barttin in MDCKII cells.....	52
Fig.20 Quantification of surface membrane fraction of barttin (A) and hClC-Ka (B).....	53
Fig.21 Fluorescent SDS-PAGE gel of biotinylated, surface exposed proteins of MDCKII cells cotransfected with plasmids coding for WT barttin CFP and YFP hClC-Ka and normalized surface membrane fraction of hClC-Ka in presence of different amounts of barttin.....	54
Fig.22 Plot of surface membrane fraction of hClC-Ka versus the relative expression of barttin.....	55
Fig.23 Confocal images of MDCKII cell expressing hClC-Ka without or with WT barttin.....	56
Fig.24 Confocal images of MDCKII cells expressing hClC-Ka with F24W or M26W barttin.....	57
Fig.25 Confocal images of MDCKII cells expressing M40W, G41W or V45W barttin (A) with or (B) without hClC-Ka.....	57
Fig.26 Confocal images of MDCKII cells expressing hClC-Ka (red) and barttin mutants (green) with impaired chaperone function.....	58
Fig.27 Confocal images of MDCKII cells expressing hClC-Ka (red) and barttin mutants (green) that cannot activate the channel.....	59

---

Fig.28 Topology model of barttin and its functional determinants on hCIC-Ka.....	60
Fig.29 Whole cell patch clamp recordings of HEK293T cell expressing (A) V166E rCIC-K1 alone, or (B) together with WT barttin and corresponding activation curves (C+D).....	62
Fig.30 Representative whole cell current recordings of HEK293T cells coexpressing V166E rCIC-K1 with barttins that were mutated within TM1.....	64
Fig.31 Representative whole cell current recordings of HEK293T cells coexpressing V166E rCIC-K1 with barttins that were mutated within TM2.....	65
Fig.32 Comparison of steady state mean macroscopic current amplitudes at -155 mV and 125 mV of HEK293T cells coexpressing V166E rCIC-K1 and barttin.....	66
Fig.33 Changes in relative open probabilities of the slow gate.....	68
Fig.34 Changes in relative open probabilities of the fast gate.....	69
Fig.35 Effect of barttin mutation on activation of the slow and the fast gate.....	71
Fig.36 Topology models of barttin and the effects of substituted residues on the hCIC-Ka (left) or V166E rCIC-K1 (right).....	75
Fig.37 Pore-coordinating amino acids in <i>EcCIC</i> and their proximity to the B-helix.....	84
Fig.38 Pore-coordinating amino acids in <i>EcCIC</i> and their proximity to the J-helix as well as the R-helix...	87
Fig.39 two hypothetical binding possibilities of barttin to CIC-K channels.....	89
Fig.40 Topology model of barttin with color-coded effects of tryptophan substitution.....	90
Fig.41 Time constants of activation at 125 mV of all scanned barttin mutants.....	104
Fig. 42 Representative whole cell current recordings of HEK293T cells expressing (A) WT barttin and V166E rCIC-K1, or concatenated (B) WT barttin/V166E rCIC-K1, (C) WT barttin/V166E rCIC-K1 together with additional WT barttin, (D) YFP-WT barttin/V166E rCIC-K1, (E) M40W barttin/V166E rCIC-K1, (F) G41W barttin/V166E rCIC-K1 and (G) V45W barttin/V166E rCIC-K1.....	106
Fig.43 Normalized I-V-plots illustrate impaired function of concatamers with mutant barttin.....	107
Fig.44 Comparison of the effects of mutant concatamers on the slow gate of V166E rCIC-K1.....	108
Fig.45 Changes in relative open probability of the fast gate and time constants of activation at +125 mV of concatamers in comparison to cell expressing the channel only or co-expressing WT barttin.....	109
Fig.46 Representative whole cell current recordings of HEK293T cells expressing A) hCIC-2 or B) hCIC-2 with B-helix of rCIC-K1.....	111
Fig.47 (A) Mean current amplitudes and (B) representative whole cell current recordings of HEK293T cell expressing chimeric CIC-2 in presence and absence of barttin are compared with the expression level (C) and subcellular distribution (confocal images in B).....	112
Fig.48 Confocal images of MDCKII cell co-expressing V166E rCIC-K1 YFP together with WT, T36W or M44W barttin mCFP .....	113

## LIST OF TABLES

Tab.1 Types of Bartter syndrome, their cause and the affected tissues.....	8
Tab.2 Alignment of two regulatory domains of ClC proteins.....	11
Tab.3 Mix for PCR reactions.....	18
Tab.4 PCR program.....	18
Tab.5 List of primers designed for Quikchange® (Stratagene) site directed mutagenesis.....	19
Tab.6 Composition of buffers.....	22
Tab.7 Primers used for concatenation of barttin and (V166E) rClC-K1.....	26
Tab.8 Primers used for tagging YFP to concatamers.....	26
Tab.9 PCR program.....	28
Tab.10 List of primers used for generation of chimeric channels.....	28
Tab.11 Composition of lysis buffer.....	39
Tab.12 Composition of the wash buffer.....	39
Tab.13Composition of the Lämmli buffer.....	41
Tab.14 Composition of running and stacking gel.....	41
Tab.15 Comparison of WT barttin and barttin mutants that alter slow and fast gate regulation.....	74
Tab.16 Comparison of WT barttin and barttin mutants that alter regulation of only one gate.....	75
Tab.17 TM1 of barttin and its unpolar residues.....	85
Tab.18 Alignment of B-helices of <i>EcClC</i> , ClC-Ka and ClC-K1 and residues proposed to build a leucine zipper	
Tab.19 Alignment of J-helices of <i>EcClC</i> , ClC-Ka and ClC-K1.....	88

## Abbreviations

(n,p)A	(nano,pico)ampere
Å	Ångstrom = $10^{-10}$ m
aa	amino acid
APS	ammoniumpersulphate
bp	base pairs
BP	bandpass filter
BSA	bovine serum albumine
CBS	cystathionin- $\beta$ -synthase/catabolic binding site
(m)CFP	(monomeric) cyan fluorescent protein
CIC	chloride channel
CMV	cytomegalovirus
<i>CmCIC</i>	Cyanidioschyzon merolae chloride channel
DMEM	Dulbecco's modified eagle medium
DNA	deoxyribonucleic acid
dNTP	deoxyribonucleotide triphosphate
DTT	dithiothreitol
<i>EcCIC</i>	Escherichia coli chloride channel
EDTA	ethylenediaminetetraacetic acid
EGTA	ethylene glycol-bis(2-aminoethylether)-N,N,N',N'-tetraacetic acid
ER	endoplasmatic reticulum
F	Faraday constant $96485.3365 \text{ C mol}^{-1}$
FBS	fetal bovine serum
HEK	human embryonic kidney
HEPES	4-(2-hydroxyethyl)-1-piperazine-N'-ethane sulfonic acid
IRES	internal ribosome entry site
kDa	kilodalton
l	liter
LB medium	Luria Berani medium
LP	longpass filter
M	$\text{mol l}^{-1}$
MDCK	Madin Darby canine kidney
MEM	modified essential medium
min	minute
MOPS	3-(N-morpholino)propansulfonic acid
ms	millisecond
NHS-SS-biotin	N-hydroxysulfosuccinimide disulfide biotin
OD	optical density
$p_o$	open probability
$p_{\text{slow}}$	open probability of the slow gate
$p_{\text{fast}}$	open probability of the fast gate
PBS	phosphate buffered saline
PCR	polymerase chain reaction
R	universal gas constant $8.3144621 \text{ J K}^{-1} \text{ mol}^{-1}$
RFP	red fluorescent protein
SDS	sodium dodecylsulphate
SDS-PAGE	sodium dodecylsulphate polyacrylamide gel electrophoresis
SP	shortpass filter
SV40	simian virus 40
T	absolute temperature
TEMED	N,N,N',tetramethyl-ethylene diamine
TAE	tris-acetate-EDTA
UV	ultraviolet
(m)V	(milli)Volt
WT	wild type
YFP	yellow fluorescent protein

## Abstract

ClC-K chloride channels, members of the ClC membrane protein family, are needed for the function of the kidney and the inner ear. They are organized as dimers while each monomer builds a discrete pore, called protopore. They can be gated individually by a fast protopore gate, or in common by a slow gate. Both gates are under the control of the  $\beta$ -subunit barttin. Besides gating modulation, barttin facilitates membrane trafficking of all ClC-K chloride channel orthologs.

The human chloride channel hClC-Ka is only active in presence of barttin, the rodent ortholog rClC-K1 is already conducting without, but barttin changes its voltage dependence. The effect of barttin on gating, and thus its binding, becomes more obvious when a pore-lining valine of rClC-K1 channels is mutated to the so called 'gating glutamate' V166E.

Little is known about functional determinants within the structure of barttin. It consists of 320 amino acids which form two transmembrane helices near the N-terminus (aa9-26 and aa35-55) that are crucial for binding to ClC-K channels as shown by barttin truncation Y57X. Chaperone function of this barttin is still conserved.

To figure out binding amino acids, we performed site-directed mutagenesis, substituting every single amino acid of the two proposed helices to tryptophan in order to prevent binding due to the introduction of a bulky amino acid. The binding of mutant barttin to hClC-Ka or V166E rClC-K1 was analyzed by confocal microscopy, biotinylation assays and whole cell patch clamp recordings in heterologous expression systems. Surprisingly, binding could not be prevented by a single point mutation.

Several mutations (I12W, G15W, A20W, G48W, S52W and Q55W barttin) lead to a reduction in chaperone function and are therefore likely to be part of the binding interface. These residues also modulate the gating behavior of the channels, also indicating their interaction. While almost the entire first helix is thoroughly needed for the activity of the fast gate, several residues within the second transmembrane helix of barttin alter mainly the slow gating of V166E rClC-K1. T36W and M44W barttin lost all their capability to modulate gating, but still bind to both observed channels. Different structure of the channel is assumed at the positions which bind to the residues G10, V13, L14, A39 and M40. In contrast to other positions, mutation of one of the mentioned five evokes effects on regulation of hClC-Ka that cannot be compared with the effects on V166E rClC-K1.

Besides the interface, the binding stoichiometry should be determined. Therefore, we covalently linked barttin to V166E rClC-K1. Our results suggest a stoichiometry barttin:ClC-K of at least 2:1.

Within the channel structure, two binding domains were published. Here, we validate the binding of barttin to the B-helix of the channel by a chimeric channel protein. Furthermore, we postulate that this binding to the B-helix occurs via the first transmembrane helix of barttin.

## Zusammenfassung

ClC-K Chlorid Kanäle sind Mitglieder der ClC Membranproteinfamilie und werden für die Funktion der Niere und des Innenohrs benötigt. Sie sind als Dimer organisiert, wobei jedes Monomer eine eigenständige Pore bildet, die Protopore genannt wird. Diese können individuell durch das schnelle Protoporengate, oder gemeinsam durch das langsame Gate reguliert werden. Beide sind unter der Kontrolle der  $\beta$ -Untereinheit Barttin. Neben der Veränderung der Spannungsabhängigkeit ermöglicht Barttin den verstärkten Membraneinbau der Kanalproteine.

Im Gegensatz zum humanen hClC-Ka Chlorid Kanal ist das Rattenortholog rClC-K1 auch ohne Barttin leitend. Allerdings verändert Barttin dessen Spannungsabhängigkeit. Der Effekt des Barttins auf das Schaltverhalten von rClC-K1 – und damit deren Interaktion - wird nach Mutation eines porenständigen Valins zum sogenannten 'Gatingglutamat' V166E deutlicher.

Über die Funktionsweise des Barttins ist bisher wenig bekannt. Es besteht aus 320 Aminosäuren, die in der Nähe des N-Terminus zwei transmembrane Helices bilden (Aminosäuren 9-26 und 35-55). Dieser transmembrane Kern ist für die Bindung an ClC-K Kanälen notwendig, wie am Beispiel eines stark verkürzten Barttins deutlich wird. Y57X Barttin zeigt noch immer einen verstärkten Membraneinbau des Kanals.

Wir führen einen Mutagenese Scan durch, bei der jede einzelne Aminosäure der beiden Helices des Barttins gegen Tryptophan ausgetauscht wurde. Falls die Mutation innerhalb der Interaktionsdomäne liegt, sollte theoretisch die Bindung verhindert werden. Die Bindung des mutierten Barttins mit hClC-Ka oder V166E rClC-K1 wurde mittels konfokaler Mikroskopie, Biotinylierungsassays und elektrophysiologischen Ganzzelleitungen in heterologen Expressionssystemen untersucht. Überraschenderweise wurde die Bindung durch keine Mutation verhindert.

Mehrere Mutationen (I12W, G15W, A20W, G48W, S52W und Q55W Barttin) führen zu einem verminderten Membraneinbau des Kanals und sind daher Teil der Interaktionsdomäne. Diese Aminosäuren beeinflussen auch das Schaltverhalten, ein weiteres Indiz der Interaktion. Die Regulierung des Schaltverhaltens scheint komplexer zu sein, da viele Aminosäuren an der Bindung beteiligt sind. Während annähernd die gesamte erste Helix des Barttins die Aktivität des schnellen Gates von V166E rClC-K1 reguliert, konnte der Einfluss einiger Aminosäuren der zweiten Helix auf das langsame Gate gezeigt werden. Durch die Mutationen T36W und M44W hat Barttin seine Funktion auf das Schaltverhalten, aber nicht auf den Membraneinbau beider untersuchter Kanäle verloren. Unterschiedliche Strukturen der Kanäle werden an

Positionen vermutet, an denen Barttin via G10, V13, L14, A39 oder M40 bindet. Im Unterschied zu anderen Positionen, führt hier eine Mutation zu Effekten auf die Regulierung von hCIC-Ka, die nicht vergleichbar sind mit den Effekten auf V166E rCIC-K1.

Neben der Bestimmung der Interaktionsdomäne sollte die Bindungsstöchiometrie ermittelt werden. Dazu wurde Barttin kovalent an den V166E rCIC-K1 verlinkt. Unsere Ergebnisse deuten auf eine Stöchiometrie Barttin:V166E rCIC-K1 von 2:1 oder höher hin.

Bisher wurden zwei Bindungsdomänen für Barttin in der Kanalstruktur nachgewiesen. In dieser Studie belegen wir die Bindung des Barttins an die B-Helix des Kanals mittels eines chimären Kanals. Weiterhin postulieren wir, dass diese Bindung an die B-Helix über die erste Transmembranhelix des Barttins stattfindet.



# 1 Introduction

Barttin is an accessory subunit of ClC-K chloride channels (Estévez et al. 2001). The protein with unknown high-resolution structure consists of 320 amino acids. Secondary structure prediction (HHpred – University of Tübingen) reveals two transmembrane helices (TM) near the N-terminus (TM1 aa9-26 and TM2 aa35-55) and a long C-terminus. The transmembrane core of barttin is needed for channel transport, post-translational modification and gating regulation of ClC-K chloride channels (Scholl et al. 2006, Fischer et al. 2010). A sorting motif for basolateral plasma membrane insertion of ClC-Ka lies within the long C-terminal tail of barttin (Janssen et al. 2009).

Up to date, it is unknown how barttin regulates the  $\alpha$ -subunit of ClC channels. Moreover, the binding stoichiometry is not solved yet.

ClC proteins are found in many kingdoms, such as bacteria (Fujita et al. 1994), fungi (Huang et al. 1994), plants (Hechenberger et al., 1996) and animals (Miller, 1982, Jentsch et al., 1990). They mediate ion flux/transport over cell membranes. Unique features of ClC family members are their organization in homo-dimers (Middleton et al. 1996, Dutzler et al. 2002) and their gating properties. Each monomer exhibits a pore, the so called protopore, which can be individually gated (Middleton et al. 1996, Ludewig et al. 1996). Additionally, there is a common gate, which opens or closes both protopores simultaneously (Fischer et al. 2010, Miller 1982, Saviane et al. 1999; Zuniga et al. 2004, de Santiago et al. 2005, Scholl et al. 2006). Due to time courses and dwell-times of the gating events, the protopore gate is called fast gate, the common gate is called slow gate. Barttin influences the fast as well as the slow gate of ClC-K channels (Fischer et al. 2010).

## 1.1 CIC chloride channel/transporter family

The family of CIC proteins consists of channels and transporters. In mammals, nine members are known, CIC-1 to CIC-7, CIC-Ka/CIC-K1 and CIC-Kb/CIC-K2. In the dendrogram of Fig.1, the relationship of these nine types of protein is depicted together with the prokaryotic *EcCIC* from *Escherichia coli* and the eukaryotic *CmCIC* from a red alga *Cyanidioschyzon merolae*, which both had been crystallized. In the upper branch, CIC-Ka to CIC-2, CIC channels are clustered together with CIC-0, the chloride channel of the electric organ from *Torpedo marmorata*. These family members are all located at plasma membranes. CIC-0 was the first CIC chloride channel protein that was cloned (Jentsch et al. 1990, Steinmeyer et al. 1991).

The lower branch includes the H<sup>+</sup>/Cl<sup>-</sup>-transporters CIC-3 to CIC-7 which are all located in membranes of intracellular compartments. *EcCIC* and *CmCIC* both act as transporter, although from their sequences of amino acids, they are closer related to the channels. Channels and transporters share the homodimeric organisation. The formation of protopores is unique within the known channels. Channels and transporters within the same family of membrane proteins is another rare feature and serves as an example for the close functional relationship of these two transport mechanisms.

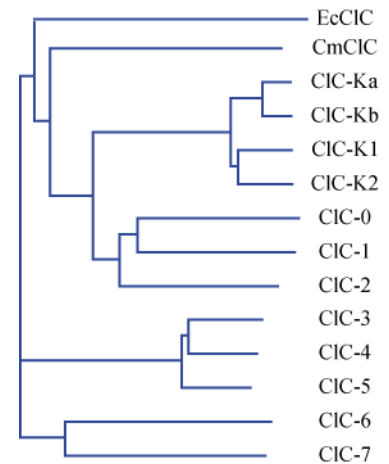


**Fig.1 Dendrogram of the CIC protein family**

Channels (CIC-Ka to CIC-2) and transporters (CIC-3 to CIC-7) are closely related. Bacterial *EcCIC* represents prokaryotic CIC transporters. *EcCIC* and *CmCIC*, a chloride transporter from a red algae, are closer related to the channel branch than to the transporters. CIC-0 is the closest relative to CIC-1.

### 1.1.1 Structure of CIC proteins

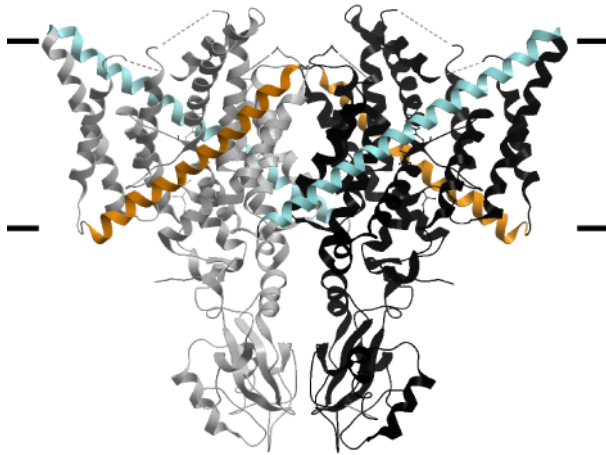


**Fig.2 Crystal structure of homodimeric CmCIC**  
Highlighted are the monomers (silver and black) with the B- (blue) and J- (orange) helices. The black lines indicate the plasma membrane. Beyond the plasma membrane, two CBS domains per monomer are shown. Modified from Feng et al. 2010.

Dutzler et al. crystallized *EcCIC* in 2002 at 2.5 Å resolution. Further X-ray structure analyses followed. But there is no structure available from mammalian CIC proteins at present. In 2010, the eukaryotic *CmCIC* protein was crystallized at 3.5 Å resolution (Fig.2, Feng et al. 2010). Like formerly crystallized CIC proteins, *CmCIC* is a transporter. Nevertheless, because of the high homology of the CIC proteins, these crystals give insights into the CIC channel function-structure relationship as well. The two

monomers are shown in silver and black. It is a side view with denoted plasma membrane segments. The highlighted B- (blue) and the J-helices (orange) are proposed to bind the  $\beta$ -subunit barttin in CIC-K2 (Tajima et al. 2007). Fig.3 shows a topology model of the  $\alpha$ -subunit.

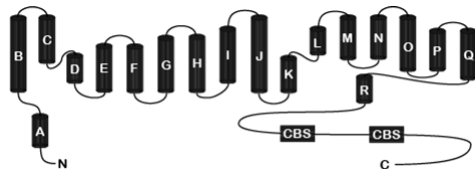


**Fig.3 Topology model of CIC proteins**  
16 transmembrane helices, two more helical stretches and two CBS domains form the tertiary structure of a monomer.

A pore-forming monomer, a so called protopore, consists of 16 transmembrane helices, two adjacent helices (A+R helix) and two cytoplasmatic CBS domains. CBS domains were first identified in name-giving cystathionine  $\beta$ -synthetase (Bateman 1997, Ignoul and Eggermont 2005). Further studies have proven CBS domains to regulate catalytic activity of enzymes by binding to nucleotides (Scott et al. 2004, Townley and Shapiro 2007). Adenosine nucleotides were shown to regulate some CIC channels and transporters via CBS domains (Stölting et al. 2013, Vanoye and George 2002, Hebeisen et al. 2004, Hebeisen and Fahlke 2005, Bennetts et al. 2005, Meyer et al. 2007). *EcCIC* lacks this cytoplasmatic domain (Dutzler et al. 2002). CBS domains of several CIC proteins have been crystallized (CIC-Ka Markovic and Dutzler 2007, CIC-5 Meyer et al. 2007, CIC-0 Meyer and Dutzler 2006, *CmCIC* Feng et al. 2010) and stated to participate in channel gating and dimerization (Bykova et al. 2006, Pusch et al. 1997,

Fong et al. 1998, Estévez et al. 2004). By comparison of nucleotide-binding CBS domains of ClC-0 and ClC-5 with CBS domains of hClC-Ka, it became clear that the CBS domains of hClC-Ka do not bind nucleotides.

The pore region of *EcClC* (Dutzler et al. 2002, 2003, 2004A+B, 2006, 2007, Cohen and Schulten 2004) and *CmClC* (Feng et al. 2010) is well described. Fig.4A depicts the pore coordinating amino acids of *EcClC*. The high homology of the pore region is shown in alignments in Fig.4B. Three chloride binding sites are formed by highly conserved amino acids. The external binding site for chloride, the peptidical bound amino group of F357 at the end of  $\alpha$ N, is not always accessible, because of a glutamate side chain (E148) swinging in and out the pore in a voltage dependency and/or upon protonation. This glutamate E148 is proposed to be the fast gate (Fig.4A, Fahlke et al. 1997, Dutzler et al. 2003, Zuñiga et al. 2004, de Santiago et al. 2005) and again highly conserved throughout the family.

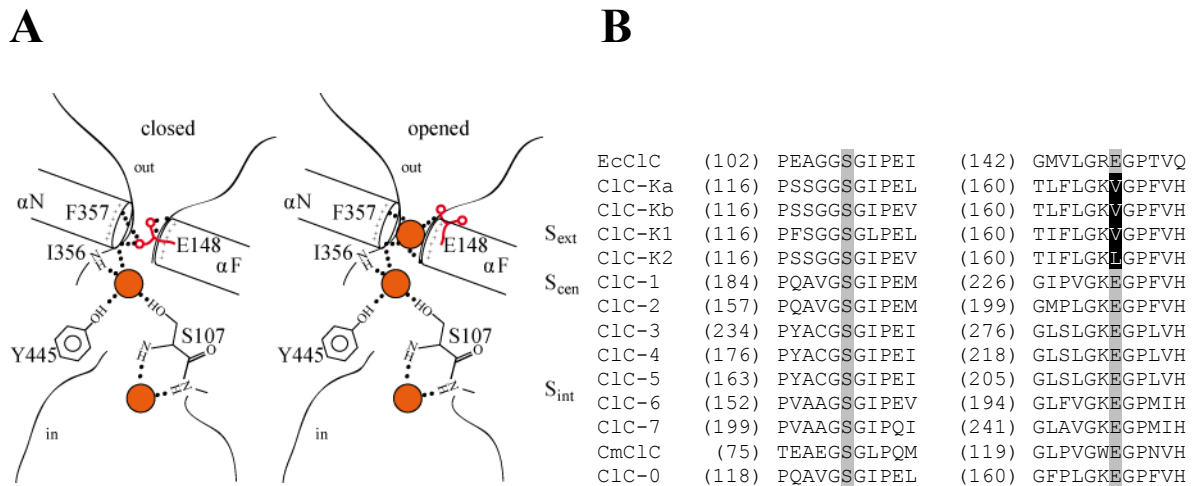


**Fig.4 (A) Scheme of the open and closed pore conformation of *EcClC* and (B) an alignment of the highly conserved chloride binding sites of ClC family members**

(A) modified from Dutzler et al. 2003. In closed conformation, the anion-binding sites *S<sub>int</sub>* and *S<sub>cen</sub>* are occupied by chloride ions (red circles), while *S<sub>ext</sub>* is occupied by the side chain of E148 (red). Movement of the side chain of E148 opens the channel, *S<sub>ext</sub>* is now occupied by a third chloride ion. S107 is the internal binding site, the central binding site is coordinated by I356, F357 and Y445, and the external binding site is formed by F357.

(B). The binding sites are highly conserved throughout the family. S107, F357 and Y445 are always present (grey bars). The gating glutamate E148 is substituted by valine/leucine in ClC-K channels (grey and black; upper right alignment). Besides the pore coordinating tyrosine, a regulatory lysine is highlighted in the lower right alignment

All CIC family members have a now-on called 'gating glutamate' at the beginning of their F-helix, except CIC-K channels, which bear a valine/leucine at this position (Fig.4B upper right alignment). Substitution of V166 to glutamate in rCIC-K1 leads to prominent changes in gating properties (Waldegger et al. 2000). These findings will be described later in detail, illustrating the functional purpose of barttin for gating regulation. Even though CIC-K WT channels lack this gating glutamate, they exhibit fast gating as well. Thus, the mechanism of gating is not fully understood, yet.

The internal anion binding site is coordinated by a serine, localized at position S107 in *EcCIC*. The central binding is coordinated by S107, Y445 and I356. S107 and Y445 are suggested to participate in gating, they are even called 'putative gate' (Jayaram et al. 2008) or intracellular gate (Picollo et al. 2009 and 2012, Accardi and Picollo 2010). The suggestion of the participation of Y445 in gating (Chen et al. 2003, Accardi and Pusch 2003) was confirmed by Elvington et al. (2009) who showed a Y445-movement. Despite of Y445 being in the Cl<sup>-</sup>-pathway, Walden et al. (2007) showed that a decrease in side chain volume at this position disrupts H<sup>+</sup>-transport, although Accardi et al. (2006) as well as Elvington et al. (2009) stated that there is no direct involvement of this tyrosine in the H<sup>+</sup>-pathway.

Residues of the selectivity filter, S107, F357 and Y445 are highly conserved throughout the CIC family, however the mechanism of binding, especially the simultaneous occupancy of the binding sites, is discussed controversially (Lobet and Dutzler 2006, Engh and Maduke 2005, Engh et al. 2007).

Mutation of Y445 (Y512 in CIC-0) hardly influences single channel conductance of CIC-0 (Chen et al. 2003, Accardi and Pusch 2003) although it is part of the selectivity filter in cooperation with S107. Same groups and others (Chen and Chen 2003, Wang et al. 2010) reported a lysine K519 in CIC-0, corresponding to T452 in *EcCIC*, to be crucial for channel activation. This lysine is highly conserved within the adjacent R-helix of channels of the CIC-family (Fig.4 B lower right alignment) and lies within the pore mouth of the channel. FRET-analysis revealed that the C-terminal – the intracellular CBS domains next to the R-helix - of the channels moves during common, slow gating (Bykova et al. 2006).

Not only the C-terminal, but a cysteine residue at the end of the G-helix (C277 in CIC-1, C212 in CIC-0) in the interface of the two protopores was shown to influence common gating (Weinberger et al. 2012, Bykova et al. 2006, Lin et al. 1999, Accardi and Pusch 2000, Zuñiga et al. 2004, de Santiago et al. 2005). For CIC-5, many mutations within this interface were found in Dent's disease (Lourdel et al. 2012).

## **1.1.2 The family members of ClC chloride channels and transporters**

### **1.1.2.1 hClC-Ka/rClC-K1 and hClC-Kb/rClC-K2**

This study was made with the renal and inner ear family members ClC-K. "K" is the abbreviation for kidney, where these channels were found first (Kieferle et al. 1994). hClC-Ka and hClC-Kb are the human, rClC-K1 and rClC-K2 are the rodent isoforms. Due to the high homology (83 % among rat isoforms, 91 % among human isoforms and 80 % among the two orthologs, Kieferle et al. 1994, Kobayashi et al. 2002, Fahlke and Fischer 2010, Krämer et al. 2008), similar regulation is expected, but a remarkable difference between the channel orthologs is that hClC-Ka, hClC-Kb and rClC-K2 are non-conducting without barttin, while rClC-K1 is always conducting without barttin, but its voltage dependence of gating is altered upon barttin-binding. The mechanisms of binding and gating regulation of ClC-K channels are unknown at present.

ClC-K channels form a complex of homodimeric organized  $\alpha$ -subunits together with barttin as  $\beta$ -subunit. The stoichiometry  $\alpha:\beta$  is unknown at present. Besides barttin, no further ClC-K binding partner has been reported, but calcium is needed for channel activity (Waldegger and Jentsch 2000, Martinez and Maduke 2008, Gradogna et al. 2010, 2012). The physiological role of ClC-K channels is described in the following passage as well as the function of barttin.

#### ***1.1.2.1.1 Role of ClC-K channels in the kidney and the inner ear***

ClC-K channels are predominantly expressed in the ascending limb of Henle's loop in the kidney and in marginal cells of the stria vascularis in the inner ear (Vandewalle et al. 1997, Rai et al. 1999, Maulet et al. 1999, Uchida 2000A+B, Uchida and Marumo 2000, Uchida et al. 1993, 1995, Estévez et al., 2001, Qu et al. 2006). The thin ascending limb is impermeable to water (Gross et al. 1975). Morgan et al. (1970), Imai and Kokko (1976) found a conductive pathway for anions on both the basolateral and apical membrane side, while  $\text{Na}^+$ , but moreover divalent cations, seemed to diffuse paracellularly (Friedman and Gesek, 1993). Years later, it was found out that the transcellular anion conduction is mediated by a ClC chloride channel (Uchida et al. 1995) – in human hClC-Ka, respective the rodent homolog

rCIC-K1 (Kieferle et al. 1994). Fig.5 illustrates the expression sites of CIC-K channels. hCIC-Ka is expressed in the thin ascending limb of Henle's loop at the apical and basolateral sides.

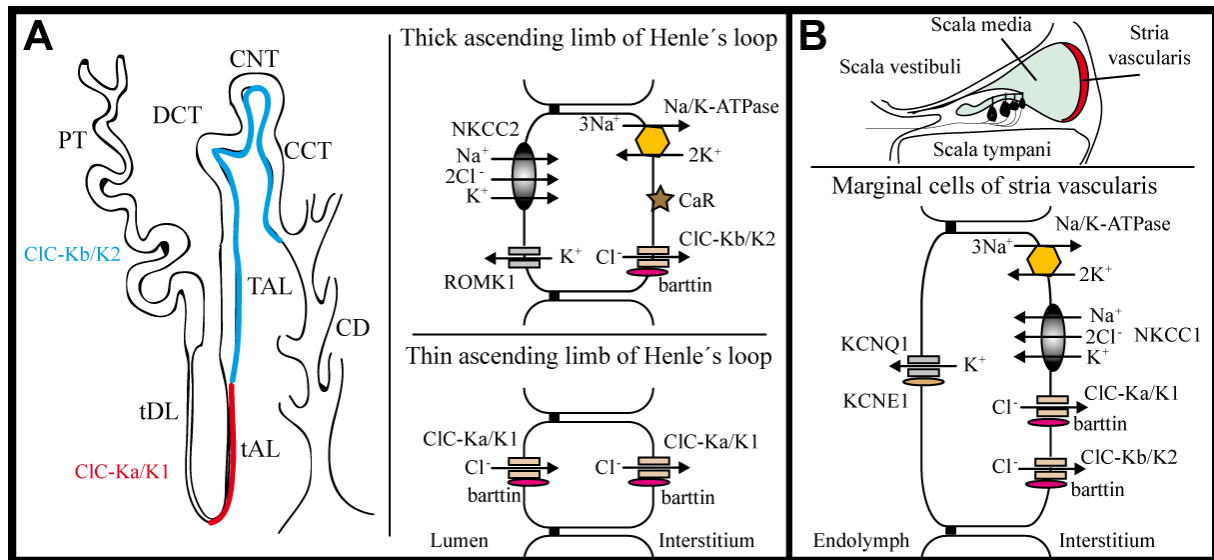


**Fig.5 Localization and physiological function of CIC-K channels in (A) the nephron and (B) the inner ear**

**A** Expression sites of hCIC-Ka/K1 (red, left panel) and hCIC-Kb/K2 (blue, left panel) in the nephron. CIC-Ka/K1 channels mediate passive NaCl reabsorption in the thin ascending limb. CIC-Kb channels are necessary for secondary active reabsorption of NaCl in the outer medulla and cortical regions of the nephron (PT proximal tubule, tDL thin descending limb of Henle's loop, tAL thin ascending limb of Henle's loop, TAL thick ascending limb of Henle's loop, DCT distal convoluted tubule, CNT connecting tubule, CCT cortical collecting tubule, CD collecting duct). **B**) Distribution of CIC-Ka/K1 and CIC-Kb/K2 in the inner ear. Both isoforms are expressed in the marginal cells of the stria vascularis, contributing to the secretion of  $K^+$  into the endolymph of the scala media. Modified from Fahlke and Fischer 2010.

The water impermeable, thick ascending limb and further distal regions shelter hCIC-Kb/rCIC-K2, but in contrast to hCIC-Ka, only on the basolateral side (Kobayashi et al. 2001A+B). To achieve salt-resorption, a secondary active transport mechanism requires more participants here. The coordinated function of a set of transmembrane proteins is needed. Apical, the inward rectifying potassium channel (ROMK1, renal outer medulla potassium channel,  $K_{ir}1.1$ ) and  $Na^+-K^+-2Cl^-$ -cotransporter (NKCC2) with basolateral anion channels (hCIC-Kb) and  $Na/K$ -ATPase work for secondarily active NaCl reabsorption (Greger et al. 1983, Greger and Schlatter 1981, 1983, Schlatter et al. 1983). A basolateral calcium sensing receptor CaR regulates ROMK1 and NKCC2 (Brown and MacLeod 2001, Naderi and Reilly 2008, Riccardi and Brown 2010) by several cascades. Phospholipase A2 activation via CaR results in arachidonic acid production (Handlogten et al. 2001, Kifor et al. 2001). Metabolic activation of arachidonic acid via cytochrome P-450 makes it an inhibitor of ROMK and probably NKCC2. With a novel statistical method to evaluate quantitative traits of multi-locus genotyped SNPs (single nucleotide polymorphism), interaction of the unlinked genes coding for CaR, CIC-Kb and NKCC2 was shown (Jung et al. 2009), but no functional investigation was performed. CIC-K channels themselves are  $Ca^{2+}$ -dependent (Gradogna et al. 2010, 2012,

Waldegger and Jentsch 2000). Two residues in the loop between the I- and J-helices were shown to bind regulatory calcium-iones. Another regulation pathway for ClC-K channels is mediated by proinflammatory cytokines that have down-regulating effects on ROMK, Na/K-ATPase and/or ClC-K (Schmidt et al. 2007).

Both isoforms, ClC-Ka/K1 and ClC-Kb/K2, co-express in the stria vascularis of the inner ear (Estévez et al. 2001). In marginal cells they are contributing to K<sup>+</sup>-secretion into the scala media. K<sup>+</sup> is needed for sensory transduction in inner hair cells. Hence a high potassium concentration in the endolymph is essential for hearing. Cooperation of NKCC1, KCNQ1 and ClC-K is needed for the maintenance of this high [K<sup>+</sup>] in the endolymph.

### 1.1.2.1.2 Bartter Syndrome

In 1962, Frederic Bartter first described a renal failure accompanied with hyperaldosteronism and hypokalemic alkalosis. Later, mutations in *CICNKB*, the gene coding for one of the two human ClC-K chloride channel homologs, were figured out to be the reason for the disease, called classical bartter syndrome. Mutation within the *BSND* gene coding for barttin may lead to atypical type of bartter syndrome with sensorineural deafness, bartter syndrome type IV (Birkenhäger et al. 2001, Miyamura et al. 2003, Estévez et al. 2001, Waldegger et al. 2001). In respect to the efforts of Frederic Bartter, barttin was named after him.

Bartter syndrome is a genetic disease with the characteristic symptoms of renal salt waste, elevation of renin and aldosteron plasma level with normal or low blood pressure, hypokalemic metabolic alkalosis, polyuria and polydipsia.

Up to now, 5 types of Bartter syndrome can be distinguished by the mutated gene (Tab.1).

<b>Bartter Syndrome</b>	<b>Dysfunctional Protein/Gene</b>	<b>affected tissue</b>
<b>Type I</b>	NKCC2/ <i>SLC12A1</i>	kidney
<b>Type II</b>	ROMK1/ <i>KCNJ1</i>	kidney
<b>Type III</b>	ClC-Kb/ <i>CICNKB</i>	kidney
<b>Type IV</b>	Barttin/ <i>BSND</i>	kidney/inner ear
<b>Type V</b>	CaR/ <i>CASR</i>	kidney

**Tab.1 Types of Bartter syndrome, their cause and the affected tissues**

5 types of bartter syndrome have been described, all affecting kidney function. Renal salt waste is caused by gene defect in genes coding for NKCC2 (I), ROMK1 (II), ClC-Kb (III), Barttin (IV) or CaR (V).



Type I-IV are inherited autosomal recessive, with Bartter syndrome type III being the classical Bartter syndrome (Jeck et al. 2000) with a defect in *ClC-Kb* coding gene causing characteristic symptoms mentioned above. Type V is inherited autosomal dominant (Pearce et al. 1996) and sums mutations in *CASR* gene, coding for the calcium receptor CaR, leading to renal failure. Mutations in *SLC12A1* or *KCNJ1*, genes coding for NKCC2 or ROMK1, may cause Bartter syndrome types I or II.

At present, no Bartter syndrome causing mutation in *ClCNKA*, coding for the other human homolog *ClC-Ka*, is known, but *ClCNKI* *-/-* mice suffer from diabetes insipidus (Matsumura et al. 1999).

Only patients with Bartter syndrome type IV suffer from hearing loss in addition to renal dysfunction (Birkenhäger et al. 2001, Hebert 2003, Landau et al. 1995, Jeck et al. 2001, Janssen et al. 2009, Riazuddin et al. 2010), because both channel homologs, *ClC-Ka* and *ClC-Kb*, are also located in the inner ear and need Barttin to become conductant.

### 1.1.2.2 *ClC-1* and *ClC-2*

*ClC-1* is expressed in adult skeletal muscle and maintains the high anion conductance at resting potentials which is inevitable for muscle fibre function (Steinmeyer et al. 1991A+B). Mutations in *ClC-1* coding gene *ClCNI* can lead to myotonia congenita (Koch et al. 1992, George et al. 1993). For a long time, *ClC-1* was called “the skeletal” chloride channel, but a recent study has shown *ClC-1* in the brain (Chen et al. 2013).

*ClC-2* is broadly expressed throughout the tissues. It was found in the central nervous system fulfilling an excitatory task (Kleefuss-Lie et al. 2009, Saint-Martin et al. 2009, Földy et al. 2010, Rinke et al. 2010), in the retina for wound healing purposes (Cao et al. 2010), and in various epithelia for anion resorption (Bösl et al. 2001, Catalán et al. 2004, Peña-Münzenmayer et al. 2005). Dysfunction of *ClC-2* can be correlated with idiopathic epilepsy (Stölting et al. 2013).

### **1.1.2.3 ClC chloride/proton antiporter**

ClC-transporters are predominantly expressed in intracellular compartments (Friedrich et al. 1998, Wang et al. 2006, Graves et al. 2008, Buyse et al. 1998). ClC-3 to ClC-7 are chloride/proton antiporters that usually exchange two chloride ions by one proton. Thus, the coupled electrogenic transport passes three net charges across the membrane for each transport cycle.

#### ***1.1.2.3.1 ClC-3, ClC-4, ClC-5***

ClC-3 is located in intracellular vesicles (Stobrawa et al. 2001). Although broadly expressed over the whole brain, ClC-3 knockout mice show complete postnatal neurodegeneration of the hippocampal CA1 region, only (Farmer et al. 2012). ClC-3 has been shown to be functionally linked to NMDA-receptors in hippocampal synapses (Wang et al. 2006).

Little is known about ClC-4. This transporter is expressed in the brain, muscle and liver. It contributes to acidification of endosomes (Mohammad-Panah et al. 2003). By certain extracellular anions (thiocyanate) ClC-4 transporters change their chloride/proton stoichiometry and are thought to functionally convert to regular anion channels (Alekov and Fahlke 2009).

Like ClC-4, ClC-5 is an outward rectifying chloride transporter of endosomes that supports acidification of such intracellular compartments. ClC-5 is detectable in endosomes of renal epithelial cells (Günther et al. 1998). Dysfunction of ClC-5 leads to Dent's disease, affecting endocytosis in the proximal tubule of the nephron.

#### ***1.1.2.3.2 ClC-6 and ClC-7***

ClC-6, but also ClC-2, ClC-3, ClC-4, ClC-5 are found in the retina, where they might play a role in wound healing (Cao et al. 2010). Little is known about the physiological role of ClC-6

at present (Neagoe et al. 2010). CIC-6 and CIC-7 form a distinct branch within the CIC family. CIC-6 as well as CIC-7 knockout mice develop unexpected fatal paediatric storage disorders (Pressey et al. 2010). CIC-7 is essential for bone growth and stability (Kornak et al. 2001). *Ostm1* is the  $\beta$ -subunit of CIC-7 (Lange et al. 2006, Leisle et al. 2011).

### 1.1.3 Interacting proteins of CIC channels and transporters

#### 1.1.3.1 Adaptor proteins

Several binding partners are reported for CIC channels and transporters (Stauber and Jentsch 2010), like adaptor proteins (AP1-4), clathrin or GGA (golgi-localized,  $\gamma$ -ear containing, Arf-binding). Dileucine motifs (DE)XXXLL or tyrosine-based motifs NPXY or YXX $\Phi$  (with  $\Phi$  being a bulky, hydrophobic amino acid) are recognized for sorting events (Bonifacino and Traub 2003). Zhao et al. (2007) described dileucine-motif dependent sorting of CIC-3. Besides sorting function, adaptor proteins or GGA family members mediate transport between the trans-Golgi network, plasma membrane and early or late endosomes (Braulke and Bonifacino 2006, Kelly et al. 2008).

<i>Ec</i> CIC	(118)	DQRPVRWWRVLPVKFF	(---)	
CIC-Ka	(132)	GVILEDYLDIKNFGAK	(646)	NLFKTLNLQS
CIC-Kb	(132)	GVVLEDYLDIKNFGAK	(646)	NLFETLNLHS
CIC-K1	(132)	GVVLEDYLDIKNFGAK	(646)	SLFERLTLQS
CIC-K2	(132)	GVILEDYLDIKNFGAK	(646)	NLFETLNLQL
CIC 1	(200)	GVVLKEYLTMKAFVAK	(839)	TLFSLGLHL
CIC 2	(173)	GVVLKEYLTLKTFIAK	(808)	TIFSLGVVDH
CIC-3	(250)	GFIIRGYLGKWTLMIK	(773)	DIFRKLGLRQ
CIC-4	(192)	GFIIRGYLGKWTLLIK	(715)	DIFRKLGLRQ
CIC-5	(179)	GFIIRGYLGKWTLVIK	(701)	DIFRKLGLRQ
CIC-6	(168)	GVKVPGIVRLRTLCK	(825)	NLFRTMGLRH
CIC-7	(215)	GVKIPHVRLRTLVIK	(759)	KLFRATGLRH
<i>Cm</i> CIC	(91)	GFYDKMRSALRLVLF	(592)	FLFVMMPSM
CIC-0	(134)	GAVLHEVTLRLTFVAK	(739)	TLFSLGLDR

**Tab.2 Alignment of two regulatory domains of CIC proteins**

In the left panel, a tyrosine between D- and E-helix is responsible for membrane insertion and recycling, as reported for CIC-2, only. This tyrosine is highly conserved through almost the entire family. The sorting of membrane insertion is regulated by another motif (right panel). A dileucine motif is needed for sorting events, as shown again for CIC-2. This dileucine motif is highly conserved for the channel proteins within the CIC-family.

In CIC-2, another motif was found. A tyrosine based motif within the loop of D- and E-helix mediates recycling of CIC-2 between endosomes and plasma membrane (Cornejo et al. 2009). These two motifs are highly conserved within the channels and transporters of the CIC-family, as shown in Tab.2. In *Ec*CIC, this functional tyrosine is replaced by a tryptophan.

Intracellular trafficking of ClC-1 and ClC-2 is mediated via adaptor proteins. The N-terminus of ClC-1 interacts with AP-2 (Stauber and Jentsch 2010). The C-terminus (dileucine motif) of ClC-2 interacts with AP-1B for basolateral orientation (Peña-Münzenmayer et al. 2005). For ClC-K channels, no adaptor protein has been described so far. But, an auxiliary subunit, barttin, was found which fulfils analog functions like membrane trafficking and sorting of chloride channels as well as gating regulation and stability of the pore-forming subunit. The above mentioned motifs could be influenced upon barttin binding.

### 1.1.3.2 $\beta$ -subunit barttin

All ClC-K channels are regulated by a  $\beta$ -subunit called barttin. Secondary structure prediction reveals two transmembrane helices TM1 and TM2 with a short N-terminus and a long C-terminal tail. Both termini are intracellular. A topology model of barttin is shown in Fig.6.

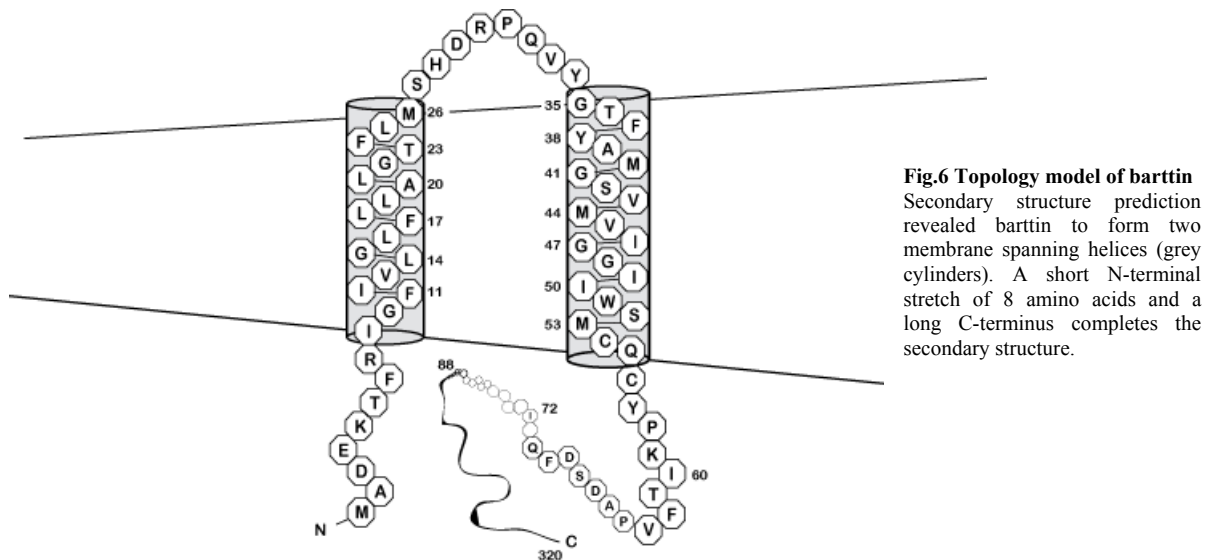


**Fig.6 Topology model of barttin**  
Secondary structure prediction revealed barttin to form two membrane spanning helices (grey cylinders). A short N-terminal stretch of 8 amino acids and a long C-terminus completes the secondary structure.

Barttin affects ClC-K channels in several ways. It is needed for channel trafficking to the plasma membrane, channel stability and modulation of the voltage dependence of gating (Estévez et al. 2001). Scholl et al. (2006) showed that the transmembrane core of barttin with

an additional short stretch of the C-terminus is sufficient to bind to ClC-K and to regulate the gating of ClC-K channels. Truncation of barttin at position 72 (I72X barttin) still activates V166E rClC-K1 in WT-barttin-like manner. Truncation at T61X reduces the unitary conductance and further truncation until Y57 still allows membrane insertion of ClC-K channels. Janssen et al. (2009) have proven E88X barttin to fulfil almost all functional purposes, besides a sorting distortion that result in pathological salt transport. hClC-Kb/E88X barttin is brought to the basolateral and to the apical membrane. In the same work, it is stated that barttins first helix alone fails to regulate ClC-K channels. Truncated Q32X barttin leads to entire loss-of-function and was found in patients suffering from Bartter Syndrome Type IV (Kitanaka et al. 2006).

A Nedd4-2 ubiquitin ligase can bind to the PY-motif of barttin via its WW-motif to mediate endocytosis (Estévez et al. 2001, Embark et al. 2004, Flores et al. 2003). A serum- and glucocorticoid-inducible kinase regulates the ubiquitin ligase (Flores et al. 2005). Interruption of this binding PY-motif, as shown for Y98A barttin (Hayama et al. 2003), leads to an extended exposure of barttin to the plasma membrane, as well as to higher stability of the barttin/ClC-K complex. Such a mutated barttin increases currents of whole cells cotransfected with hClC-Kb cDNA. Similar endocytosis regulation via Nedd4-2 ubiquitin ligase and corresponding PY-motif were found for Na<sup>+</sup>-channel ENaC or ClC-5 (Flores et al. 2003, Kamynina and Staub 2002). As described above, a tyrosine based motif for regulation of endocytosis is found for almost all ClC-family members in the cytoplasmatic loop between the D- and the E-helix. Barttin facilitates plasma membrane exposure and stability of ClC-K channels and this loop is a possible target for the regulation of this purpose.

Another regulatory mechanism is to modify barttin with palmitate. This fatty acid is attached to barttins cysteine residues C54 and C56 (unpublished data, Steinke et al. 2013). Without palmitate, hClC-Ka/Kb is non-conductant and the gating of V166E rClC-K1 is altered.

Besides Q32X and E88X barttin, which were described above, more disease-causing barttin mutations have been identified and characterized (Janssen et al. 2009). The severity of symptoms varies depending on the position of mutation in the *BSND* gene. All patients are deaf. R8L, R8W and G10S barttin evoke a severe renal phenotype, but without causing renal failure. G47R barttin provokes a late onset of the bartter syndrome with a mild phenotype (Miyamura et al. 2003, García-Nieto et al. 2006), and interestingly, I12T barttin is only affecting inner ear function (Riazzudin et al. 2010, Janssen et al. 2009, Fahlke and Fischer 2010).

Due to this huge variety of symptoms of Bartter Syndrome Type IV introduced by single point mutations, it gets obvious that barttin regulates its  $\alpha$ -subunit distinct. Several molecular determinants within the transmembrane core are expected, because of stabilizing effects and chaperone function. In addition with a short cytoplasmatic stretch (I72X), slow and fast gating of ClC-K channels is coordinated, but only the transmembrane core of barttin is needed for the binding to ClC-K channels.

## **1.2 Aim of this study**

The interaction of barttin and ClC-K channels is poorly understood. Little is known about binding interfaces, stoichiometry or possible further binding partners. At present, only one publication postulates the B- and the J-helices of ClC-K channels to bind to barttin (Tajima et al. 2007). Even less is known about the determinants important for binding to the channel protein on behalf of barttin.

The aim of this study was to determine amino acids in the transmembrane helices of barttin that interact with the pore-forming subunits of ClC-K/barttin channels. We substituted each amino acid of the two transmembrane helices by bulky tryptophan residues to investigate the interaction via this position with the  $\alpha$ -subunit.

The barttin mutants were co-expressed with hClC-Ka or V166E rClC-K1, a well described mutant of rClC-K1 (Scholl et al. 2006), in a heterologous expression system and investigated using standard patch clamp methods, biochemical approaches and confocal imaging.

We found several functional determinants within both helices of barttin that are necessary for trafficking of barttin and ClC-K/barttin to the plasma membrane, for the binding of barttin and the ClC-K  $\alpha$ -subunit, and for activation of the ClC-K/barttin channel complex. Almost the entire first transmembrane helix of barttin is needed for fast gate regulation, while several amino acids within the second transmembrane helix are needed especially for slow gate regulation.

## **2 Material and methods**

### **2.1 Material**

As long as not otherwise declared, chemicals and solutions were at least of p.A. purity. Chemicals and other material was purchased from BD (Heidelberg), BioRad (Munich), Calbiochem (Bad Soden), Fluka (Neu-Ulm), Gibco (Eggenstein), Glycon (Luckenwalde), GE Healthcare (Solingen), Harvard apparatus (March-Hugstetten), Ibidi (Martinsried), Invitrogen (Karlsruhe), Merck (Darmstadt), Moyco Dental Wax (York, PA, USA), New England Biolabs (Frankfurt), Quiagen (Hilden), Roche (Basel), Roth (Karlsruhe), Serva (Heidelberg), Sigma-Aldrich (Munich) and Thermo Scientific (Bremen).

Agilent (Waldbronn) and Roche (Basel) provided PCR Kits.

Several devices were used: Typhoon Fluorescence Scanner (GE Healthcare), Puller P-9750 (Sutter Instruments), Microforge MF-830 (Narishige, Japan), GeneGnome5 (Syngene, UK), Victor Plate reader 1420 Multilabel Counter (Perkin Elmer), Centrifuges (Table centrifuges (5415D) (Eppendorf), Heraeus cooled centrifuge, Coulter Avanti J-25 (Rotor: JLA 10.500),(Beckman)), Nanodrop Photometer (Thermo Fischer), Photometer Ultrospec 2100 pro (Amersham Bioscience), Fluorolog (Jasco), Thermoblock TDB-120 (Kisger), EnviroGenie (Scientific Industries inc.), Shaker Multitron Eco/ Infors HT PCR (Biometra Professional Trio), Gel-Doc (Bio-Rad, München) and Fusion SL (Peqlab). The equipment for electrophysiology is described in corresponding section of this chapter.

## **2.2 Methods**

For heterologous expression of proteins, corresponding genes are cloned into vectors and transfected into expressing cells. Mutations within in the gene can be introduced by PCR (polymerase chain reaction) strategies. With PCRs, proteins can also be covalently fused to another.

After the expression of the desired protein - in this case ClC-K chloride channels and their  $\beta$ -subunit barttin – they can be characterized with biochemical and electrophysiological approaches.

### **2.2.1 Molecular Biology – Vectors used**

For protein expression in HEK293T, MDCKII or Flp-in T-Rex cells, we used several vectors:

#### pSVL

This vector harbors IRES (internal ribosome entry site) with a promoter for the CD8 antigen, which can be recognized by CD8-antibody carrying Dynabeads. This binding indicates successful transfection of cells. It is a low expressing vector. An ampicillin resistance gene is encoded for selection. Initially in this study, we used a pSVL vector that encodes for YFP-hClC-Ka.

#### pRcCMV

It is a high-level expression vector for mammalian cells, due to the introduction of CMV (cytomegalovirus)-promoter which is recognized and used for biosynthesis preferentially. A polyadenylation signal leads to enhanced mRNA stability. This vector is a derivative of SV40 (simian virus 40). An ampicillin resistance gene is encoded for selection. In this study, we used pRcCMV vectors encoding for YFP rClC-K1 and YFP V166E rClC-K1.

#### pcDNA3.1(+) and pcDNA3.1(-)

This vector is derived from the pRcCMV vector. pcDNA3.1 vectors are high-level expression vectors in mammalian cells, because of the CMV promoter. Multiple cloning site in forward (+) or reverse (-) orientation is completed by a polyadenylation signal for enhanced mRNA stability. Its origin is SV40. Neomycin and ampicillin resistances genes can be used for



selection. Here, pcDNA3.1 (+) barttin (mCFP) was used. This vector was taken as template to generate all tryptophan mutants. We also used pcDNA3.1 (-) YFP hCIC-Ka.

### pcDNA5/FRT/TO

This vector has a CMV promoter for high expression in mammalian cells, a flip-in recombinase site for gene integration in Flp-In<sup>TM</sup> T-Rex host cell genom, as well as ampicillin and hygromycin resistance genes for selection. This vector was used for stable expression of chimeric channel constructs. As described later, domains of CIC-K and CIC-2 channels were exchanged on genetic level, cloned into pcDNA5/FRT/TO vectors and transfected into Flp-In<sup>TM</sup> T-Rex cells for stable expression. Transcription of these genes is tetracycline-dependent. Cells transfected with this vector were incubated with tetracycline-free medium.

## **2.2.2 PCR strategies**

As mentioned, tryptophan scanning should reveal functional determinant of barttin. Therefore, we substituted every single amino acid of the two proposed transmembrane helices by tryptophan. This was done with site directed mutagenesis PCRs. Corresponding codons within *BSND* were pointwisely mutated to TGG, coding for tryptophan.

Another PCR strategy was used to concatenate proteins. The side overlap extension PCR (SOE PCR) allows the elongation of an existing gene and the introduction of a random linker sequence which bears a complementary sequence of another gene or restriction sites. This linker and overlap is needed to fuse the two genes.

SOE PCRs were also performed to exchange single helical domains of two channels.

All primers were designed with a combination of [www.bioinformatics.org/primerX/](http://www.bioinformatics.org/primerX/) and vectorNTI software. Sigma-Aldrich provided the oligonucleotides. After arrival, the oligonucleotides were dissolved in TE-buffer (Quiagen) to an end concentration of 100  $\mu$ M.

Quikchange®-PCR was carried out with nucleotides, polymerases and buffers from Agilent (Stratagene), SOE-PCR with Fermentas High Fidelity PCR Kit (Roche). Enzymes for vector restriction and ligation were ordered at FD Fast Digest. The concentrations of template vector, primers, dNTPs, buffer and polymerase remained the same in all PCR reactions and are listed in Tab.3. For PCR-amplification of fragments of, or entire vectors, a general protocol is shown in Tab.4. An initial denaturation step was followed by 15 circles of step 2-4. The temperature of the annealing step is dependent on the length and G/C-content of primers. The

duration of the elongation step 4 is dependent on the expected length of DNA (approximately 1 min/kb). After a terminal elongation step, the PCR reaction is stopped and the sample stored at 4 °C.

PCR composition	Volume (µl)
Template vector (50 ng/µL)	1
Primer (s/as) (125 ng/µL)	1+1
10x buffer	5
50x dNTPs	1
Polymerase	1
H <sub>2</sub> O	ad. 50

**Tab.3 Mix for PCR reactions**

Template vector, primer, buffer, dNTP (deoxy-nucleotide-tri-phosphate) and polymerase are diluted in H<sub>2</sub>O as indicated.

PCR step	Temperature	Duration
1 denaturation	95 °C	1 min
2 denaturation	95 °C	20 sec
3 annealing	55 ± 3 °C	65 ± 5 sec
4 elongation	68 °C	1 min/kb
5 terminal elongation	68 °C	5 min
6 end/storage	4 °C	infinite

**Tab.4 PCR program**

Standard PCR protocols are run for amplification. Initial denaturation is followed by 15 circles of denaturation, annealing and elongation until a terminal elongation phase terminates amplification. DNA can be stored at 4 °C for long time.

### 2.2.2.1 Substitution of single amino acids to tryptophan:

#### QuikChange® site directed mutagenesis

A generalized procedure was followed stepwise. The here listed steps are explained in more detail in the next passages.

- QuikChange®PCR for point mutation
- Template digestion with DpnI
- Transformation
- Mini prep
- Control restriction and sequencing
- Subcloning
- Transformation
- Maxi prep
- Sequencing

### 2.2.2.1.1 Quikchange® PCR

Based on the backbone pcDNA3.1 (+) barttin mCFP, primers were designed to generate a tryptophan codon at desired position. The entire vector is amplified with an intended mutation, introduced by PCR reaction with a pair of complementary primers. These primers used for QuikChange® (Stratagene) site directed mutagenesis are listed in Tab. 5. The mutated nucleotides are marked in bold letters. The mutated triplet was always substituted to 5'-TGG-3' (antisense 5'-CCA-3') coding for tryptophan.

Mutation	s/as	Primer sequence (5'-3')
I9W barttin mCFP	s	GAGAAGACCTTCCGGT <b>TGGGG</b> CTTCATTGTGCTG
	as	CAGCACAATGAAGCCCCACCGGAAGGTCTTCTC
G10W barttin mCFP	s	GAAGACCTTCCGGATCT <b>TGG</b> TTCATTGTGCTGGGG
	as	CCCCAGCACAATGAACCAGATCCGGAAGGTCTTC
F11W barttin mCFP	s	GACCTTCCGGATCGGCT <b>TGG</b> ATTGTGCTGGGGCTTTTC
	as	GAAAAGCCCCAGCACAATCCAGCCGATCCGGAAGGTC
I12W barttin mCFP	s	TTCCGGATCGGCTTCT <b>TGGG</b> TGCTGGGGCTTTT
	as	AAAAGCCCCAGCACCCAGAAGCCGATCCGGAA
V13W barttin mCFP	s	GGATCGGCTTCATT <b>TGG</b> CTGGGGCTTTTCC
	as	GGAAAAGCCCCAGCCAAATGAAGCCGATCC
L14W barttin mCFP	s	CGGCTTCATTGTGT <b>TGGGG</b> CTTTTCTGTC
	as	GCAGGAAAAGCCCCACACAATGAAGCCG
G15W barttin mCFP	s	GCTTCATTGTGCTGT <b>TGG</b> CTTTTCTGCTGG
	as	CCAGCAGGAAAAGCCACAGCACAATGAAGC
L16W barttin mCFP	s	TTCATTGTGCTGGGG <b>TGG</b> TTCCTGCTGGCCCT
	as	AGGGCCAGCAGGAACCACCCAGCACAATGAA
F17W barttin mCFP	s	TTCATTGTGCTGGGGCTT <b>TGG</b> CTGCTGGCCCTCGGTACGT
	as	ACGTACCGAGGGCCAGCAGCCAAAGCCCCAGCACAATGAA
L18W barttin mCFP	s	CATTGTGCTGGGGCTTTTCT <b>TGG</b> CTGGCCCTCGGTACGTTC
	as	GAACGTACCGAGGGCCAGCCAGAAAAGCCCCAGCACAATG
L19W barttin mCFP	s	ATTGTGCTGGGGCTTTTCTG <b>TGG</b> CCCTCGGTACGTTCTCA
	as	TGAGGAACGTACCGAGGGCCACAGGAAAAGCCCCAGCACAAT
A20W barttin mCFP	s	GGCTTTTCTGCTGT <b>TGG</b> CTCGGTACGTTCTC
	as	GAGGAACGTACCGAGCCACAGCAGGAAAAGCC
L21W barttin mCFP	s	CTTTTCTGCTGGCC <b>TGGG</b> TACGTTCTCATG
	as	CATGAGGAACGTACCCAGGCCAGCAGGAAAAG
G22W barttin mCFP	s	CTTTTCTGCTGGCCCT <b>TGG</b> ACGTTCTCATGAGCCATG
	as	CATGGCTCATGAGGAACGTCCAGAGGGCCAGCAGGAAAAG
T23W barttin mCFP	s	CTTTTCTGCTGGCCCTCGGT <b>TGG</b> TTCCTCATGAGCCATGATC
	as	GATCATGGCTCATGAGGAA <b>CCA</b> ACCGAGGGCCAGCAGGAAAAG
F24W barttin mCFP	s	CCTCGGTACGT <b>TGG</b> TTGATGAGCCATGATC
	as	GATCATGGCTCATCA <b>ACC</b> ACGTACCGAGG
L25W barttin mCFP	s	CCCTCGGTACGTTCT <b>TGG</b> ATGAGCCATGATCGG
	as	CCGATCATGGCTCATCCAGAACGTACCGAGGG
M26W barttin mCFP	s	CCTCGGTACGTTCTCT <b>TGG</b> AGCCATGATC
	as	GATCATGGCTCCAGAGGAACGTACCGAGG

G35W barttin mCFP	s	GGCCCCAGGTCTACT <b>TGG</b> ACCTTCTATGCCATG
	as	CATGGCATAGAAGGT <b>TCC</b> AGTAGACCTGGGGCC
T36W barttin mCFP	s	GATCGGCCCCAGGTCTACGGCT <b>TGG</b> TTCTATGCC
	as	GGCATAGA <b>ACC</b> AGCCGTAGACCTGGGGCCGATC
F37W barttin mCFP	s	GTCTACGGCACCT <b>TGG</b> TATGCCATGGGCAG
	as	CTGCCCATGGCATA <b>ACC</b> AGGTGCCGTAGAC
Y38W barttin mCFP	s	GGTCTACGGCACCTTCT <b>TGG</b> GCCATGGGCAGCGTCATG
	as	CATGACGCTGCCCATGG <b>CCC</b> AGAAGGTGCCGTAGACC
A39W barttin mCFP	s	GTCTACGGCACCTTCTAT <b>TGG</b> ATGGGCAGCGTCATGGTG
	as	CACCATGACGCTGCCCAT <b>CCA</b> ATAGAAGGTGCCGTAGAC
M40W barttin mCFP	s	CTACGGCACCTTCTATGCC <b>TGG</b> GCAGCGTCATGGTGATC
	as	GATCACCATGACGCTGCC <b>CCC</b> AGGCATAGAAGGTGCCGTAG
G41W barttin mCFP	s	GCACCTTCTATGCCAT <b>TGG</b> AGCGTCATGGTGATCG
	as	CGATCACCATGACGCT <b>CC</b> ACATGGCATAGAAGGTGC
S42W barttin mCFP	s	CACCTTCTATGCCATGGGCT <b>TGG</b> TCATGGTGATCGG
	as	CCGATCACCATGAC <b>CCC</b> AGCCCATGGCATAGAAGGTG
V43W barttin mCFP	s	CTTCTATGCCATGGGCAG <b>TGG</b> ATGGTGATCGGGGGCATC
	as	GATGCC <b>CCC</b> GATCACCAT <b>CC</b> AGCTGCCCATGGCATAGAAG
M44W barttin mCFP	s	GGGCAGCGT <b>TGG</b> GTGATCGGGGGCATCATCTG
	as	CAGATGATGCC <b>CCC</b> GATC <b>ACC</b> AGACGCTGCC
V45W barttin mCFP	s	CAGCGTCAT <b>TGG</b> ATCGGGGGCATCATCTG
	as	CAGATGATGCC <b>CCC</b> GAT <b>CC</b> ACATGACGCTG
I46W barttin mCFP	s	CATGGGCAGCGTCATGGT <b>TGG</b> GGGGGCATCATCTG
	as	CAGATGATGCC <b>CCC</b> ACACCATGACGCTGCCATG
G47W barttin mCFP	s	GCGTCATGGTGAT <b>TGG</b> GCATCATCTGG
	as	CCAGATGATGCC <b>CCC</b> GATCACCATGACGC
G48W barttin mCFP	s	CGTCATGGTGATCGGG <b>TGG</b> ATCATCTGGAGCATG
	as	CATGCTCCAGATGAT <b>CC</b> ACCCGATCACCATGACG
I49W barttin mCFP	s	GTCATGGTGATCGGGGG <b>TGG</b> ATCTGGAGCATGTG
	as	CACATGCTCCAGAT <b>CC</b> AGCCCCGATCACCATGAC
I50W barttin mCFP	s	GTCATGGTGATCGGGGGCAT <b>TGG</b> TGGAGCATGTGCCAGTGCTAC
	as	GTAGCACTGGCACATGCT <b>CC</b> ACCAGATGCC <b>CCC</b> GATCACCATGAC
S52W barttin mCFP	s	GGGGCATCATCTGG <b>TGG</b> ATGTGCCAGTGCTAC
	as	GTAGCACTGGCACAT <b>CC</b> ACCAGATGATGCC <b>CCC</b>
M53W barttin mCFP	s	CATCATCTGGAG <b>TGG</b> TGCCAGTGCTACC
	as	GGTAGCACTGG <b>CA</b> CCAGCTCCAGATGATG
C54W barttin mCFP	s	CATCTGGAGCAT <b>TGG</b> CAGTGCTACCCCAAG
	as	CTTGGGGTAGCACT <b>GCC</b> ACATGCTCCAGATG
Q55W barttin mCFP	s	CATCTGGAGCATGTG <b>TGG</b> TGCTACCCCAAGATC
	as	GATCTGGGGTAG <b>CA</b> CCAGCACATGCTCCAGATG

**Tab.5 List of primers designed for Quikchange® (Stratagene) site directed mutagenesis**

In the left column, the introduced substitution is noted followed by the sense (s) and the antisense primer sequence(as). Both are given in 5'-3'-orientation. The template BSND gene is harbored in the pcDNA3.1(+) vector. The triplet coding for the amino acids that is substituted to tryptophan is marked in bold letters TGG.

PCR reactions were performed as recommended by manufacturer of the kit (Stratagene, Quikchange©PCR Kit) and indicated in Tab.3+4.

#### **2.2.2.1.2 *DpnI* digestion**

After the Quikchange® PCR (step 2.2.2.1.1), the sample is incubated for 20 min at 37 °C with DpnI, a restriction enzyme which cuts only methylated DNA. This is only the case for the in bacteria generated template vector, but not the PCR product. This step is needed to avoid transformation of unchanged vectors.

Before transformation, the cleared PCR product was checked for size in agarose gel electrophoresis. After transformation, the PCR product is sequenced, subcloned and again sequenced.

#### **2.2.2.1.3 *Agarose gel electrophoresis***

2 % (w/v) agarose (Invitrogen) is dissolved in 1x TAE buffer (400 mM TRIS, 200 mM acetic acid, 10 mM EDTA) with 0.005 % (v/v) ethidiumbromide or 0.01 % (v/v) SYBR®safe at 60 °C and poured into the gel chamber. Both intercalating agents can be visualized with UV-light in a Gel-Doc. DNA ladder mix was loaded as size marker. The gels were run for one hour at 20 V.

#### **2.2.2.1.4 *DNA purification – gel extraction***

Plasmids or PCR fragments are extracted of agarose gels with Quiagen® Gel Extraction Kit following manufacturers' instruction. After gel extraction and before transformation, the concentration of the vector-DNA is measured photometrically.

#### **2.2.2.1.5 *Competent cells***

*E.coli* cells (DH5- $\alpha$ ) are made competent chemically according to Sambrook and Russell (2006). 100 ml antibiotic-free LB-Medium was incubated with cells until the optical density reached values of  $OD_{600} \approx 0.5 - 0.6$ . After centrifugation (10 min, 3000 g, 4°C), the cells are

resuspended in 60 ml TFB I buffer and incubated on ice for 20-90 min. A second centrifugation step (10 min, 3000 g, 4°C) is followed by resuspension of the cells in 8 ml TBF II buffer. Aliquots of 200 µl are taken and frozen in nitrogen. Tab.6 shows the ingredients of the two used buffers.

Composition	TBF I buffer	TBF II buffer
RbCl	100 mM	10 mM
MnCl <sub>2</sub> x 2 H <sub>2</sub> O	50 mM	---
CH <sub>3</sub> CO <sub>2</sub> K	30 mM	---
CaCl <sub>2</sub> x 2 H <sub>2</sub> O	10 mM	75 mM
Glycerin (99.9 %)	15 % (v/v)	15 % (v/v)
MOPS	---	10 mM
pH	5.8	8.0

**Tab.6 Composition of buffers**

Two buffers are needed for chemical generation of competent DH5-α cells.

### ***2.2.2.1.6 Growth of transformed bacteria in LB-medium/ on LB-Agar plates***

Transformed bacteria are plated on LB-agar plates. After 14 hours of incubation at 37 °C, colonies are picked and further incubated in LB medium before plasmid recovery. LB-medium contains Bacto-yeast extract (5 g/L), NaCl (10g/L) and Bacto-tryptone (10 g/L). The medium is autoclaved at 121 °C for 20 min.

For LB-Agar plates, Bacto-Agar is added to the LB-medium to a final concentration of 20 g/L. After sterilization in an autoclave and cooling down to approximately 60 °C, the LB-agar can be inoculated with ampicillin (100 µg/ml) and poured into dishes.

### ***2.2.2.1.7 Transformation***

For transformation, 40 µl of competent DH5-α cell suspension were mixed with 4-10 ng of DNA of step 2.2.2.1.4, and kept for 20 min at 42 °C. After 2 min on ice, 300 µl SOC-medium was added, follow by a 45 min incubation period at 37 °C while shaking.

SOC-medium contains

- 2 % bacto-tryptone
- 0.5 % bacto-yeast extract
- 10 mM NaCl
- 2.5 mM KCl

After sterilization, MgCl<sub>2</sub> and glucose are added to a final concentration of 20 mM. pH is set to 7.0. SOC-medium contains no antibiotics.

After incubation, the cells are spun down (1 min, 800 x g). 260 µl of medium are discarded leaving 40 µl medium in the eppendorf tube. The cells are resuspended before plating on LB-agar. The presence of ampicillin in the LB-agar and the ampicillin resistance gene on the vector allows selection of transformed cells. Plates are incubated at 37 °C for 16-20 hours. Colonies are picked and incubated in 5 or 200 ml LB-medium in presence of ampicillin for Mini or Maxi preparation. Amplified vectors are isolated with Quiagen Kits for plasmid recovery.

#### ***2.2.2.1.8 Vector recovery***

For vector recovery, Quiagen® Kits are used. Depending on the culture volume, Mini Preparation Kit or HiSpeed Plasmid Maxi Kits are used following manufacturers instruction. The concentrations of the purified vectors are either measured with the Nanodrop photometer or calculated densitometrically.

#### ***2.2.2.1.9 Glycerol stock***

For long time storage, an aliquot of every transformed bacterial culture is taken. Therefore, equal volumes of cultured LB medium and 50 % glycerol are mixed and frozen in liquid nitrogen before storage at -80 °C. Depending on the volume of culture medium 100 µl or 500 µl of inoculated LB medium are taken.

#### ***2.2.2.1.10 Control restriction***

After vector recovery, size and quality is checked by cutting 1.5 µg of the vector with restriction enzymes. Ideally, a restriction site is introduced or deleted by PCR. This alteration results in different band patterns after enzymatic restriction and agarose gel electrophoresis

compared to template vector. However, this was the exception within the here performed Quikchange© PCRs. Only vectors of correct size and restriction pattern were sequenced.

#### **2.2.2.1.11 Sequencing**

Sequencing PCRs are performed by GATC (Lindau/Düsseldorf).

#### **2.2.2.1.12 Subcloning**

Sequenced fragments of vector are subcloned. This means that the DNA of the mini or maxi preparation (2.2.2.1.8) is restricted within the sequence provided of GATC and cloned into the template vector. By doing so, replication errors are minimized.

DNA restriction was always performed with two single cutting enzymes (most often AgeI and NheI). Sticky end restriction allows control of orientation of the insert. Restriction results in two fragments – one sequenced fragment which bears the mutation, and the rest of this amplified vector lacking this fragment. Same restriction is performed with the template vector that was already sequenced entirely. Before ligation of template vector and mutated DNA, the fragments are separated by agarose electrophoresis. DNA-gel extraction and ligation are described in following.

#### **2.2.2.1.13 Ligation**

T4 DNA ligase (Fermentas) is used to ligate DNA fragments according to manufacturers' instruction. In molar ratio, three DNA fragments of the insert are mixed with one fragment of template vector, ATP containing buffer and T4 DNA ligase and incubated for 20 minutes at 37 °C. Transformation and plasmid recovery completes the Quikchange© protocol. In this study, only sticky end ligation was performed.

For the calculation of the mass of the insert, we used following equation for 3:1 stoichiometry:

$$m(\text{insert}) = m(\text{vector}) \times \frac{3}{1} \times \text{size}(\text{insert/vector}) \quad (\text{eq.1})$$



### 2.2.2.2 Side overlap extension PCR (SOE-PCR)

SOE-PCR strategies are performed to fuse two proteins on DNA level. Concatenated proteins should ensure a 1:1 stoichiometry. To guarantee an open reading frame coding for the fusion protein, the stop codon of the first protein needs to be mutated. Another important aspect is the finding of an appropriate linker sequence, coding for a peptide long enough to allow typical protein-protein interaction. This linker must not lead to a frame shift. Here, SOE-PCR was performed to link barttin to the N-terminus of CIC-K channels.

SOE-PCR was also performed to generate chimeras. The B- and/or J-helices of CIC-K1 and CIC-2 were exchanged in order to validate the binding of barttin to these domains. Therefore, the linker sequence of the SOE-PCR is the sequence of the corresponding helix.

#### 2.2.2.2.1 Covalent link of barttin to rCIC-K1 and V166E rCIC-K1

Barttin was covalently linked to the N-terminus of rCIC-K1, respective V166E rCIC-K1 with a PCR strategy depicted in Fig.7.

As templates, pcDNA3.1 (+) barttin and pSVL (V166E) rCIC-K1 IRES CD8 were used for SOE-PCR. The sequence of barttin was modified in two aspects. The stop codon was mutated from TGA to TGG resulting in non-stop barttin. Additionally, the sequence was C-terminally

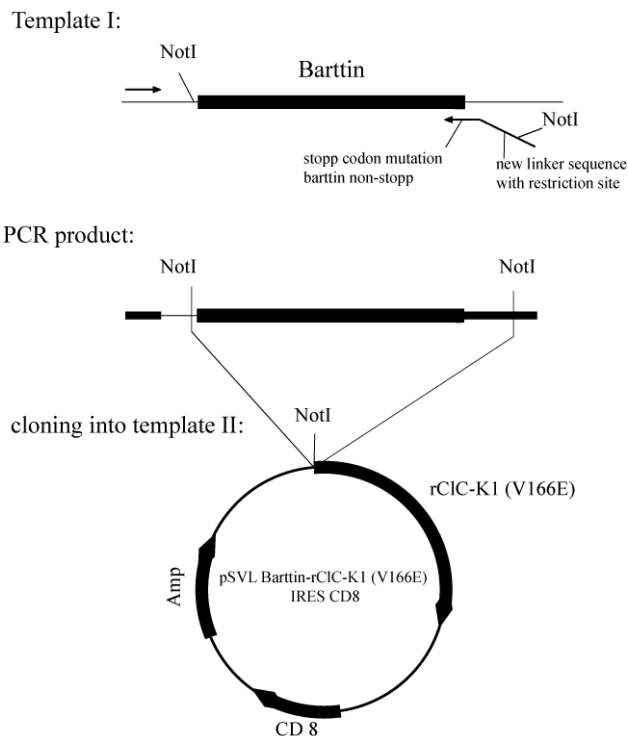


**Fig.7 Scheme of SOE-PCR**

For covalent linkage of barttin to V166E rCIC-K1 on genetic level, two primers are needed. One primer binds to the template with its full length. Here, the forward primer bound to the vector upstream the gene encoding for barttin as a start for amplification. The second primer fulfills several tasks. For C-terminal elongation of barttin, the stop codon is mutated to tryptophan. Therefore a point mutation in the complementary part of the reverse primer is generated. This primer additionally encodes a peptide linker carrying a restriction site for the subcloning into the host vector. Frame shift must not occur by the introduction of the linker. The second gene, here coding for (V166E) rCIC-K1 must be within the same reading frame starting with ATG of the first protein.

elongated with the desired linker sequence. Both tasks were managed by the antisense primer. A restriction site (NotI) was introduced in the linker sequence for further cloning into the host vector.

In Tab.7, the primers are listed. The mutated stop codon and the linker sequence are marked in bold letters.

fw within pcDNA3.1(+)	s	5'-GCAGAGCTCTCTGGCT-3'
rev barttin nonstop and linker sequence with restriction site	as	5'-TGCAGCGGCCGCT <b>CCACTCCATCTAGACGG</b> <b>AGCACAAACATCCCAGCCTTGGGTGCAG</b> -3'

**Tab.7 Primers used for concatenation of barttin and (V166E) rCIC-K1**  
Mutated stop codon and new linker sequence is marked with bold italic letters

The SOE-PCR product of extended barttin was restricted with NotI for 30 min at 37 °C. Agarose gel electrophoresis yielded in purified DNA fragment, which was ligated into linearised pSVL vector (pSVL rCIC-K1 IRES CD8, resp. pSVL rCIC-K1 V166E IRES CD8). Transformation, colony picking, plasmid recovery and sequencing were performed as described.

#### 2.2.2.2.2 N-terminal link of the concatamers with mYFP (Quikchange)

For easier detection, the built concatamers were N-terminally labeled with mYFP with Quikchange® strategy. The stop codon of the mYFP coding gene was mutated to TGG and at the N-terminus of the concatamer coding gene, an additional AgeI-restriction site was introduced by a point mutation. Cloning in into pSVL concatamers barttin-(V166E) rCIC-K1 IRES CD8 resulted in N-terminally mYFP-labeled concatamer mYFP-barttin-(V166E) rCIC-K1. The primers used for this PCR reaction are given in Tab.8.

fw primer mYFP stopp mutation	s	5'-CGAGCTGTACAAGTTTAAAGCGGCCGCTC-3'
rev primer mYFP stopp mutation	as	5'-GAGCGGCCGCTTTAAACTTGTACAGCTCG-3'
fw primer concatamer N-terminus AgeI introduction	s	5'-CTGCTCTAAACCGGTTCGATCCCTCGAG-3'
rev primer concatamer N-terminus AgeI introduction	as	5'-CTCGAGGGATCGAACCGGTTTAGAGCAG-3'

**Tab.8 Primers used for tagging YFP to concatamers**

Two PCR reactions were performed. In a first PCR step reaction, the stop codon of mYFP is mutated to enable N-terminal labeling of the concatamers with mYFP in one open reading frame. For cloning in the mutated reporter gene, an additional restriction site within the vector coding for the concatamer is needed and introduced by indicated primers.

### 2.2.2.2.3 Generation of CIC-2 and V166E rCIC-K1 chimera (SOE-PCR)

Chimaeric channels are built for validation of barttin binding to the B- and/or J-helix. Substitutions of B- and J-helix of CIC-2 with the ones of CIC-K are expected to be a good tool to determine binding of barttin. For helix substitution, following three-step SOE-PCR strategy was used and sketched in fig.8. The three small boxes mark the initial PCRs (PCR1, PCR2 and PCR3 in Fig.8) and the grey box illustrates the second step in which two PCR products are combined (PCR4). Terminally, the product of PCR3 is added to the already combined DNA fragment (big black box, PCR5).

There here used variation of the general PCR protocol that was run is listed in Tab.9.

In one of the initial PCRs (PCR1), a helix sequence of the donor gene (black intermission in grey bar) is amplified with appropriate primers a+b, shown in Tab.10. In the two other initial PCRs, the future host gene (white bar) is amplified upstream (PCR 2, primer c+d) and downstream of the helix (PCR 3, primer e+f) that is to be substituted with extended primers. These three PCR products are combined stepwise in two further PCR reactions.

In PCR4 (grey box), the PCR products 1 and 2 are mixed with primers c and b. The product of PCR4 is linked to the PCR3 product with primers c and f and boxed as PCR5.

This PCR product was cloned in the host gene vector with appropriate restriction enzymes and ligation methods. The PCR products all were purified and checked for size in agarose gels.

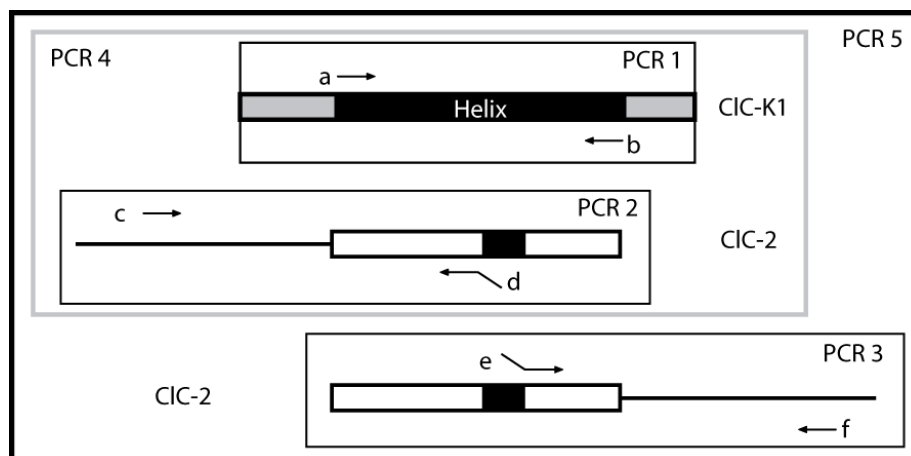


**Fig.8 Scheme of PCR reaction needed for helix substitution between rCIC-K1 and CIC-2**

Bars (grey: CIC-K1, white: CIC-2) represent the genes with the sequences of a helix indicated in black. Five PCRs (PCR 1-5) are needed together with six primers (a-f). PCR 1 amplifies the helix to be substituted (black bar) without any other parts of the donor gene (grey bar). PCR 2+3 amplify helix-corresponding upstream (PCR 2) and downstream (PCR 3) regions of the future host gene (white bar). PCR 2 and 3 are performed with overlapping primers, whereas the overlap is complementary to the helix to be introduced (PCR 1 product). Two PCR products serve as template in further PCRs. PCR 4 combines PCR products 1 and 2 by a PCR with primers c and b. In PCR 5, this upstream prolonged helix (PCR 4 product) is further combined with PCR 3 product by a PCR with primers c and f. PCR product 5 can now be cloned in the template host gene vector, here CIC-2, with appropriate restriction enzymes.

PCR-Program:

PCR-Step	Temperatur (°C)	Duration (sec)
1 initial denaturation	94	120
2 denaturation	94	10
3 annealing	52	70
4 elongation	72	330
5 denaturation	94	15
6 annealing	52	30
7 elongation	72	330
8 terminal elongation	72	420
9 end/storage	4	infinite

**Tab.9 PCR program**

Initial denaturation was followed by 10 cycles of 10 sec denaturation, 70 sec annealing and 5.5 min elongation (steps 2-4). Additional 20 cycles of steps 5-7 as indicated were performed for amplification. Terminal elongation and storage ended the PCR program.

<b>a</b> Helix B CIC-K1 s	GACTGGCACTTCCTGGTGGC
<b>b</b> Helix B CIC-K1 as	CCGGTATAGCCATTTGTGTGCTC
<b>c</b> Helix B downstream CIC-K1 in CIC-2 s	<b>CACAAATGGCTATAACGGG</b> GGCTTGAACACCAGCATCTTG
<b>d</b> Helix B downstream CIC-K1 in CIC-2 as	GCCAGCATCTCTGTGTCCG
<b>e</b> Helix B upstream CIC-K1 in CIC-2 s	GAGCAAAGACCCCAACGAGAAG
<b>f</b> Helix B upstream CIC-K1 in CIC-2 as	<b>CCACCAGGAAGTGCCAGTC</b> TTACCAACCTGGATACTAGGAAC
<b>a</b> Helix J CIC-K1 s	GACCTGCCTGAAATCTTCTTCTTG
<b>b</b> Helix J CIC-K1 as	CAACAGTCTGGAGGTGTACCGATTG
<b>c</b> Helix J downstream CIC-K1 in CIC-2 s	<b>GTACACCTCCAGACTGTTG</b> ATGAGGAAACGCCTGCTCTTC
<b>d</b> Helix J downstream CIC-K1 in CIC-2 as	CAGGCACAATCCGGTAGGTG
<b>e</b> Helix J upstream CIC-K1 in CIC-2 s	CATTGGGCTGACCTGCGC
<b>f</b> Helix J upstream CIC-K1 in CIC-2 as	<b>GAAGATTCAGGCAGGTC</b> AAAGGGGAAGTCGAGCCGG
<b>a</b> Helix B CIC-2 s	GATTGGATCTTCTGGTCCTG
<b>b</b> Helix B CIC-2 as	CCGGGACATCCACTGCTGAG
<b>c</b> Helix B downstream CIC-2 in CIC-K1 s	<b>CAGCAGTGGATGTCCGG</b> GAGGTTGGGGACGCCAC
<b>d</b> Helix B downstream CIC-2 in CIC-K1 as	GTAGATGGAGGTGATGGTCTCCTG
<b>e</b> Helix B upstream CIC-2 in CIC-K1 s	GGTCCTGCTGGAGTTCGTGAC
<b>f</b> Helix B upstream CIC-2 in CIC-K1 as	<b>CCAGGAAGATCCAATC</b> CTCACCCACACGGAACAACC
<b>a</b> Helix J CIC-2 s	GACCTGCAGGAGCTGCCAG
<b>b</b> Helix J CIC-2 as	GAGGAAGCGATTGATGGTTTTTC
<b>c</b> Helix J downstream CIC-2 in CIC-K1 s	<b>CCATCAATCGTTCCTC</b> CGCTACAAGCAAGCCGTCCTACG
<b>d</b> Helix J downstream CIC-2 in CIC-K1 as	GCCATCAGCACAGGCAGTGC
<b>e</b> Helix J upstream CIC-2 in CIC-K1 s	GCTTCTCGCAGAGCATCTCACC
<b>f</b> Helix J upstream CIC-2 in CIC-K1 as	<b>GGCTGGCAGCTCCTGCAGGTC</b> AAAGGGCACATCCACTCGG

**Tab.10 List of primers used for generation of chimeric channels**

B- and J-helices of CIC-K channels are supposed to bind barttin. These helices are exchanged by the corresponding domains of CIC-2 and vice versa. Here, four groups of primers are built each containing six primers (a-f). The first group is needed for building CIC-2 with B-helix of CIC-K. CIC-2 with the J-helix of CIC-K is generated with the second group of primers. The third and fourth group facilitate the generation of chimeric channels with the backbone of CIC-K and the B-/J-helix of CIC-2. All primers are given in 5'-3' orientation and the SOE-sequences marked in bold italic letters.

## **2.2.3 Cell culture**

### **2.2.3.1 Cell lines**

Due to different tasks, several cell types are used. The here used cell lines are described in following passages.

#### ***2.2.3.1.1 MDCKII for confocal microscopy and biotinylation assay***

This cell line is derived by S.H. Madin and N.B. Darby from the kidney tissue (distal tubule or collecting duct) of an adult female cocker spaniel in 1958. Main feature is their polarized epithelia. They shelter an extracellular matrix at the basal lamina for adhesion to adjacent tissues. This extracellular matrix makes these cells very hard or even unable to patch. This cell line is commonly used as a general model for epithelial cells, especially to investigate the sorting of proteins. (HAMAMATSU.COM)

#### ***2.2.3.1.2 HEK293T for electrophysiology***

This cell line is derived from human embrionic kidney (HEK) cells from a healthy aborted fetus. It was cultured by Graham and van der Eb in the 1970s. F.Graham, inventor of the calcium-phosphat precipitation method for transfection, and co-workers (1977) succeeded in his 293<sup>rd</sup> experiment to transform HEK cells with sheared fragments of adenovirus 5 DNA (hence HEK293). Later on, simian virus 40 DNA was transformed. These cells constitutively express SV40 large T antigen for higher transfectability, but moreover this antigen can bind to promoter sequences for higher expression.

Cells need nutrients to grow. MDCKII and HEK293T cells are cultured and transfected in DMEM (Dulbecco modified eagle medium) containing 10 % FBS, 200 µM L-Glutamine and in presence of penicillin (50 U/ml) and streptomycin (50 µg/ml).

### **2.2.3.1.3 *Flp-in*<sup>TM</sup> T-REx for stable cell lines**

This cell line is designed for rapid generation of stable cell lines that ensure stable expression of a certain protein. In a transcriptional active genomic locus, a recombinase site (Flp) allows targeted integration of a gene of interest. For integration, a designed Flp-In<sup>TM</sup> expression vector, here pcDNA<sup>TM</sup>5/FRT/TO, is co-transfected with Flp recombinase vector, here pOG44. The FRT (flippase recognition target) coding vector is then inserted into the Flp site within the host cell genom.

The basal medium consists of DMEM, 10 % FBS and L-glutamine. The expression of the inserted protein is under the control of a tetracycline promoter. Therefore, tetracycline-free FBS must be purchased. 0.1 % (v/v) zeocin and 0.15 % (v/v) blasticidin are recommended for cultivation of untransfected cells. The zeocin resistance gene lies within the Flp site and is interrupted upon gene insertion. Therefore, the medium for transfection contains only blasticidin. The vector encodes a hygromycin resistance gene. So, successful transfection can be checked by addition of 0.2 % (v/v) of hygromycin to the medium. Picking of single colonies and further passaging in selecting medium was performed several times (4-8 times) before the cells were frozen in liquid nitrogen for long time storage.

### **2.2.3.2 Splitting**

Cells grown in 10 cm dishes are washed with PBS. 3 ml trypsin-EDTA (Gibco) is added until the cells detached. Harsh pipetting with a transfer pipette separates the cells. Air bubbles are avoided as good as possible. Addition of 7 ml medium inactivates the trypsin reaction, because of neutralization of the pH. The desired amounts of cells are transferred to a new dish, prefilled with 10 ml culture medium.

### **2.2.3.3 Transfection**

DNA cannot pass the plasma membrane, because of size and charge. Here, two different protocols were performed to transfect cells with the desired DNA. Ca<sub>2</sub>PO<sub>3</sub>-precipitation is a cheap method used for the transfection of HEK293T and Flp-in<sup>TM</sup> T-Rex cells. MDCKII cells

cannot be transfected with this method. Therefore, transfection with Lipofectamin™2000 was performed.

#### **2.2.3.3.1 $Ca_2PO_3$ -precipitation**

The calcium phosphate precipitation method was first described by Graham and van der Eb (1973). DNA coprecipitates with calcium phosphate on a monolayer of cells which take up the DNA by an unsolved mechanism. The desired amount of plasmid DNA is diluted in 10 µl salmon sperm and 500 µl 100 mM  $CaCl_2$ . This mix is added dropwise to 2x HEBS solution (274 mM NaCl, 40 mM Hepes, 12 mM dextrose, 10 mM KCl, 1.4 mM  $Na_2HPO_4$ ) and mixed thoroughly. After 20-30 minutes at RT, the mix is added dropwise to 80 % confluent cells with 10 ml medium while shaking the 10 cm dish.

#### **2.2.3.3.2 Lipofectamin™ 2000**

MDCKII cells were transfected with Lipofectamin™ 2000 according to manufacturers' instructions. 80 % confluency of cells was attained. The desired amount of DNA is diluted in OptiMEM. Lipofectamin™ is diluted in OptiMEM, too. After 5 minutes, the DNA-containing mix is added dropwise to the Lipofectamin-mix while mixing thoroughly after each drop. After 30-60 min incubation at RT, the mix is given to the cells in standard culture medium. For confocal microscopy, cells were grown in Ibidi 35µm high dishes. For biotinylation assay, 10 cm dishes were used for culturing MDCKII cells.

#### **2.2.3.4 Freezing cells**

Cultured cells can be stored for long time at -80 °C. For that purpose, the cells are washed with PBS in a dish. Addition of 3 ml trypsin-EDTA detaches the cells. Trypsin is inactivated by addition of 7 ml medium. The cells are spun down (3 min, 1500 rpm, the supernatant is discarded) and resuspended in 3 ml MEM containing 20 % FBS. Aliquots à 0.5 or 0.75 ml are taken and mixed with same volume of MEM containing 20 % FBS and 33 % (v/v) DMSO (di-methyl-sulf-oxid). In a Nunc-box, the cells are slowly cooled down to -80 °C.

### **2.2.3.5 Thawing cells**

Frozen cells are thawed at room temperature. Washing of cells is recommended to get rid of dispensable DMSO. Therefore, cells are spun down (5 min, 800 rpm) and resuspended in standard culture medium for at least one time before transferring the cells into a culture dish.

### **2.2.4 Electrophysiology**

We used standard whole cell patch clamp techniques as described by Sakmann and Neher in 1984. Two electrodes as references record the potential between the interior and exterior of the cell. The quality of the Gigaseal was checked with a test pulse of 5 mV for 10 ms. Spikes at the beginning and end of the test pulse before and after opening of the cell were compensated by an analog procedure to minimize voltage errors due to capacitances of the pipette, respective cell. By application of voltages to the interior of the cell, the voltage dependence of over-expressed channels is displayed by the resulting current measured with a feedback amplifier.

#### **2.2.4.1 Setup**

All patch clamp recordings were digitized by Digidata 1440 and amplified by an Axopatch 200B. We used the pClamp 8-10 software for recordings in combination with Excel and SigmaPlot for data analysis. A Leica inverted microscope was placed on a shock dampened table (TMC, Peabody, USA). The setup was protected against electrical radiation by a Faraday cage. A piezoelectric micromanipulator (SM-1, Luigs & Neumann, Ratingen) was used to move the pipette to the cell.

#### **2.2.4.2 Pipettes and electrodes**

Pipettes were pulled from borosilicate glass capillaries (Harvard apparatus) with a micropipette puller (Sutter instruments). Heat polish of the pipettes with a microforge (MF-



830, Narishige Japan) smoothed the edges. The opening tip of the pipettes had diameters of about 5  $\mu\text{m}$ , resulting in resistances of 1-2.2  $\text{M}\Omega$ . For stationary noise analysis the pipettes were covered with dental wax (Moyco) to reduce their capacitance. Therefore the pipettes were pulled, polished, waxed and again polished.

Silver wires were used as electrodes. These were chlorinated with hypochloric acid.

### **2.2.4.3 Preparation of cells**

HEK293T and Flp-In T-Rex cells were used for whole cell patch clamp recordings. For transfection of HEK293T cells, the calcium phosphat precipitation protocol was chosen as described above. 2  $\mu\text{g}$  pcDNA3.1 (-) YFP hClC-Ka, 2  $\mu\text{g}$  pRcCMV YFP V166E rClC-K1 or 4  $\mu\text{g}$  of pcDNA3.1 (+) XX barttin mCFP (XX = WT or mutation, e.g. G10W) were transfected.

When hClC-Ka was expressed, 12 hours after transfection the cells were splitted. After additional three hours, patch clamp recording started. When V166E rClC-K1 was expressed, splitting took place after 24 hours. 36h after transfection, patch clamp recordings started.

Flp-In T-Rex cells were stable transfected as described (1.5.1.3) and splitted 12 hours before patch clamp recordings.

The cells are washed three times with 5 ml bath solution before having 5 ml bath solution in a 6 cm dish.

### **2.2.4.4 Solutions**

Extracellular solution contained (in mM): NaCl (140), KCl (4),  $\text{CaCl}_2$  (2),  $\text{MgCl}_2$  (1), HEPES (5), pH 7.4; intracellular solution contained (in mM): NaCl (120),  $\text{MgCl}_2$  (2), EGTA (5), HEPES (10), pH 7.4. Chloride is the only anion present with almost symmetrical distribution. Nernst-equation results in a chloride reversal potential of -4.8 mV at room temperature (22°C). After splitting the cells in 6 cm dishes containing 3 ml medium and at least 3 hours incubation at 37 °C, the cells were washed 3x with 5 ml extracellular solution, before adding 5 ml of the same solution for whole cell patch clamp recordings.

### 2.2.4.5 Determination of relative open probabilities and times constants of activation

In this study we investigated human and rodent ClC chloride channels. To determine the voltage dependencies of the channel, a voltage protocol is used. First, voltage steps between -155 and +125 mV were applied followed by a test pulse to -125 mV. For activation curves, the current amplitudes at the beginning of the tail pulse are plotted versus the applied voltage. Fitting this data with Boltzmann functions (eq.2) and normalizing the activation curves to the maximum of the fit results in relative open probabilities of the channels.

$$I(V) = I_{\min} + \frac{I_{\max} - I_{\min}}{1 + e^{\frac{z_d F}{RT} (V - V_{0.5})}} \quad (\text{eq.2})$$

In eq.2,  $V_{0.5}$  corresponds to the voltage of half-maximal activation. The current amplitude at certain voltages  $V$  can be estimated, as well as the minimal  $I_{\min}$  and maximal  $I_{\max}$  amplitude at very negative or positive potentials. The activation curves are now normalized to  $I_{\max}$  to obtain relative open probabilities of the channel  $p_{\text{channel}}$ .

As mentioned in the introduction, ClC channels are organized as dimers consisting of two protopores which are under the control of a fast protopore gate and a slow common gate. These gates are assumed to move independently and can be separated by a short interpulse of 5 msec to +180 mV prior to the test pulse. The instantaneous test pulse current amplitude is then only dependent on the steady state slow gate open probability  $p_{\text{slow gate}}$  that has been reached during the long prepulses of varying potentials. Same fitting procedure like before is used to obtain  $p_{\text{slow gate}}$ . Then, the open probability of the fast gate  $p_{\text{fast gate}}$  can be calculated by dividing the total channel open probability  $p_{\text{channel}}$  by its slow gate open probability  $p_{\text{slow gate}}$ :

$$P_{\text{fastgate}} = \frac{P_{\text{channel}}}{P_{\text{slowgate}}} \quad (\text{eq.3})$$

For normalization, the calculated activation curve of the fast gate is fitted with Boltzmann functions analog to the fitting procedure mentioned above. For that purpose,  $I_{\max}$  and  $I_{\min}$  are substituted by  $p_{\max}$  and  $p_{\min}$  in eq.2.

$$p(V) = p_{\min} + \frac{p_{\max} - p_{\min}}{1 + e^{\frac{z_d F}{RT} (V - V_{0.5})}} \quad (\text{eq.4})$$

$P_{\text{channel}}$  is now recalculated by multiplication of  $p_{\text{fast gate}}$  and  $p_{\text{slow gate}}$ .

To determine the time course of activation  $\tau$ , whole cell current recordings at +125 mV were fitted with a mono-exponential function:

$$\tau(t) = \Delta I \times e^{\frac{-t}{\tau}} + I_{\max} \quad (\text{eq.5})$$

In this study,  $\tau$  is the elapsed time until 63.2 % of  $\Delta I$  is reached after a stimulus of a certain voltage.

#### 2.2.4.6 Noise analysis

Here we performed stationary noise analysis of HEK293T cells coexpressing hClC-Ka together with barttin in order to receive single channel conductance, absolute open probabilities and the number of active channels in the plasma membrane. All recordings were filtered with a 10 kHz low pass Bessel filter. Noise analysis could be performed due to a dramatic increase in current variance upon hyperpolarization. This flickering is caused by statistical closure and reopening of some channels in the membrane. The highest variance can be observed, when the open probability of the channel is at 50 %. Then spontaneous opening and closing of the channel occurs with highest probability.

The macroscopic current ( $I$ ) is the product of the number of channels ( $N$ ), single channel amplitude ( $i$ ) and the single channel open probability ( $p_o$ ):

$$I = N \times i \times p_o \quad (\text{eq.6})$$

Current variance ( $\sigma^2$ ) is related to the single-channel properties as:

$$\sigma^2 = i \times I - \frac{I^2}{N} \quad (\text{eq.7})$$

It is assumed that the single channel conductance and the number of channels do not change during measurement. Background noise was subtracted. Plotting the variance, normalized by the product of the mean current ( $I$ ) and the electrical driving force ( $V - V_r$ ), versus the macroscopic conductance  $\frac{I}{V - V_r}$  leads to a linear regression of data point, whereas the slope is the negative reciprocal number of channels.

$$\frac{\sigma^2}{I \times (V - V_r)} = \frac{i}{V - V_r} - \frac{1}{N} \times \frac{I}{V - V_r} \quad (\text{eq.8})$$

$-\frac{1}{N}$  equals the slope, whereas  $\frac{i}{V - V_r}$  is the y-axis intercept of the linear regression corresponding to single channel conductance. The x-axis intercept is the maximum conductance of the whole cell. Normalization of conductance levels by maximum conductance and plotting versus applied voltage results in absolute open probabilities.

### **2.2.5 Confocal imaging**

Live cell confocal imaging was carried out with MDCK II cells on a Leica DM IRB inverted microscope with a TCS SP2 AOBS scan head. Subcellular distribution of barttin-mCFP was investigated using 405 nm excitation wavelength and fluorescence detection within the range of 450-500 nm. Excitation wavelength at 514 nm and fluorescence detection at 520-600 nm was used to study the distribution of YFP-CIC-Ka channels.

MDCKII cells were transfected with the Lipofectamin™ protocol (see 2.2.3.3.2). 0.8 µg pcDNA3.1 (-) YFP-hCIC-Ka and 1.2 µg pcDNA3.1 (+) XX barttin mCFP (XX = WT or mutation, e.g. I9W) were cotransfected in corresponding OptiMEM (2x100 µl) and Lipofectamin (4 µl) concentrations and 1 ml of culture medium in the Ibidi dishes. The culture medium was renewed after 20 hours. 48 hours after transfection, the imaging started.

### **2.2.6 Protein biochemistry**

Barttin is the functional subunit of CIC-K channels. One of the tasks of barttin is to facilitate enhanced membrane insertion of the channel proteins. This can be quantified by biotinylation assay. Therefore, a ratio of surface membrane exposed and expressed protein is built to obtain the surface membrane fraction.

Western blot analyses were performed as qualitative check of the biotinylation assay as well as check for the correct size of the built concatamers barttin/V166E rCIC-K1.

#### **2.2.6.1 Biotinylation assay**

Surface exposed proteins with extracellular primary amino-groups can be labeled with a modified biotin and purified via this label. Here, we want to quantify the amount of CIC-K channel protein or barttin that is brought to the membrane. The target proteins are labeled with fluorescence reporter genes. By comparing the fluorescence membrane fraction with the

fluorescence of the whole cell lysate, a relative surface membrane fraction is calculated. The fluorescence of the whole cell lysate corresponds to the relative expression level when normalized to the fluorescence of WT barttin or hCIC-Ka in presence of WT barttin.

In the following passages, the reaction steps are described in detail before Fig.10 gives an overview about the several steps of the protocol.

### 2.2.6.1.1 Labeling with biotin

MDCKII cells were transfected with 2  $\mu\text{g}$  plasmids coding for barttin, respective barttin mutants together with 1  $\mu\text{g}$  hCIC-Ka coding plasmid (in 200  $\mu\text{l}$  OptiMEM) using Lipofectamin™ (in another 200  $\mu\text{l}$  OptiMEM) in 10 cm dishes in 6 ml transfection medium. 12-18 hours after transfection, the medium was changed. 44 hours after transfection, EZ-linked sulfo-NHS-SS-Biotin was dissolved in cold PBS to a concentration of 0.5 mg/ml. The cells were washed gently three times with PBS at RT (3 ml). PBS was removed by a vacuum pump. Preceding steps all were performed at 4 °C. Solutions should be cooled. Cells were incubated with 0.5 mg EZ-linked NHS-sulfo-SS-biotin for 30 min. Surface exposed primary amino groups, e.g. found in lysine or arginine, are bound by thioester-linked biotin.

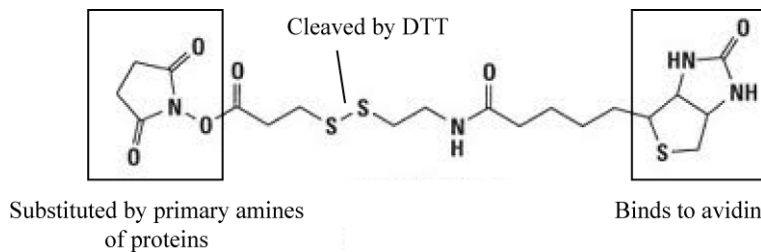


**Fig.9 Molecular structure of EZ-linked NHS-sulfo-SS-biotin**

Reactive centers are indicated. The left box is substituted by a primary amino group of a protein. After binding of the protein, biotin (right box) can bind to an avidin matrix for purification. The thiol-bond is cleaved by DTT to elute the protein of the avidin matrix.

### 2.2.6.1.2 Whole cell lysate

100 mM glycine/PBS is used for 3 washing steps. The last washing step was let stand for 20 min. Free glycine quenches unbound biotin. After two additional washing steps with PBS, lysis was performed with 1 ml of modified RIPA buffer. The components of the here used RIPA and washing buffer are listed in Tab.11+12.

RIPA buffer	concentration
HEPES	20 mM
NaCl	100 mM
EGTA	1 mM
Na-orthovanadate	1 mM
NaF	50 mM
NP-40 alternate	1 % (v/v)
Na-Deoxycholate	1 % (w/v)
SDS (Sodium dodecyl sulphate)	0.1 % (v/v)
Pi-mix complete	1 % (v/v)
Benzonase	8 U/ml
pH	7.4

Washing buffer	concentration
Triton X-100	0.1 % (v/v)
NaCl	500
EDTA	5 mM
Tris	50 mM
Pi-mix complete	1 % (v/v)
pH	7.4

**Tab.11 Composition of lysis buffer (left)**  
A modified RIPA-buffer was used for cell lysis.

**Tab.12 Composition of the wash buffer (up)**  
The detergent is change to exchange to micelles and their interior to purify resin bound proteins.

The lysate was cleared by a centrifugation step for 15 min at 4 °C with 13.000 g. Protein concentration was determined by BCA-Assay (Pierce) following manufacturers instruction. Comparable amounts of protein ( $\approx 50\mu\text{g}$ ) were loaded onto SDS-PAGE gel for densitometric analysis of relative expression. WT barttin was present in all gels as reference. The fluorescence intensity of the bands corresponding to barttin, respective channel protein, was normalized to the one found in the presence of WT barttin to determine the relative expression level.

### 2.2.6.1.3 Surface membrane fraction

Surface membrane exposed proteins were labeled with enzyme linked biotin, as described above. Comparable amounts (around 1 mg per sample and experiment) of cleared lysates were incubated with High Capacity NeutrAvidin Resin™ (Thermo Scientific) that was equilibrated with RIPA-buffer. Biotin binds to the avidin-coated beads during a 2 hour incubation period at 4 °C while rotating. Proceeding, the beads were washed once with RIPA buffer and five times with washing buffer. The last washing step must not contain fluorescent protein. This was checked by SDS-PAGE (**p**oly**a**crylamide **g**el **e**lectrophoresis) analysis. In

case of false positive fluorescence in gels of washing fractions, additional washing steps were performed. DTT containing Lämmli-buffer was used to cleave the disulfide bond within the spacer arm of SS-biotin, thereby eluting formerly surface exposed proteins of the matrix. SDS-PAGE gels and densitometric analysis quantifies the amount of surface exposed protein. The ratio of fluorescence of biotinylated protein and the fluorescence of protein in the cleared lysate marks the surface exposed fraction. The found ratio was normalized to the one found for WT barttin or hC1C-Ka in presence of WT barttin.

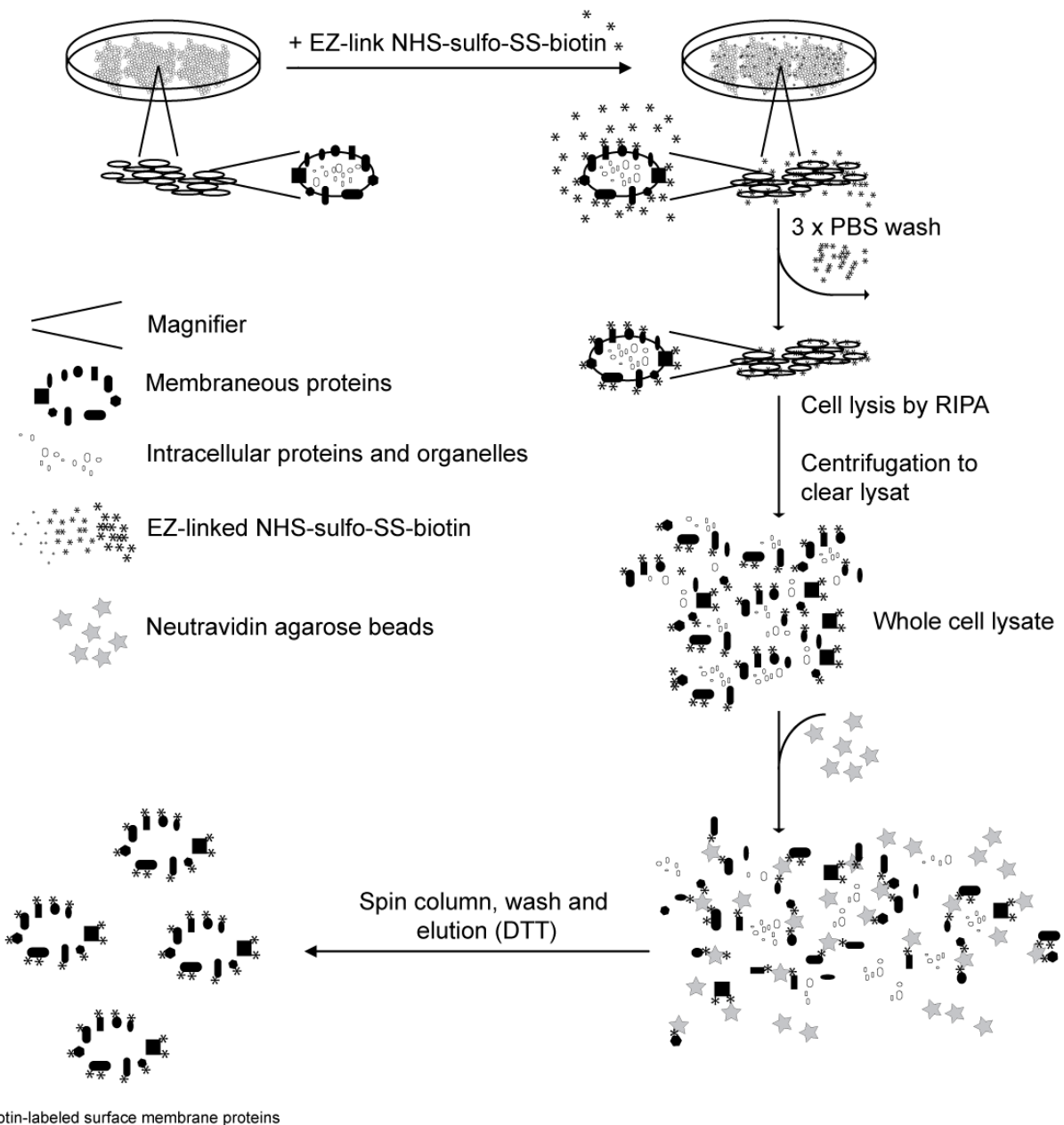


**Fig. 10 Scheme of biotinylation assay procedure**

Cells are incubated with a modified biotin. The modification (Fig.9) allows labeling of primary amino groups exposed to the extracellular side of the cells. After washing and lysis of the cells, surface exposed proteins can be purified via the biotin-label along a NeutrAvidin Agarose resin.



### 2.2.6.2 SDS-PAGE gel

12 % SDS-PAGE gels were poured for separation of proteins. In Tab.13, components of running and stacking gel are listed. Ammoniumpersulphate (APS) was freshly prepared in deionised water and crosslinks acrylamid monomers. N,N,N'-tetramethyl-ethylene diamin (TEMED) was purchased from Serva and is the catalysator of this crosslink reaction.

SDS-PAGE gel	12 % running gel	4 % stacking gel
H <sub>2</sub> O	1.65 (ml)	1.525 (ml)
1.5 M Tris pH 8.8	1.25 (ml)	---
1.5 M Tris pH 6.8	---	0.625 (ml)
Protogel	2 (ml)	0.325 (ml)
10 % SDS	50 (µl)	25 (µl)
10 % APS	50 (µl)	12.5 (µl)
TEMED	5 (µl)	2.5 (µl)

Tab.14 Composition of running and stacking gel

Lämmli buffer	concentration
TrisHCl pH 6.8	250 mM
SDS	10 %
Glycerol	10 %
DTT	100 mM
Bromphenole blue	0.05 %

Tab.13 Composition of the Lämmli buffer  
This buffer is needed to load the sample on the gel.

Samples were dissolved in 5 x Lämmli buffer (Tab.14). Dual Color marker (DC) was loaded for size estimation. Running buffer contained 25 mM Tris-Base, 192 mM glycine and 3.5 mM SDS. Gels were run at 90 V during stacking and 180 V for running gel.

### 2.2.6.3 Typhoon laser scanning

Fluorescent bands in SDS-PAGE gels were visualized with a fluorescence scanner (Typhoon, GE Healthcare). CFP was excited with coherent light of 457 nm, YFP was excited with 488 nm. For emission detection, a 40 nm broad band pass filter was used with the center peak at 520 nm for both channels.

For marker (Dual Color DC marker, BioRad) visualization, RFP was excited with 457 nm or 633 nm. For emission detection, same filter as above or a red light corresponding 30 nm broad band pass filter was used with the center peak at 670 nm.

### 2.2.6.4 SDS-PAGE gel analysis

Fluorophore-tagged proteins allow quicker detection and more accurate densitometric analysis of SDS-PAGE gels than Western blot analysis. Therefore, mCFP (monomeric cyan fluorescent protein) was covalently linked to barttin and YFP (yellow fluorescent protein) to hClC-Ka. For almost all biochemical experiments, MDCKII cells were cotransfected as described.

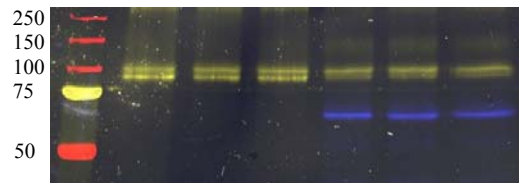


**Fig. 11 Fluorescence scan of SDS-PAGE gel of MDCKII cells expressing YFP hClC-Ka (yellow) alone or with WT barttin mCFP (blue)**  
hClC-Ka typically shows two bands without barttin. Barttin facilitates channels ER-exit by complex glycosylation. This additional mannose weighs on hClC-Ka resulting in a third band. DC size marker was loaded.

Loading of cleared lysate onto SDS-PAGE gels leads to a distinct band pattern, when scanned with a fluorescence laser scanner. An example is shown in Fig.11. Without barttin, a yellow double band of the channel can be detected at approximately 100 kDa. With barttin, a third smeary channel band appears at approximately 110 kDa, and the barttin band (colored in blue), of course. Janssen et al. showed in 2009 three channel bands are caused by different glycosylation states – unglycosylated, core glycosylated and complex glycosylated. The complex glycosylation of hClC-K channels only takes place in presence of barttin. By that, hClC-K can exit the ER and is further transported to the plasma membrane, together with barttin.

To figure out the expression level and the surface membrane fraction of hClC-Ka and barttin, gels like the shown were run and densitometrically analyzed.

Some gels were analysed with a different imaging device, the Fusion SL (Peqlab). This device uses diodes and no lasers for excitation. In contrast to the Typhoon, the Fusion device detects emitted light over the whole plate and not spotwise with confocal application. These two differences lead to lower fluorescence intensities and lower resolution. So, only one band corresponding to YFP hClC-Ka is detected Fig. 16 and 21.

### **2.2.6.5 Densitometric analysis**

Fluorescent band intensities were quantified using Image Quant TL software. Lanes were set manually and background subtraction was performed with the rolling ball algorithm. Bands with a minimum slope of 100 were detected and normalized to the band intensity of WT barttin or hCIC-Ka coexpressed with barttin.

To quantify the expression level of hCIC-Ka, the intensity of the three bands were summed.

For surface membrane fraction, the intensity of the fluorescent band of biotinylation protein is divided by the intensity of the fluorescent band of whole cell lysate (in case of hCIC-Ka the sum of three bands was built).

### **2.2.6.6 Western blot**

General western blot protocol was used for transfer onto PVDF membranes (GE Healthcare). Protein transfer was performed at pH 9.9 for 1 h with 90 V at room temperature or for 16 hours and 20 V at 4 °C. Blot membranes were blocked for at least 1 hour in TBS with 3 % BSA (bovine serum albumin). Before and after incubation with antibody-containing buffer, the membranes were washed twice with TBS/0.1 % Triton X-100 and once with TBS. Each washing step took 5 minutes while shaking. Incubation with primary or secondary antibody was performed for at least one hour at room temperature or overnight at 4 °C while shaking.

#### ***2.2.6.6.1 Qualitative control for surface membrane proteins***

The elution fraction of the biotinylation assay should not contain intracellular proteins as GAPDH (glycerin-aldehyde-3-phosphate-dehydrogenase) for instance. Therefore we performed western blots of gels loaded with this fraction. A primary antibody raised in mouse against human GAPDH (Santa Cruz, mouse anti-GAPDH, dilution 1:2500 in TBS with 1 % BSA) was used for detection. For visualization, a chemiluminescent procedure was used. A HRP- (horseradish-peroxidase) conjugated secondary antibody was used (HRP-anti-mouse, dilution 1:20000 in TBS with 3 % BSA) and detected with SuperSignal West Pico Chemiluminescent Substrate™ (Thermo Scientific). This substrate leads to enhanced chemiluminescence (ECL).

#### ***2.2.6.6.2 Qualitative check for built concatamers***

As shown in the results, fluorophore labeled concatamers are no longer functional. Therefore we performed a western blot for detection of unlabeled concatamers. HEK293T cells expressing WT barttin and mutant barttin concatamers were lysed. The lysates were electrophoresed and western blotted. Two detection strategies were tried. First, a primary antibody that was raised in goat against human barttin (Santa Cruz, goat-anti-barttin, dilution 1:2000 in TBS with 1 % BSA), and second, a primary antibody raised in rabbit against rat rCIC-K1 were used. Detection with appropriate secondary antibodies (HRP-anti-goat, or HRP-anti-rabbit) and SuperSignal West Pico Chemiluminescent Substrate™ (Thermo Scientific) took place.

### 3 Results

In this study, we examined sequence determinants at the functional modification of ClC-K chloride channels by barttin. For this purpose, we analyzed the effects of tryptophan-substituted barttin on two ClC-K channel orthologs – the human hClC-Ka and the rodent rClC-K1 with the earlier mentioned gating glutamate introduced at amino acid position 166 (V166E). We found residues to be crucial for the stability, trafficking or chaperone function of barttin, as well as residues that may play a major role in channel activation/gating regulation.

#### **3.1 hClC-Ka and the effects of barttin and mutant barttins**

##### **3.1.1 hClC-Ka is activated by WT barttin – and only by four helix 1-mutants**

HEK293T cells were co-transfected with plasmids encoding an N-terminally labeled fusion protein of hClC-Ka and YFP and a C-terminally labeled fusion protein of barttin and mCFP. Barttin was transfected with DNA amount 2-4 times larger than ClC-K encoding plasmids to ensure that all ClC-K proteins are complexed with barttin. Only cells with an obviously exceeding mCFP-fluorescence were selected for patch-clamp experiments to ensure a higher amount of barttin.

Whole cell patch clamp measurements of HEK293T cells that express hClC-Ka channels in absence of barttin reveal currents that were indistinguishable from untransfected cells. Co-expression of WT barttin induces hClC-Ka currents over the whole measured voltage range between -245 mV and +145 mV (Fig.12A). At very negative potentials the hClC-Ka/barttin current amplitudes decrease and current noise values increase (Fig.12A right panel). Fig.12B depicts an I-V-plot showing the voltage dependence of hClC-Ka currents in presence and absence of barttin. hClC-Ka/barttin currents display a hook-shaped I-V-dependence with a current maximum at around -150 mV.

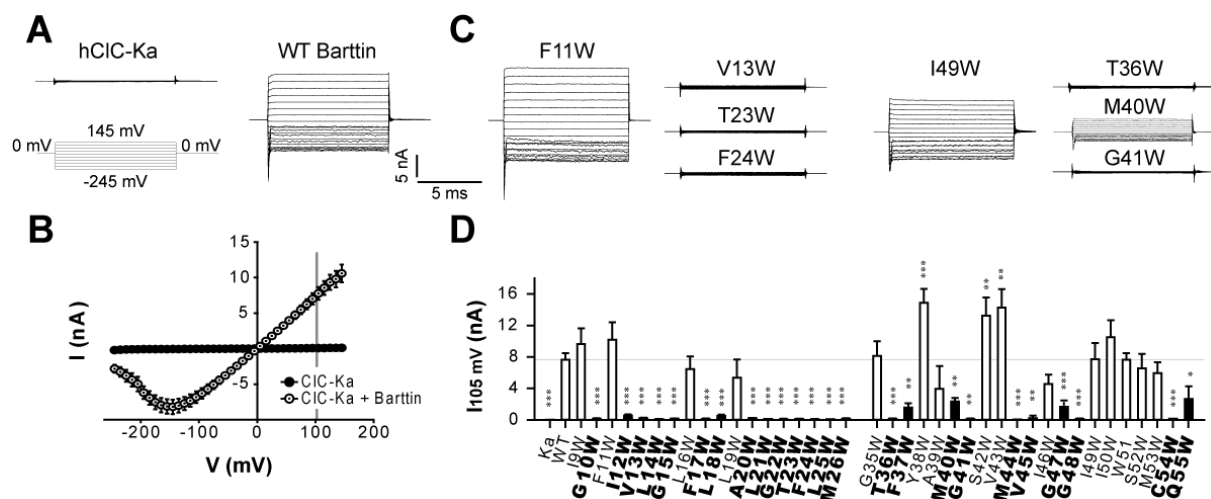


**Fig.12 (A)** Representative recordings of HEK293T cells expressing hCIC-Ka (left) or hCIC-Ka with WT barttin (right) Voltage steps of 10 mV from -245mV to 145mV were applied with an in between holding potential of 0mV. **(B)** I-V-plot of hCIC-Ka without and with WT barttin; reduction of amplitude is registered beyond -150mV with raising noise. **(C)** Representative recordings of hCIC-Ka coexpressed with mutant barttins. F11W, M40W and I49W are examples for WT-like current traces, however with different amplitudes. V13W, T23W, F24W, T36W and G41W barttin are exemplary for mutations which inhibit currents of hCIC-Ka. **(D)** Comparison of hCIC-Ka amplitudes at 105mV. Only 4 of 18 barttins of helix 1 evoke hCIC-Ka currents, as well as 15 of 21 barttins of helix 2 (highlighted with white bars). Black bars and bold letters represent residues which diminish the currents amplitude.

Fig.12C shows representative recordings of hCIC-Ka channels for some exemplary barttin mutants. Some evoke larger currents, like F11W barttin and some evoke smaller currents, like M40W or I49W barttin. However, the voltage dependence of current amplitudes remained unchanged in any case. The reversal potential and the potential of maximum current at negative range were not shifted. V13W, T23W, F24W, T36W and G41W barttin are examples for barttin mutations that failed to activate hCIC-Ka. There are many possible reasons for these effects of tryptophan insertion on barttin function. Misfolded or degraded barttin proteins, or barttins that fail to bind to the CIC channel will lead to a loss of function. Mutants that impair subcellular trafficking or proper gating of hCIC-Ka would evoke smaller or no currents. Lower expression of barttin could result in lower amplitudes.

In Fig.12D hCIC-Ka/barttin mean current amplitudes at a voltage of +105 mV are compared for the whole set of barttin mutants. Substitution of single amino acids by tryptophan in transmembrane helix 1 of barttin, TM1, impairs channel function for most residues. Only mutations at position I9, F11, L16 and L19 allow proper channel activation. hCIC-Ka/barttin seems to be more resistant to tryptophan substitutions in helix 2 of barttin. 15 of 21 tryptophan substitutions in the second transmembrane helix of barttin, TM2, do not impair activation of hCIC-Ka. Four out of these mutantions evoke lower mean current amplitudes (F37W, M40W, G47W and Q55W barttin). In contrast to all other mutants marked with asterisks, the I-V-plots in presence of these four mutants show the characteristic hook-shaped

I-V-dependence. All mutants that significantly reduce mean current amplitudes are marked with bold letters in Fig.12D. Since lowering of the mean current amplitude can be due to multiple reasons, we examined single channel properties and trafficking of hCIC-Ka co-expressed with mutant barttin.

### **3.1.2 Functional barttin mutants leave single channel properties of hCIC-Ka/barttin unaffected**

The amplitude of macroscopic hCIC-Ka/barttin currents depends on the product of the single channel amplitude ( $i$ ), the number of active channels in the plasma membrane ( $N$ ) and the open probability of the channels ( $p_o$ ) (see material & methods, eq.6). We used stationary noise analysis to investigate these channel properties. Plotting the macroscopic current variance, normalized by the product of the mean current amplitude  $I$  and the electrical driving force  $V-V_r$  ( $V$  = applied voltage,  $V_r$  = reversal potential), versus the macroscopic conductance  $I/(V-V_r)$  reveals the unitary channel conductance as y-axis-intercept. The number of active channels in the membrane can be obtained from the slope of the linear regression line of the same plot (material & methods, eq.7+8).

Fig.13A shows representative noise analyses for hCIC-Ka currents in presence of WT barttin or M40W barttin. The unitary channel conductance of about 20 pS is comparable for WT and mutant barttin, but the number of active channels and therefore the maximum conductance of the whole cell (x-axis intercept) is clearly reduced for M40W barttin. The quotient of the actual conductance at certain voltages by the maximum conductance gives the absolute open probability of the channel. Fig.13B illustrates the voltage dependence of absolute open probabilities indicating that there is no difference between M40W and WT barttin. M40W barttin was chosen as example for a barttin mutant that results in rather low hCIC-Ka current amplitudes. However, even such a barttin mutant is able to transfer hCIC-Ka channels into an open state with unaltered pore properties.

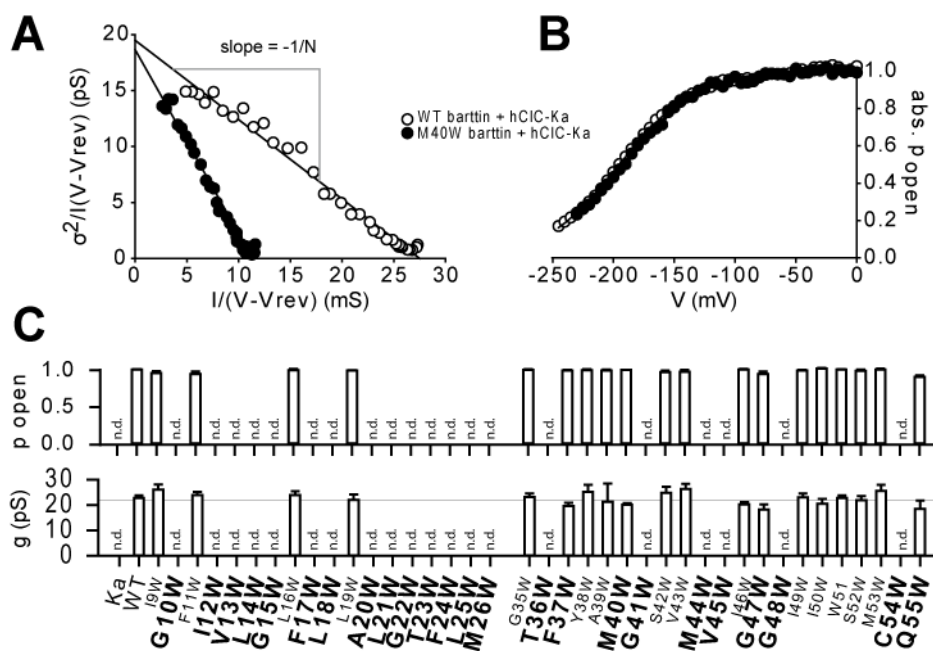


**Fig.13 Stationary noise analysis of currents of HEK293T cells coexpressing hCIC-Ka and barttin**  
**(A)** Noise analysis of WT barttin and exemplary mutant M40W barttin reveals same unitary conductance (y-axis intercept). **(B)** Absolute maximal open probability of hCIC-Ka coexpressed with WT barttin or exemplary barttin mutant M40W barttin. No changes in open probability are observed. **(C)** Bar charts sum noise analysis results of all scanned barttin mutants. No changes in unitary conductance or absolute maximal open probability could be examined. Due to very tiny currents, noise analysis was not performed for mutants marked with n.d. = not determinable.  $n \geq 4$ , all data + S.E.M. Students t-test was performed to test for significance. Bold letters highlight residues with still unknown reasons for low current amplitudes (Fig. 12).

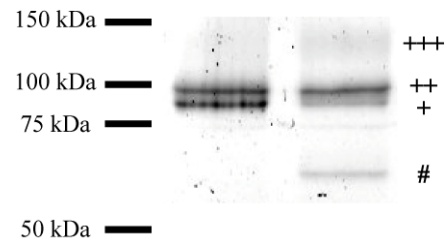
Noise analyses were carried out for all mutants that activate hCIC-Ka and results are summarized in Fig.13C. No difference in absolute maximal open probability at +5 mV or single channel conductance of hCIC-Ka was detected in presence of WT barttin and any barttin mutant. We conclude that barttin mutants that activate hCIC-Ka channels do not change the pore properties of the channel.

Changes in current amplitudes therefore are caused by differences in the number of channels in the plasma membrane or by complete insufficiency of barttin to switch membrane inserted channels into an active state.



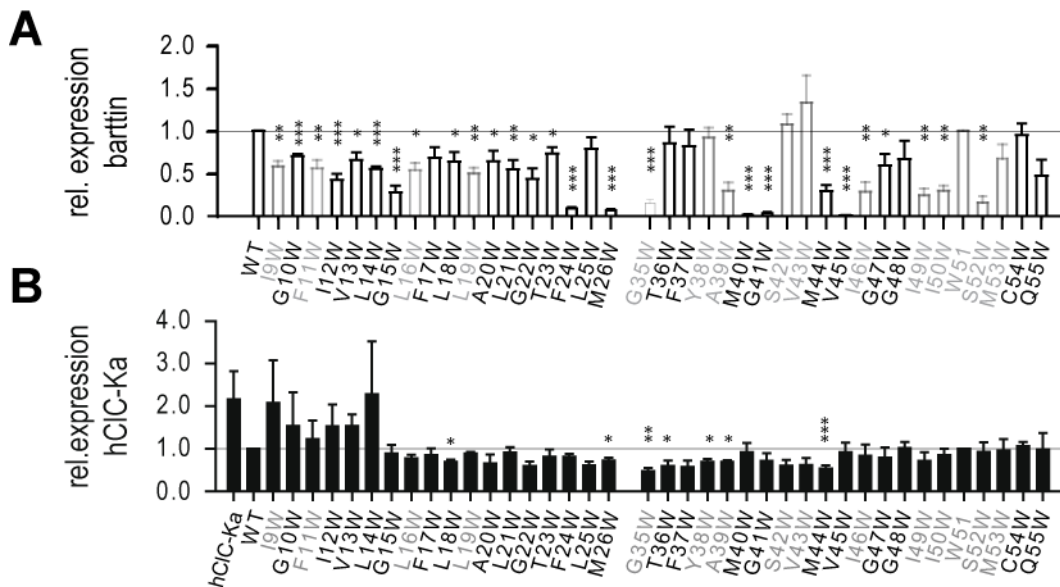
### 3.1.3 Expression level of mutant barttin and hClC-Ka

Fig.14 shows a fluorescence scan of a representative SDS-PAGE gel from lysed MDCK II cells that expressed YFP-hClC-Ka in absence (left lane) or in presence (right lane) of WT barttin. Without barttin, two YFP bands can be seen between 75 and 100 kDa. In presence of WT barttin, a third YFP band appears at around 115-130 kDa. Barttin-mCFP migrates at around 60-65 kDa (#). The different molecular weights of hClC-Ka proteins are caused by different glycosylation states (Janssen et al. 2009). The lightest band corresponds to unglycosylated channel (+) protein. During maturation the protein becomes core-glycosylated in the ER (++). Binding of additional oligosaccharides results in complex glycosylated channel proteins (+++), which may facilitate Golgi-exit and membrane trafficking. For the determination of relative expression levels, the fluorescence intensities of all YFP bands were summed and corrected for the protein concentration of the cleared cell lysates, as determined using a BCA-assay.



**Fig.14 Fluorescent SDS-PAGE gel of whole cell lysate of MDCKII cells expressing hClC-Ka without or with barttin**

Without barttin (left lane) two prominent bands are visible corresponding to unglycosylated (+) and core glycosylated (++) channel protein. In the presence of barttin (hashtag #, right lane), hClC-Ka is complex glycosylated (+++).



**Fig.15 SDS-PAGE gel analysis; quantification of fluorescent band intensities of (A) barttin, normalized to WT barttin and (B) hClC-Ka, normalized to hClC-Ka in presence of WT barttin**

(A) Most barttin mutants do not express as well as WT barttin (asterisks), but low barttin expression does not correlate with low current amplitudes (black letters). Residues illuminated in light grey did not reduce mean current amplitude. For the others, the reason for low current amplitude needed to be found out. Reduced barttin expression often did not result in diminished mean current amplitude (e.g. I46W, I49W, I50W or S52W compared with Fig.12D). The minimal expression level for unaltered current amplitudes is below 16% (S52W) and above 1.6% (M40W). (B) Channel expression remains constant upon cotransfection with most barttins. Lower channel expression must not necessarily lead to a reduction in mean current amplitude (Y38W). Reduced barttin and reduced channel expression not necessarily lead to a decrease in current amplitude (G35W, A39W compared with Fig.12D). (Mann-Rank-Sum-Test was performed to check for significance \*  $p < 0.05$ ; \*\*  $p < 0.01$ ; \*\*\*  $p < 0.001$ ). Data are mean + S.E.  $n \geq 3$ .

In Fig.15, expression levels were normalized to the expression of WT barttin in (A) and to the expression of hClC-Ka in presence of WT barttin in (B). In absence of WT barttin, the expression level of hClC-Ka increases by a factor 2. For determination of the expression level of hClC-Ka without barttin, no second plasmid was present. Cotransfection of additional plasmids influences the transcription of the first plasmid, as shown in Fig.16. Therefore, the relative expression level of hClC-Ka expressed without barttin is higher.

Light grey letters and bars in A and B mark barttin mutations that did not lower the mean current amplitude. Black letters indicate mutations that lower the mean current amplitude for still unknown reason.

The majority of barttin mutations affect the protein biosynthesis, because 29 out of 38 investigated mutants displayed reduced expression levels. The hClC-Ka expression was slightly, but significantly reduced (asterisks) in presence of only 7 out of 38 barttin mutants. There is no clear correlation between both expression patterns. Low expressing barttin mutants like G35W or M40W do not evoke higher hClC-Ka expression, as might be expected if plasmids coding for these barttin mutants were not transcribed. As shown in Fig.16, the more barttin is expressed, the less channel protein is built.

**Fig.16 Fluorescent SDS-PAGE gel to illustrate the lower expression level of hClC-Ka with raising concentration of co-transfected plasmids coding for barttin**  
HEK293T cells were co-transfected with (upper row) 2 µg pcDNA3.1(-) YFP hClC-Ka and (lower row) various amounts of pcDNA3.1(+) barttin mCFP.

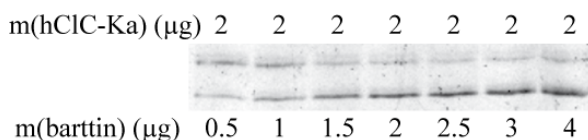
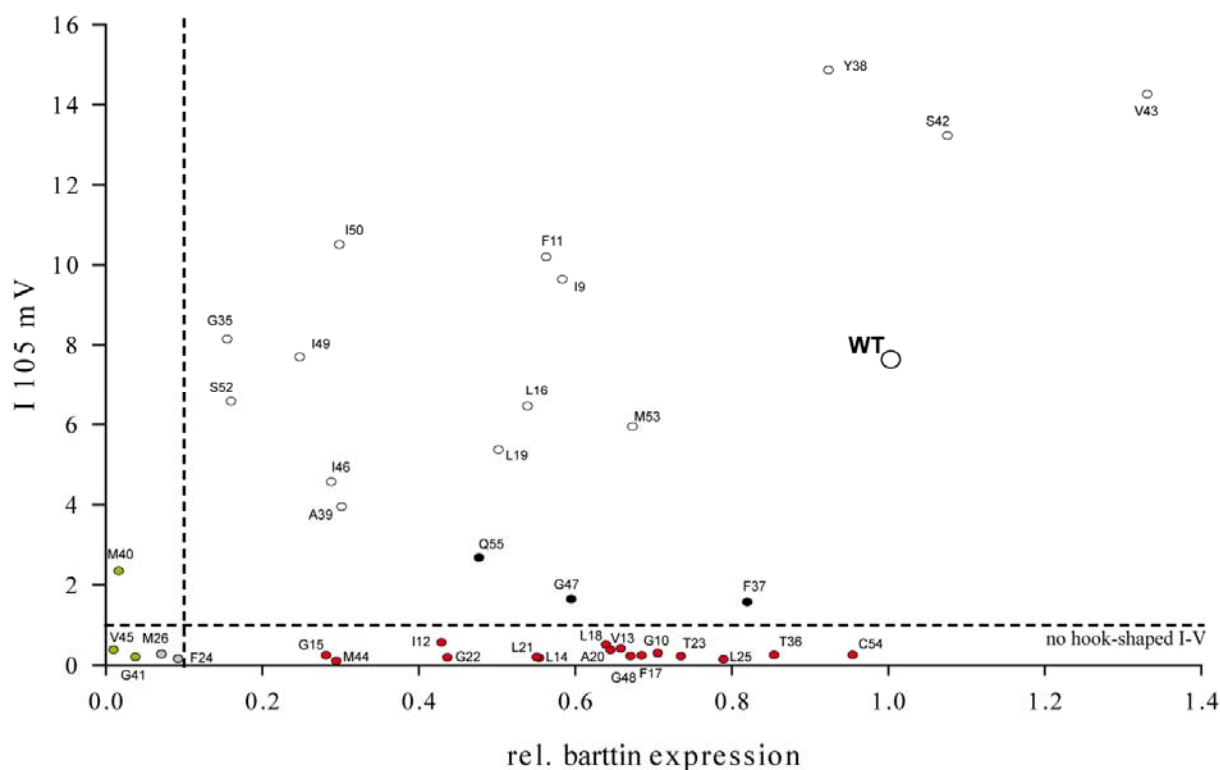


Fig.17 illustrates relative expression levels of barttin and current amplitudes of hClC-Ka/barttin channels in one plot. Dashed lines arbitrarily separate relative expression levels of barttin lower than 10 % and currents lower than 1 nA.



**Fig.17 Plot of macroscopic hCIC-Ka current amplitudes at 105 mV versus barttin expression levels**

A lower relative expression of barttin does not explain low currents or impaired activation of hCIC-Ka. Dashed lines mark 10 % expression level and 1 nA current amplitude. Mutant barttins that show a significant reduction in mean current amplitude are marked in green, black and red. Green marked mutants are hardly expressed. Mutants marked in black activate hCIC-Ka with unaltered pore properties, but these three mutants and M40W barttin reduce the mean current amplitude. Red marked barttin tryptophan mutants evoke low hCIC-Ka current amplitudes although the rel. expression level is higher than 25 %. Even with lower expressing barttin mutants, regular current amplitudes could be recorded. Currents lower than 1 nA avoid noise analysis.

Expression levels of five mutant barttins are below 10 %. Of those, only M40W barttin activates hCIC-Ka. Mutations F24W, M26W, G41W and V45W abolish hCIC-K/barttin currents. A lot of barttin mutations reduce current amplitudes (bold letters in Fig.12D), even though expression levels are high and cells with excessive barttin expression were preferentially selected for electrophysiological recordings. These mutants include hCIC-Ka activating F37W (n=6), G47W (n=12) and Q55W (n=8) (labeled in black in Fig.17) and many mutants that reveal current amplitudes below 1 nA (labeled in red).

We conclude that significantly reduced current amplitudes in patch clamp recordings are in most cases not easily explained by reduced expression of barttin. Instead, one has to consider additional factors like impaired trafficking of barttin or channel protein to the plasma membrane, declined binding affinities between barttin and hCIC-Ka or failures in activation of hCIC-K channels.

### 3.1.4 F24W and M26W barttin are misfolded or degraded

Fig.18 shows a CFP fluorescence scan of a representative SDS-PAGE gel with mCFP-barttin bands at 60-65 kDa. F24W and M26W barttin, however, migrate differently in the gel as compared to all other barttin mutants and WT barttin. Only F24W barttin and M26W barttin show a smaller band at around 55 kDa. Accordingly, these two barttin mutants are misfolded or degraded and the missing hCIC-Ka channels activation is explained by improper barttin structure and function.

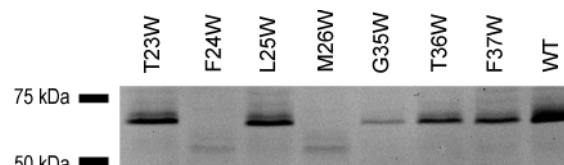


**Fig.18 Excerpt of a fluorescence scan of SDS-PAGE gel of mutant barttins coexpressed with hCIC-Ka**  
Only barttin bands are shown. F24W and M26W barttin show altered refraction fronts. All other barttin mutations did not alter refraction front and could be detected at a same height as WT barttin or here shown exemplary mutants.

### 3.1.5 Surface membrane insertion of CIC-K/barttin channels is impaired for some barttin mutants

We next investigated surface membrane insertion of hCIC-Ka/barttin channels. MDCKII cells, coexpressing hCIC-Ka and barttin, were incubated with modified biotin in the bath solution that labels primary amino groups of plasma membrane inserted proteins from the extracellular side. After lysis of

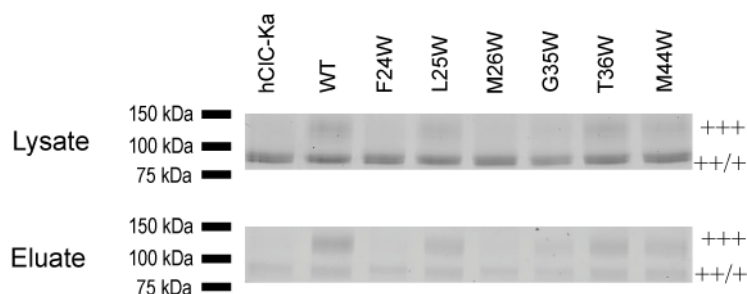


**Fig.19 Fluorescence scan of SDS-PAGE gels of hCIC-Ka coexpressed with mutant or WT barttin in MDCKII cells**  
Cleared lysates (upper panel) and eluates (lower panel) are depicted for exemplary mutants (+++complex glycosylated band, ++core- and +unglycosylated bands). Only hCIC-Ka bands are shown.

the cells, labeled proteins were purified using a neutrAvidin matrix. SDS-PAGE gel analysis of the protein amount in whole cell lysates and of biotinylated proteins after purification (eluate) were used to quantify the plasma membrane inserted fractions of barttin and hCIC-Ka. Representative fluorescence scans of SDS-PAGE gels are shown in Fig.19. The relative amount of complex glycosylated hCIC-Ka proteins is obviously higher in the eluate than in the lysate.

To quantify the plasma membrane inserted fraction of barttin and hClC-Ka, the fluorescence intensity of biotinylated protein (eluate) was divided by the fluorescence intensity of the cleared lysate. The results are depicted in Fig.20. Fractions were normalized to the values obtained from WT barttin (A) or hClC-Ka in presence of WT Barttin (B). Besides the two misfolded barttins (F24W and M26W, marked as grey bars), three mutant barttins, M40W, G41W and V45W, are hardly brought to the membrane (Fig.20A) and marked in green, analog to Fig.17. In presence of these mutants the surface membrane insertion of hClC-Ka channels was also significantly reduced. We conclude that impaired subcellular trafficking of M40W, G41W and V45W barttin is responsible for low hClC-Ka/barttin current amplitudes. There are more barttin mutants that impair trafficking of hClC-Ka, even though these barttins themselves insert adequately into the surface membrane. They are highlighted as red bars in Fig.20B. Four of them (I12W, G15W, A20W and G48W) have been previously shown to be sufficiently expressed, but were not able to produce hClC-Ka/barttin currents larger than 1 nA (compare Fig.17). Q55W and low expressing S52W barttin significantly decrease surface membrane insertion of hClC-Ka. These mutants, however, activate the channel protein, resulting in reduced current amplitudes for Q55W only.

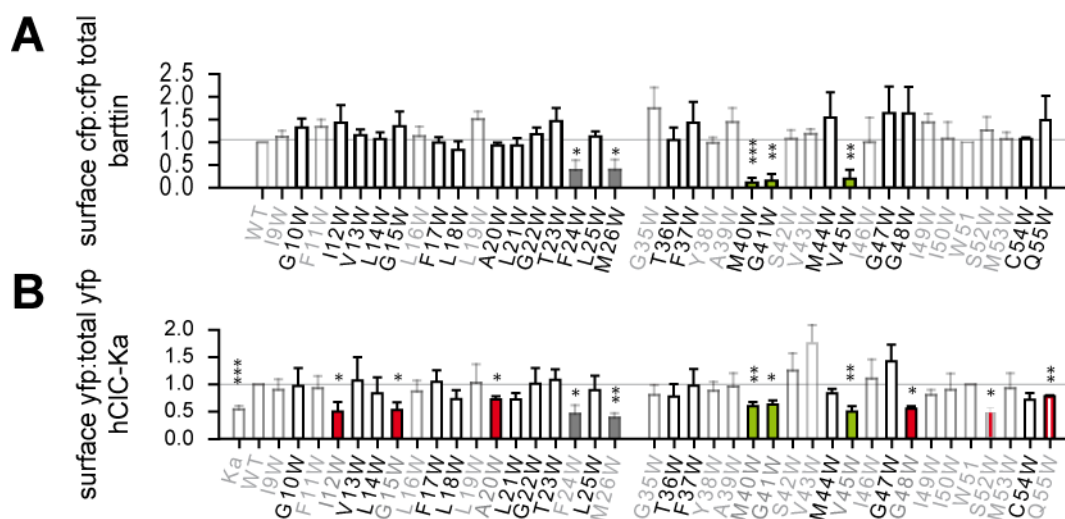


**Fig.20 Quantification of surface membrane fraction of barttin (A) and hClC-Ka (B)**  
 For mutations marked with black letters in (A), low mean current amplitude has been recorded (compare with Fig.12D). Besides (F24W, M26W,) M40W, G41W and V45W, all barttin mutants are WT-like in their trafficking behavior. Despite regular barttin trafficking, I12W, G15W, A20W, G48W, S52W and Q55W barttin cannot bring as many channels to the plasma membrane as WT barttin. This explains the observed low mean current amplitude of hClC-Ka evoked by these mutant barttins. For mutations marked with black letters in (B), no explanation for low mean current amplitude was found. Mann-Rank-Sum test was performed to check for significance versus WT barttin or hClC-Ka in presence of barttin (\* p<0.05; \*\* p<0.01; \*\*\* p<0.001). All data are mean  $\pm$  S.E. n  $\geq$  3.

In summary, mutations M40W, G41W and V45W hinder trafficking of barttin and subsequently trafficking of the channel to the surface membrane. The mutations I12W, G15W, A20W, G48W, S52W and Q55W significantly interfere with the chaperone effect of barttin, which reduces the plasma membrane insertion of hClC-Ka channels. Lowered mean current amplitude of hClC-Ka evoked by Q55W barttin may be explained with fewer channels in the plasma membrane. S52W and Q55W barttin can activate hClC-Ka in contrast to I12W, G15W, A20W and G48W barttin. Therefore we assume only a partial loss of chaperone function.

Several barttin mutations do not affect channel trafficking. The channel protein and its subunit are inserted into the plasma membrane, but hClC-Ka is not activated in presence of G10W, V13W, L14W, F17W, L18W, L21W, G22W, T23W, L25W, T36W, M44W or C54W barttin. The mean current amplitude is smaller than 1 nA and the I-V-plot does not show the characteristic hook-shaped I-V-dependence (compare with Fig.17). We assume effects of these barttin mutants on gating properties of hClC-Ka. The reasons for reduced current amplitudes remain unclear for F37W and G47W barttin.

As shown before, the expression levels of barttin mutants differ (Fig.15) and the surface membrane fraction of hClC-Ka is expected to depend on the concentration of barttin. To estimate a relative amount of barttin that is needed to guarantee an excess by biotinylation assays, MDCKII cells were cotransfected with 2  $\mu$ g of plasmids coding for hClC-Ka and varying amounts of plasmids coding for WT barttin. Fig.21A shows a representative fluorescent SDS-PAGE gel of the surface membrane fraction of hClC-Ka (upper row) and barttin (lower row) bands.

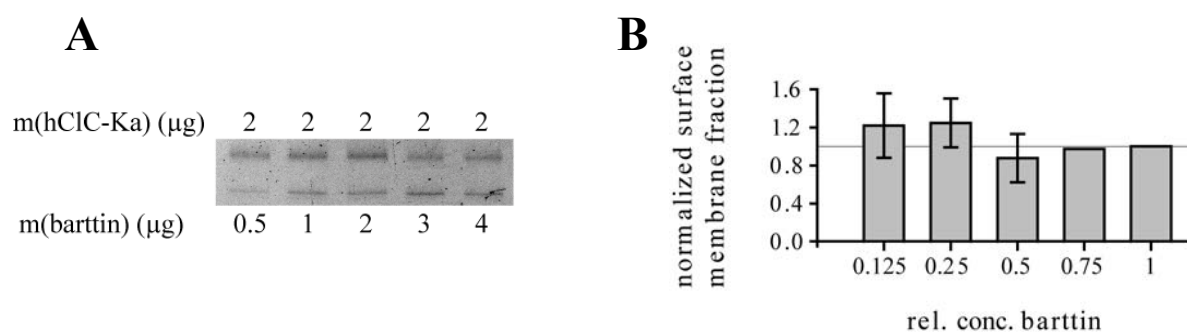


**Fig.21 A) Fluorescent SDS-PAGE gel of biotinylated, surface exposed proteins of MDCKII cells cotransfected with plasmids coding for WT barttin CFP (lower row) and YFP hClC-Ka (upper row) and (B) normalized surface membrane fraction of hClC-Ka in presence of different amounts of barttin**

The amounts of transfected plasmids are indicated. Analog to Fig.15, the amount of built channels decreases with raising barttin concentration. **B)** The ratio of membrane fraction and total lysate fraction corresponds to the relative surface membrane fraction which were normalized to the value found with the highest barttin concentration. This ratio is the same for all observed barttin concentrations indicating that a relative barttin concentration of 12.5 % suffices to saturate all possible barttin binding sites in hClC-Ka when co-expressing 2  $\mu$ g of vectors expressing hClC-Ka and 4  $\mu$ g of vectors expressing barttin.

By normalizing the ratio of the band intensities of the whole cell lysates (Fig. 16) and the surface membrane fraction (Fig. 21A), it gets obvious that co-transfecting 0.5  $\mu\text{g}$  (rel.  $c_{\text{barttin}} = 0.125$ ) or 4  $\mu\text{g}$  barttin (rel.  $c_{\text{barttin}} = 1$ ) coding plasmids together with 2  $\mu\text{g}$  hCIC-Ka coding plasmids results in comparable relative surface membrane fractions of the channel (Fig.21B). This indicates that barttin is present in excess even when the relative amount of barttin is reduced to around 12.5 %.

Since chaperone function of barttin is certainly dependent on the availability of the accessory subunit, we correlated surface membrane insertion of hCIC-Ka channels to the expression level of barttin mutants (Fig.22) to demonstrate whether the loss-of-chaperone function is caused by the mutation or if it is artificially caused by low expression. A vertical dashed line indicates the minimal relative expression level needed to guarantee an excess of barttin. Because of this excess above 12.5 % relative barttin expression, a regression line is missing. The correlation of surface membrane fraction and expression level allows evaluations of the chaperone effects of barttin mutants. The membrane insertion of hCIC-Ka is unchanged even for low expressing barttin mutants like G35W barttin, or in contrast, S52W barttin, which is comparably low expressed, but fails to take as many channels to the membrane. The loss-of-chaperone function of S52W barttin is not an effect of low expression, but caused by the mutation.

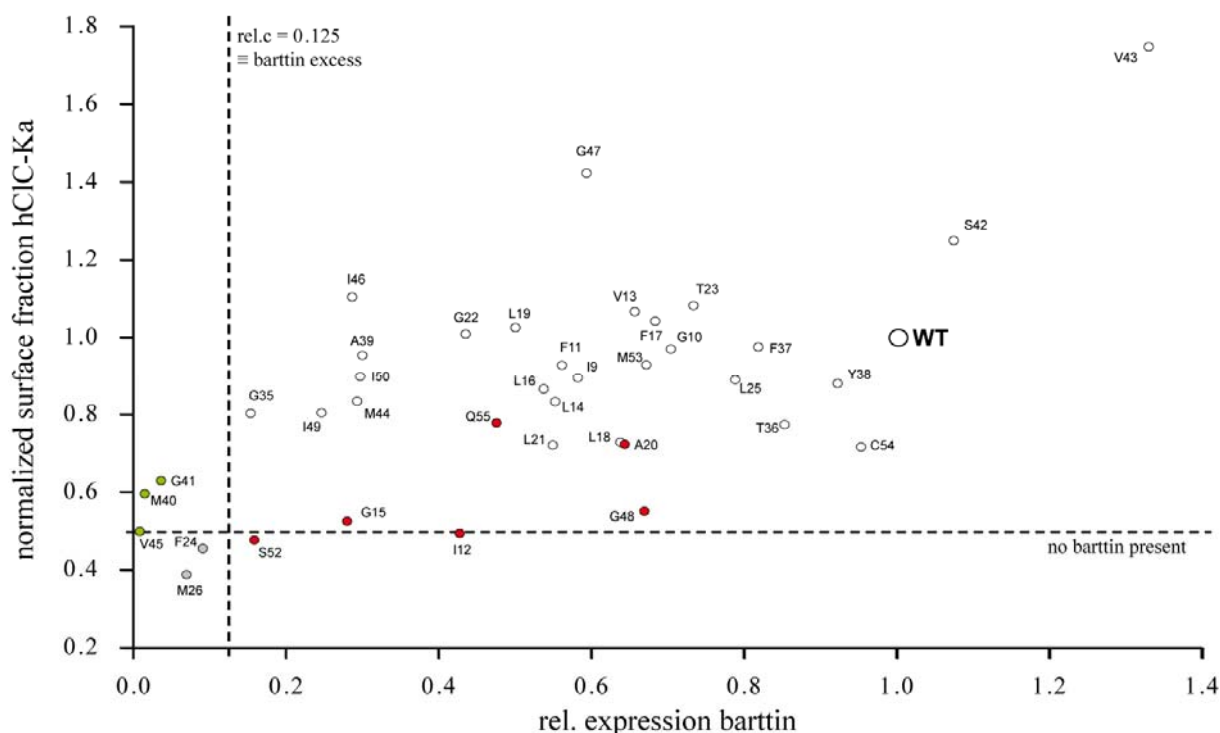


**Fig.22 Plot of surface membrane fraction of hCIC-Ka versus the relative expression of barttin**

The values of Fig.20B were plotted versus the values of Fig.15A. White circle represent WT-like mutants, green circles mark low expressing or misfolded/degraded barttins. Red circles depict barttin mutants that evoke significant reduction in hCIC-Ka surface membrane trafficking. A vertical dashed line marks the minimal relative barttin expression level and separates green marked mutants from the rest. A horizontal dashed line indicates a relative level of surface membrane inserted channel proteins in absence of barttin.



### 3.1.6 Investigation of subcellular barttin and hClC-Ka distribution by confocal imaging

We next investigated subcellular distribution of barttin-mCFP and YFP-hClC-Ka channels using confocal microscopy. MDCKII cells were transfected with vectors encoding barttin-mCFP and YFP-hClC-Ka and live cell imaging was performed 48 hours after transfection. hClC-Ka remains mostly in intracellular compartments, when barttin is absent. In presence of WT barttin both proteins, barttin and hClC-Ka, are co-localized in the plasma membrane (Fig.23).

As expected from biotinylation experiments (Fig.20), some barttin mutants differ in their intracellular distribution, and co-localization with hClC-Ka is affected. When the chaperone function of barttin is impaired, larger amounts of channel protein are retained in intracellular compartments.

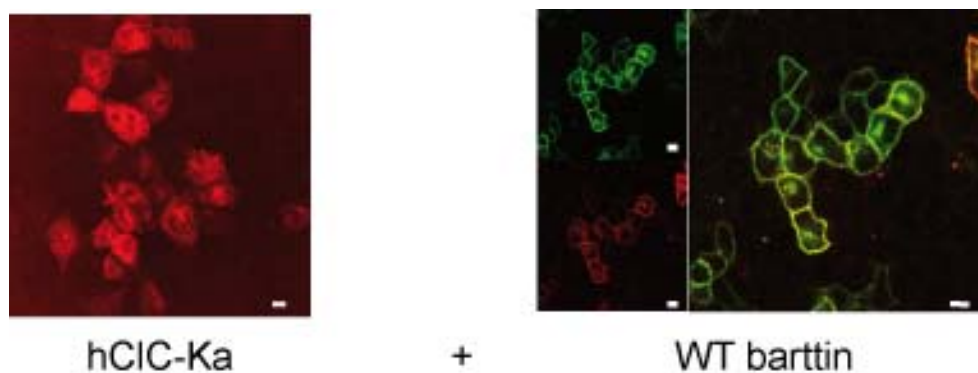


**Fig.23 Confocal images of MDCKII cell expressing hClC-Ka without or with WT barttin**  
Without barttin, most of expressed hClC-Ka (red) retains in intracellular compartments. Upon the presence of barttin (green), hClC-Ka is predominantly in the plasma membrane with its  $\beta$ -subunit. Scale bar = 10  $\mu$ m



F24W and M26W barttin are misfolded or degraded, so no chaperone effect was observed, the channel was not complex glycosylated and here, confocal imaging showed that these two barttin proteins and hCIC-Ka retain in intracellular compartments (Fig.24).

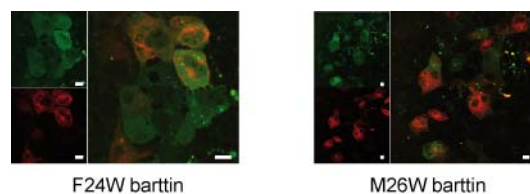


**Fig.24 Confocal images of MDCKII cells expressing hCIC-Ka with F24W or M26W barttin**  
These two misfolded or degraded barttins cannot bring hCIC-Ka to the plasma membrane. Scale bar = 10  $\mu$ m

M40W, G41W and V45W barttin are very low expressed and biotinylation experiments predict that these mutants are retained intracellularly together with coexpressed hCIC-Ka. This is also confirmed by confocal imaging (Fig.25).

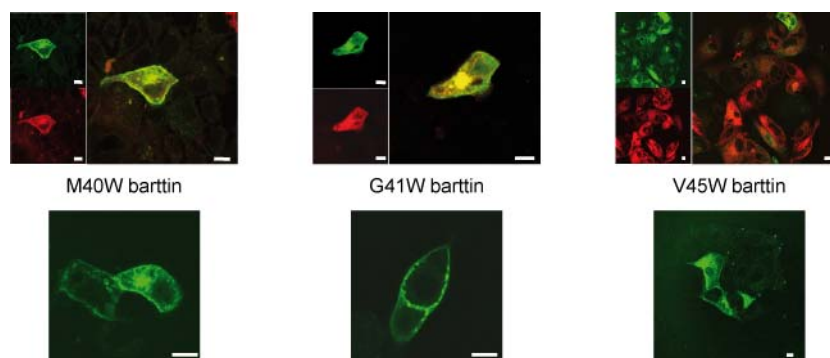


**Fig.25 Confocal images of MDCKII cells expressing M40W, G41W or V45W barttin (A) with or (B) without hCIC-Ka**  
Chaperone function of these three barttin (green) mutants seems to be impaired. Very low expression levels leave many questions. M40W barttin colocalize with hCIC-Ka in the plasma membrane, while hCIC-Ka (red) trafficking is impaired upon cotransfection with G41W and most severe with V45W barttin. The trafficking of barttin itself is impaired for V45W barttin. Scale bar = 10  $\mu$ m

Interruption of the chaperone function (Fig.25 upper lane) is obvious for G41W and V45W barttin and in full agreement with the results from biotinylation experiments. Membrane insertion of M40W barttin and coexpressed hCIC-Ka is not as obviously impaired as expected from biotinylation experiments, explaining the relatively large current amplitudes with respect to a very low M40W barttin expression.

Trafficking of M40W, G41W and V45W was also investigated in absence of hCIC-Ka (Fig.25 lower lane). Those confocal images show these barttins mainly in the cytoplasm. The trafficking of M40W barttin is distorted, but not entirely inhibited. In contrast, G41W barttin seems to be transported near, but not into the plasma membrane, whereas V45W barttin retains mainly in intracellular compartments.

Regular barttin trafficking, but loss of its chaperone function was observed for six mutations. Confocal images (Fig.26) are not well-suited to discriminate between hClC-Ka channels that are located close to the membrane and those channels that interact with barttin and insert into the membrane. However, we found clear intracellular staining originating from YFP-hClC-Ka and clear membrane staining from barttin-mCFP for mutations G15W, A20W, and G48W. Images for I12W, S52W and Q55W barttin display some overlapping YFP and CFP fluorescence in the plasma membrane. Electrophysiological recordings irrevocably predict a colocalization of hClC-Ka and S52W or Q55W barttin in the membrane. Nevertheless, there might be a partial loss of chaperone function.

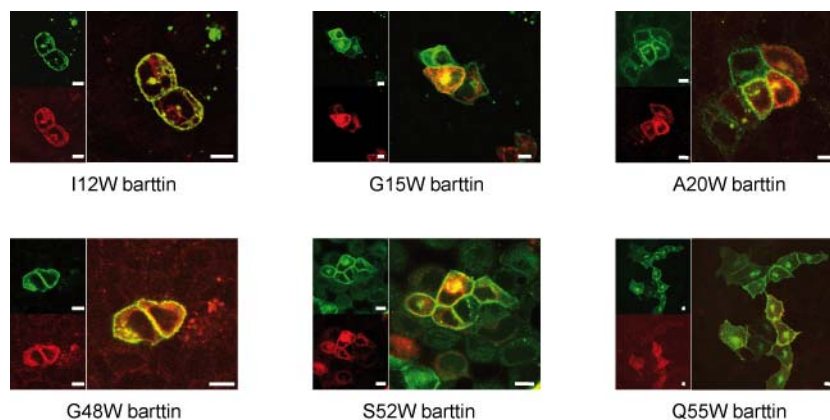


**Fig.26 Confocal images of MDCKII cells expressing hClC-Ka (red) and barttin mutants (green) with impaired chaperone function**

The six depicted barttin mutants were shown to transport less channel protein to the membrane (Fig.20+22). Confocal images support these findings. However, S52W and Q55W barttin colocalize with the channel in the membrane which is expected, because only these two barttins can activate hClC-Ka with unaltered pore properties. Scale bar = 10  $\mu$ m

For many barttin mutants, expression level and surface membrane insertion are not altered. Some barttin mutants (I9W, F11W, L16W, L19W, G35W, Y38W, A39W, S42W, V43W, I46W, I49W, I50W and M53W, confocal images not shown) activate hClC-Ka like WT barttin. However, there are a number of mutations that prevent activation of hClC-Ka, even though the interaction between  $\alpha$ - and  $\beta$ -subunits and channel insertion into the plasma membrane is not altered. Confocal images from hClC-Ka and these mutants (G10W, V13W, L14W, F17W, L18W, L21W, G22W, T23W, L25W, T36W, M44W or C54W) confirm the results of biotinylation experiments (Fig.20). Channel proteins and barttin are co-localized in the plasma membrane in Fig.27.

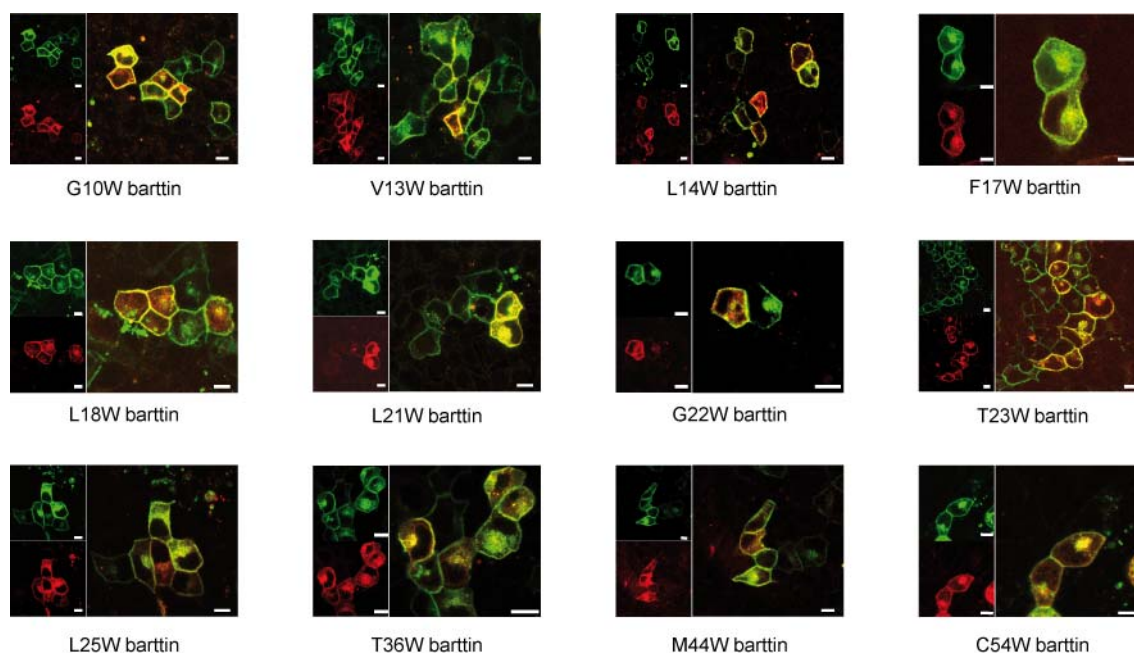


**Fig.27 Confocal images of MDCKII cells expressing hClC-Ka (red) and barttin mutants (green) that cannot activate the channel**

All of the here shown images confirm results of biotinylation (see Fig.20+22). Barttin and inactive hClC-Ka are in the plasma membrane. Scale bar = 10  $\mu$ m

Fig.28 summarizes the results of tryptophan substitution in a topology model of barttin. White circles represent residues that result in fully functional barttin proteins after substitution to tryptophan. F24W and M26W barttin (dark grey circles) are misfolded or degraded and thus abolish hClC-Ka/barttin currents. Red circles mark mutants with an impaired chaperone function. S52W and Q55W are labeled in red and white for their ability to produce considerable current amplitudes through interaction with hClC-Ka, even though the interaction with the channel protein seems to be altered. Mutations that produce trafficking deficient barttins are displayed with green circles. Here again M40W is labeled green and white, since it allows some membrane insertion resulting in notable current amplitudes of hClC-Ka/barttin. The remaining residues that prevent hClC-Ka currents are labeled with yellow circles. Substitution of these residues by tryptophan is assumed to impair exclusively the gating of hClC-Ka.

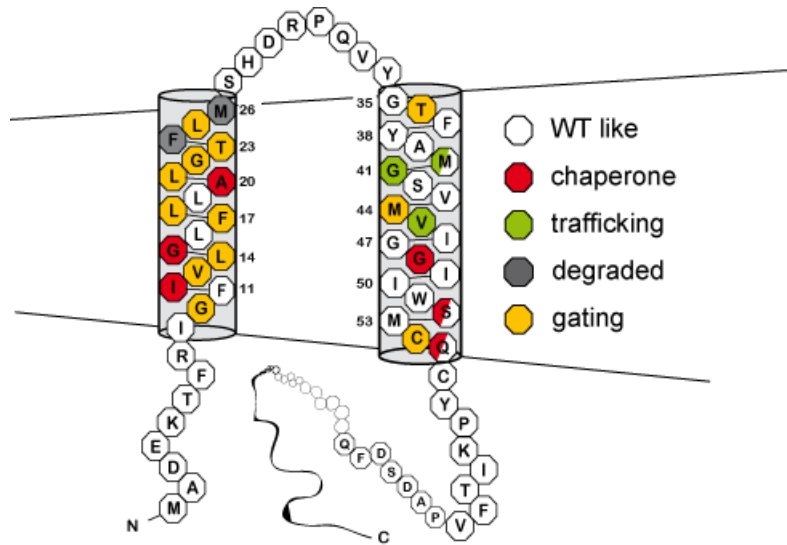


**Fig.28 Topology model of barttin and its functional determinants on hClC-Ka**

Two proposed transmembrane helices are illustrated by grey cylinders. Straight lines indicate the plasma membrane. N- and C-terminal of barttin are intracellular. By color coding residues, the effects on function are demonstrated. Residues marked in white can be substituted to tryptophan without any loss of function. F24 and M26 are needed for stability (dark grey). Residues 40, 41 and 45 are important for barttin trafficking (green). I12, G15, A20, G48, S52 and Q55 are needed for chaperone function (red). Residues marked in yellow avoid activation of hClC-Ka.

## **3.2 V166E rClC-K1 and the effects of barttin and barttin mutants**

### **3.2.1 Barttin modifies gating of V166E rClC-K1**

rClC-K1 is the rodent ortholog of hClC-Ka. This channel is active even without barttin (Adachi et al. 1994, Kieferle et al. 1994, Uchida et al. 1996, Scholl et al. 2006). The mutation V166E introduces the so called 'gating glutamate' that is lacking in ClC-K channels (Waldegger and Jentsch 2000). This mutation leads to prominent changes in gating behavior of the channel, especially in presence of barttin (Fischer et al. 2010). In whole cell patch clamp current recordings of HEK293T cells expressing V166E rClC-K1 without barttin, two gating processes can be seen (Fig.29 A).

A fast gate opens at positive and closes at negative potentials. After a holding potential of 0 mV, the fast gate closure at hyperpolarizing potentials is almost entirely masked by the slow gate that is closed at the holding potential. The slow gate opens at hyperpolarizing and closes at depolarizing potentials. To investigate gating properties of V166E rClC-K1, voltage steps between -155 and +125 mV were applied each followed by a test pulse to -125 mV. After a prepulse to -155 mV, voltage step to -125 mV illustrate both the fast and the slow gating process, since there is a fast activation followed by a slow deactivation (Fig.29A lower inset). Assuming that the two gates move independently, the two gating processes can be separated by introducing a short interpulse to +180 mV (5 msec) prior to the test pulse (upper inset Fig.29A). Such an interpulse opens the fast gate but leaves the slow gate nearly unaffected (Fischer et al. 2010). In this case, the instantaneous test pulse current amplitude is only dependent on the steady state slow gate open probability that has been reached during the long prepulses of varying potentials. Then, the open probability of the fast gate  $p_{\text{fast gate}}$  can be calculated by dividing the total channel open probability  $p_{\text{channel}}$  by its slow gate open probability  $p_{\text{slow gate}}$  (eq.3, material and methods).

Fig.29C shows the activation curves of V166E rClC-K1 channels in absence of WT barttin depicting the described gating processes. Without barttin, V166E rClC-K1 activates bidirectionally. Boltzmann functions (eq.2 and 4) have been fit to the activation curves of the channel as well as to the slow and fast gate yielding values for  $V_{0.5}$ , the voltage of half-maximal activation, of  $-96.1 \pm 3.4$  mV for the entire channel,  $-105.5 \pm 4.2$  mV for the slow gate and  $+67.7 \pm 7.4$  mV for the fast gate.

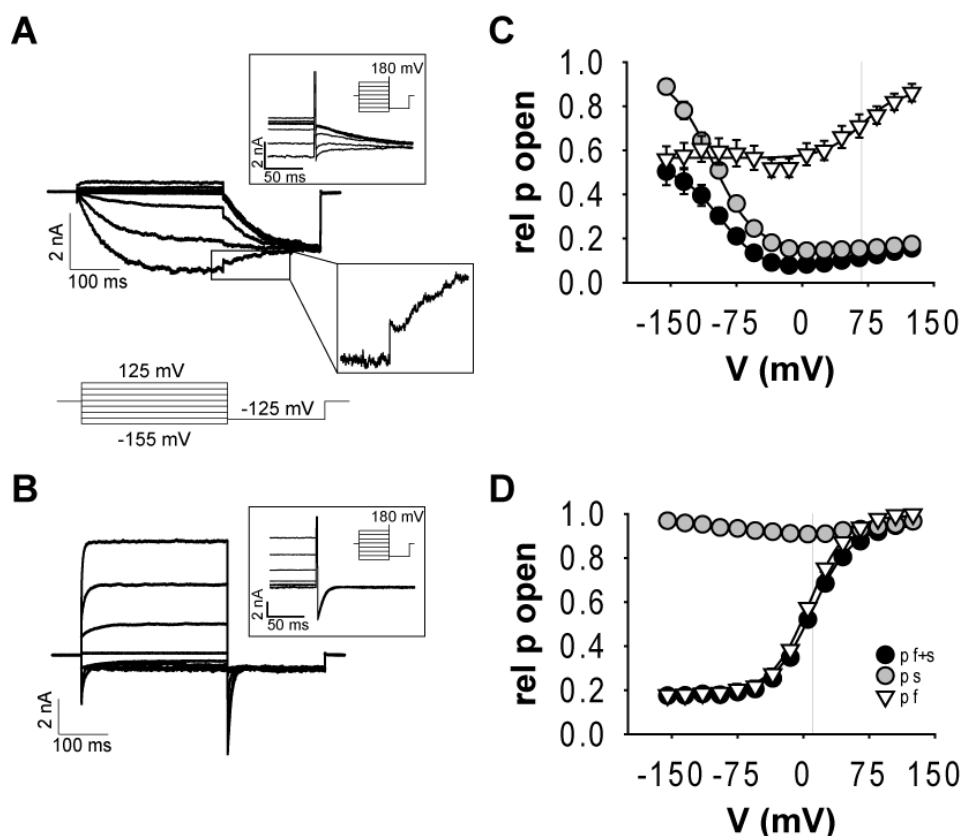


**Fig.29 Whole cell patch clamp recordings of HEK293T cell expressing (A) V166E rCLC-K1 alone, or (B) together with WT barttin and corresponding activation curves (C+D)**

Without barttin, V166E rCLC-K1 activates bidirectional with a fast opening at positive and a slow opening at negative potentials. Both gating processes can be seen after a voltage jump from -155 mV to -125 mV (lower inset in A). The current amplitudes immediately after the voltage jump are plotted versus the voltage of the prepulse. Fitting procedure with Boltzmann functions leads to (C) relative open probabilities of the entire channel ( $p_{f+s}$ ). The relative open probability of the slow gate ( $p_s$ ) can be determined by the set of a short interpulse that entirely opens the fast gate (upper inset in A). The resulting current amplitude immediately after the voltage jump to -125 mV is then only dependent on the prepulse initiated opening state of the slow gate. Plot of the current amplitude of the test pulse versus the voltage of the prepulse and normalization to the maximum of the Boltzmann fit results in  $p_s$ . The relative open probability of the fast gate can be calculated by dividing  $p_{f+s}$  by  $p_s$  (see text and eq.3). Without barttin, the slow gate (grey circles) closes under depolarizing conditions.

(B) Upon barttin binding, the channel mainly propagates a chloride inward current. Analog to A+C, voltage protocols (inset in B) and fitting procedures lead to (D) activation curves. The slow gate is set open over the whole measured voltage range. Barttin also shifts the activation curve of the fast gate to the left (light grey line in C and D).

Data of activation curves are mean  $\pm$  S.E.;  $n = 17$  cells expressing channel only,  $n = 14$  for cells coexpressing channel and WT barttin.

WT barttin (Fig.29B+D) locks the slow gate to an open state (changes in relative open probability are less than 7 % over the measured voltage range) and changes the voltage dependence of fast gating. V166E rCLC-K1/barttin is activated only monodirectionally with a  $V_{0.5}$  of  $+11.5 \pm 1.1$  mV, mainly depending on the fast gate activity. The changes in relative open probability of the slow gate are minimized with an unaltered  $V_{0.5}$  of  $-103.4 \pm 7.4$  mV.  $V_{0.5}$  of the fast gate activation dramatically shifts by about 60 mV to  $+7.4 \pm 0.9$  mV, a value that shows that the channel activity is mainly or only dependent on the fast gate activity.

The fast gate activation is left-shifted and faster than without barttin. Current traces at +125 mV can be fit with mono-exponential functions (eq.5) which results in values  $\tau$  corresponding to the time course of activation. Without barttin we obtained a  $\tau$  of  $7.7 \pm 1.5$  ms which is shifted to  $+2.6 \pm 0.2$  ms in presence of barttin.

To sum up, WT barttin affects V166E rClC-K1 gating in several ways. The open probability of the slow gate is no longer voltage dependent and set to an open state. This and additional effects on fast gating were used as criteria to examine the interaction of V166E rClC-K1 with barttin mutants.

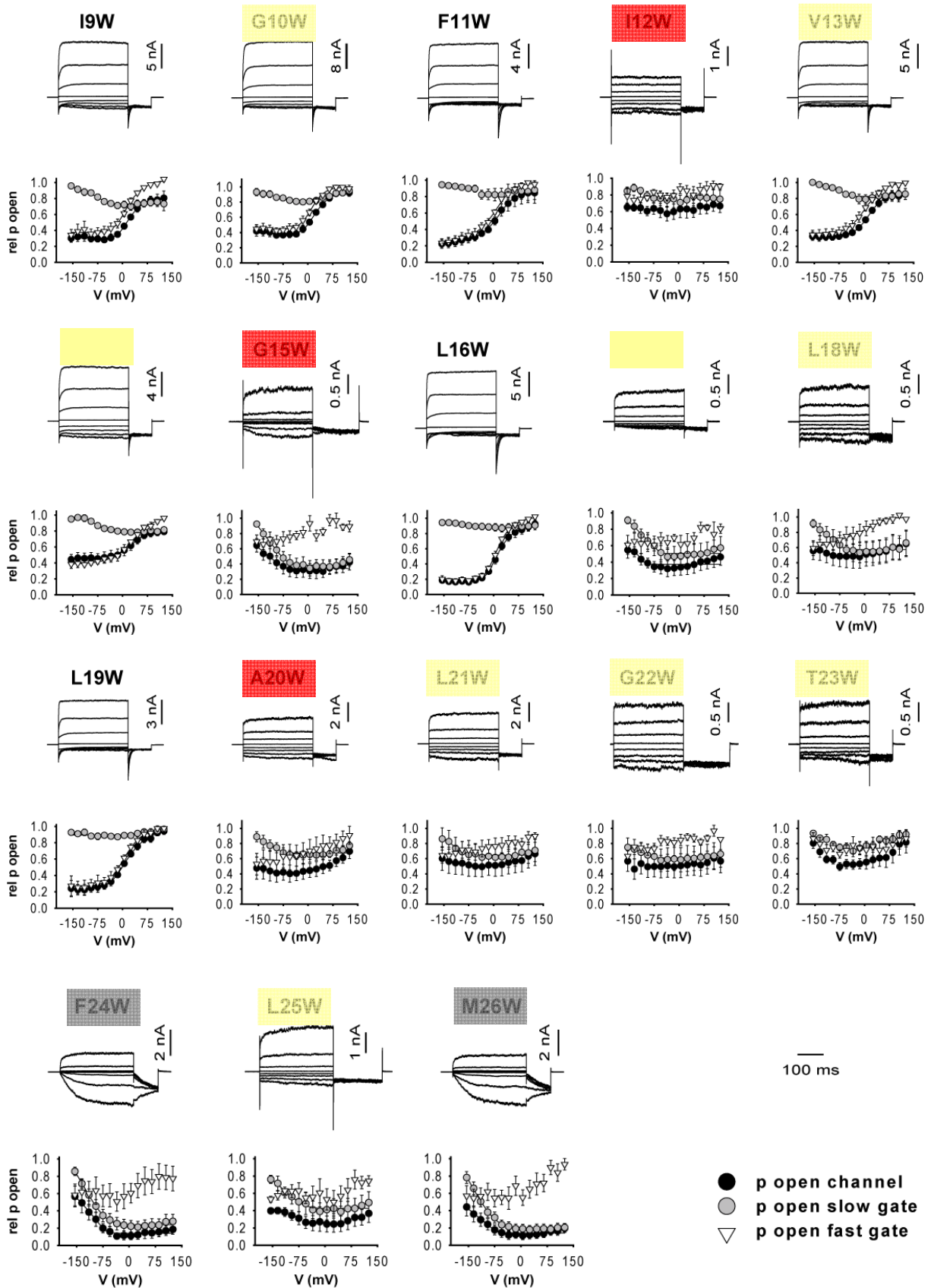
### **3.2.2 Mutant barttins interact with V166E rClC-K1 - and many alter the gating**

Fig. 30 and 31 show representative whole cell current recordings and activation curves of HEK293T cells co-expressing V166E rClC-K1 with barttin mutated within the first and second transmembrane helix, TM1 and TM2. Activation curves depict the voltage dependence of the channel (black circles) and the two gates (white triangles = fast gate, grey circles = slow gate). By color coding the letters, the here depicted current traces and activation curves measured with V166E rClC-K1 are compared with the results found for hClC-Ka (white = not affected, green = trafficking deficient barttin, red = partial loss of chaperone function, grey = degraded barttin, yellow = no activation of hClC-Ka). These two figures give a first overview of the effects of mutant barttins on the rodent channel homolog. Further analyses to quantify open probabilities,  $V_{0.5}$  and time constants of activation reveal deeper insights into functional determinants within the primary structure of barttin.

Many mutations in TM1 of barttin lead to dysfunction of V166E rClC-K1/barttin channels. Since F24W and M26W barttin are degraded (Fig.18), V166E rClC-K1 currents and activation curves in presence of these mutants do not differ from measurements in absence of barttin.

The rodent channel shows dramatically reduced current amplitudes in presence of I12W, G15W, F17W, L18W, A20W, L21W, G22W, T23W and L25W barttin. Since current amplitudes are smaller than in absence of barttin and time dependent gating is often diminished, there must be an interaction with inhibitory effect between these barttin mutants and the pore-forming subunit. Compared with the results found with hClC-Ka, chaperone-function deficient barttin mutations I12W, G15W and A20W still allow interaction with V166E rClC-K1.





**Fig.30 Representative whole cell current recordings of HEK293T cells coexpressing V166E rCIC-K1 with barttins that were mutated within TM1**

Activation curves depict the voltage dependence of the channel modified by mentioned barttin, separated by gates. All hCIC-Ka-activating barttin mutants (left in white) seem to regulate V166E rCIC-K1 like WT barttin. In correspondence to the results with hCIC-Ka, red boxes highlight residues with a reduction in chaperone function, grey boxes mark misfolded or degraded barttins whereas yellow marks illustrate gating deficient barttin mutants. All marked residues evoke altered regulation of V166E rCIC-K1 as well. G10W, V13W and L14W barttin failed to open hCIC-Ka, but the regulation of the rodent channel has tendencies to be like the regulation of WT barttin.



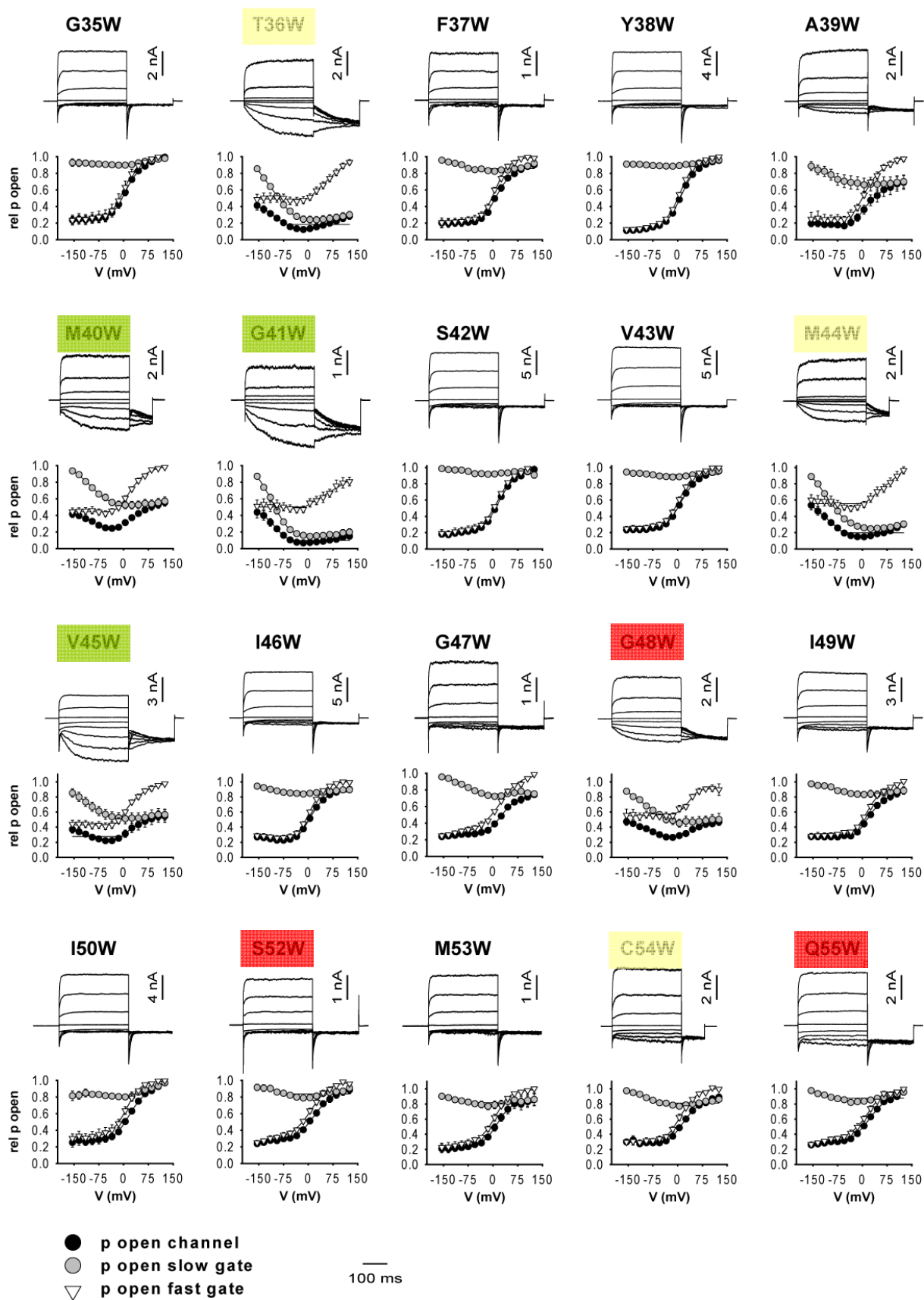


**Fig.31** Representative whole cell current recordings of HEK293T cells coexpressing V166E rClC-K1 with barttins that were mutated within TM2

Activation curves depict the voltage dependence of the channel modified by mentioned barttin, separated by gates. Almost all hClC-Ka activating barttin mutants seem to regulate V166E rClC-K1 like WT barttin. Only A39W, M40W, G47W, I49W and Q55W barttin appear to evoke alternate gating of the rodent channel. None-hClC-Ka activating barttins (T36W, G41W, M44W, V45W, G48W and C54W barttin) also fail to regulate V166E rClC-K1 like WT barttin. The color code of the boxes is analog to Fig.30.

Voltage dependent gating over the entire measured voltage range can only be seen for seven barttin mutants (I9W, G10W, F11W, V13W, L14W, L16W and L19W barttin). Of those, I9W, F11W, L16W and L19W barttin also activate hCIC-Ka. However, gating of V166E rCIC-K1 seems to be altered with I9W barttin that provokes currents like G10W, V13W and L14W barttin. These barttins do not lock the slow gate to an open state over the measured voltage range and/or they exhibit altered fast gate regulation.

Substitution of amino acids of TM2 left the function of barttin often unaltered. At first sight, barttin function is conserved for mutations G35W, F37W, Y38W, S42W, V43W, I46W, I50W, S52W and M53W. All barttins evoke currents with clear gating at negative and positive potentials. Upon coexpression with T36W, M40W, G41W, M44W, V45W and G48W barttin, time dependent current relaxations are similar to V166E rCIC-K1 in absence of barttin. Of those mutants, only M40W barttin activates hCIC-Ka. A39W, G47W, I49W, C54W and Q55W barttin do not entirely open the slow gate, as seen by activation at negative potentials. Of those, only C54W barttin fails to activate hCIC-Ka.

### 3.2.3 Helix 1 is necessary for channel activation

Fig.32 compares mean steady state current amplitudes at +125 mV and -155 mV. Such a plot illustrates that the channel without barttin (V166E) mainly conducts at negative potentials, and that WT barttin (WT) inverts the voltage dependence of gating. Additionally, this figure shows the dramatically reduced mean current amplitudes evoked by many mutations, especially within TM1.

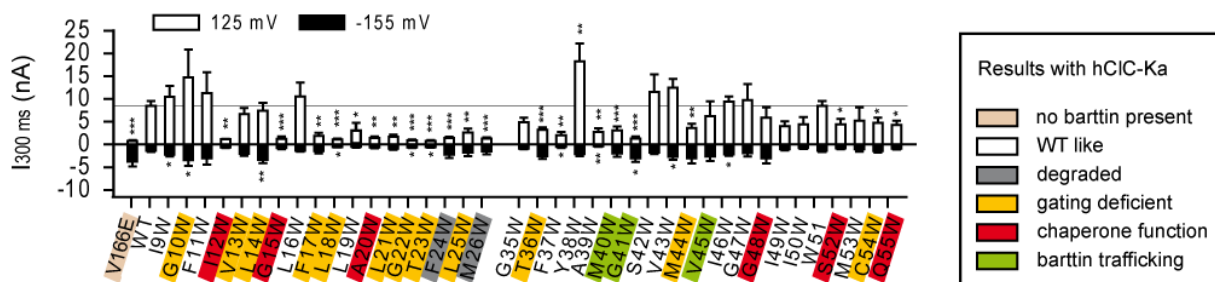


**Fig.32 Comparison of steady state mean macroscopic current amplitudes at -155 mV and 125 mV of HEK293T cells coexpressing V166E rCIC-K1 and barttin**

Variations in current amplitude are often observed, as indicated with asterisks (student's t-test versus WT). At positive range, most often, a reduction in current amplitude is recorded. Especially mutations within helix 1 have dramatic effects on channel activation. At negative range, an increase in current amplitude corresponds to slow gate opening. By color-coding the letters (legend in box), the results of both channel orthologs can be compared. All data are mean  $\pm$  s.e.;  $n \geq 4$  (\*  $p < 0.05$ , \*\*  $p < 0.01$ , \*\*\*  $p < 0.001$ ).

Residues whose substitution to tryptophan lead to barttin degradation or gating (grey letters), trafficking (green) or chaperone function deficiency (red) for hClC-Ka (see box in Fig.32) all cause altered gating of V166E rClC-K1. Regarding the red labeled residues, there is no doubt about their interaction with V166E rClC-K1. The activation of the rodent channel homolog is hindered over nearly the entire measured voltage range coexpressed with I12W, G15W and A20W barttin. If these barttins did not interact with the channel, macroscopic currents like the ones seen in absence of barttin would be expected. G48W, S52W and Q55W barttin clearly bind to the channel, as shown by the stronger activation at positive than at negative potentials. The results for barttin mutants that failed to activate hClC-Ka (yellow letters) are diverse, but all seem to interact with V166E rClC-K1, as shown by gating regulation (G10W, V13W, L14W, and C54W barttin) or low mean current amplitudes (F17W, L18W, A20W, L21W, G22W, T23W and L25W barttin). T36W and M44W barttin seem to interact, too, as they evoke strong activation of the channel at positive potentials.

The absolute values of mean current amplitudes are not sufficient to describe the effect of tryptophan insertion on gating. For example, L19W barttin exhibits small current amplitudes, but modifies channel gating like WT barttin. In contrast, L14W barttin evoke large currents at positive potentials, but the slow gate is not set to an open state over the entire voltage range as seen at negative potentials. We therefore analyzed the regulation of gating in more detail.

### **3.2.4 Functional determinants important for slow gating of V166E rClC-K1**

The voltage dependence of relative slow gate open probabilities was fit with Boltzmann functions. From these functions, the minimal and maximal relative open probabilities were obtained. We display the range of voltage dependent changes (Fig.33) by calculating the difference between the minimal and maximal open probabilities ( $\Delta p_{\text{open}}$ ). For some mutants, the fitting procedure was not reliable (I12W, L21W, G22W, T23W). In this case we simply subtracted minimal and maximal values of open probabilities obtained in the voltage range between -155 mV and +125 mV. Blue and black colored bars represent barttin mutations that significantly differ in their slow gate activation of V166E rClC-K1 from WT barttin. When slow gate activation is additionally not distinguishable from V166E rClC-K1 in absence of barttin, bars are labeled in black. These mutants are either misfolded or degraded (F24W,

M26W) or lost the capability of slow gate regulation (T36W, G41W and M44W). It appears as if they can no longer bind to the channel or fail to regulate its gating. White bars represent mutations that similarly activate the slow gate as WT barttin. Letters of the residues have been color-coded to compare the results with the effects on hCIC-Ka.

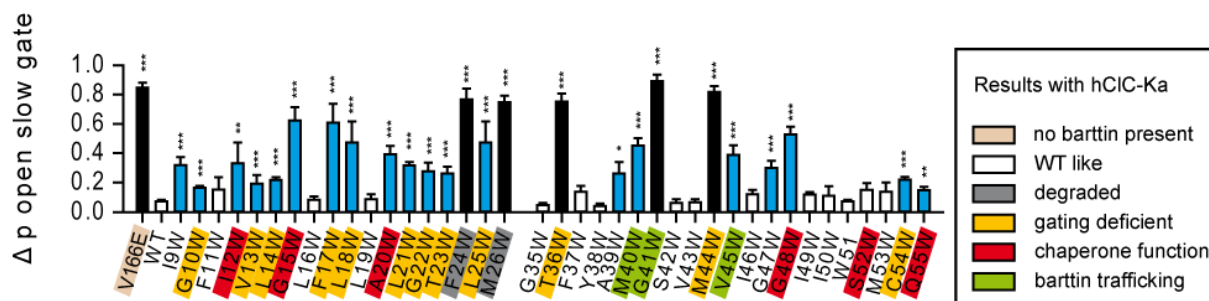


**Fig.33 Changes in relative open probabilities of the slow gate**

Mutants marked with black bars have no effect on the slow gate, while white marked residues behave like WT barttin. Blue marked residues show significant differences to V166E and WT (channel alone or in presence of WT barttin). Mutants marked with asterisks exhibit significant differences to values found in presence of WT barttin. All data are mean  $\pm$  s.e.;  $n \geq 4$  (\*  $p < 0.05$ , \*\*  $p < 0.01$ , \*\*\*  $p < 0.001$ ). Color-code of the letters compares the results with the results found with hCIC-Ka.

The results for the two channels superimpose almost perfectly. hCIC-Ka activating mutations behave like WT barttin on V166E rCIC-K1 as well. Exceptions are I9W, A39W and G47W barttin that do not completely open the slow gate in V166E-rCIC-K1, but activate hCIC-Ka. Barttins that do not appropriately regulate hCIC-Ka (marked in colored letters) also exhibit a deficient slow gate regulation in V166E rCIC-K1.

S52W barttin completely opens the slow gate of V166E rCIC-K1, despite showing the biggest defect in chaperone function on hCIC-Ka. All other chaperone function reducing mutations (red letters in Fig.33) modify slow gating of V166E rCIC-K1, hence not like WT barttin. This indicates again that the interaction of these barttins with the  $\alpha$ -subunit (rodent and human version) is not completely inhibited.

The analysis of the changes of the relative slow gate open probability demonstrates that almost the entire first helix is needed for accurate slow gating, although the activation curves are often hard to evaluate. Only for three mutants the function could be conserved. In contrast to TM1, TM2 again is more resistant to mutations. However, T36, G41 and M44 seem to be crucial for slow gating. Upon substitution to tryptophan, coexpression of one of these barttin mutants results in slow gate regulation of V166E rCIC-K1 as if no barttin is present.

### 3.2.5 Many mutant barttins lower minimal fast gate open probability

We used the same fitting procedure to determine voltage-dependent changes in relative open probabilities of the fast gate ( $\Delta p_{\text{open}}$ ). Results are shown as bar charts in Fig.34. Again, white bars represent substitutions which conserve the function of barttin and blue bars represent barttin mutations that lead to significant differences in fast gate regulation compared with WT barttin or barttinless channels while black bars indicate that no difference to fast gate regulation in absence of barttin is recorded. Many fast gate activation curves cannot be fit with Boltzmann functions (I12W, G15W, F17W, L18W, A20W, L21W, G22W, T23W and L25W), because of low current amplitudes and lack of gating. In these cases, the difference between minimal and maximal values obtained between -155 mV and +125 mV were calculated. All of these barttins evoke changes in relative fast gate open probability comparable to V166E rClC-K1 without barttin (black bars) or even below (grey bars, I12W and L21W barttin) values observed when no barttin is present.

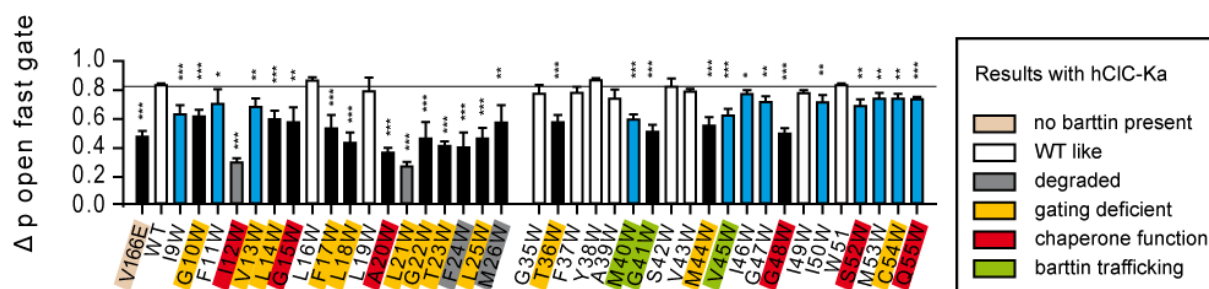


**Fig.34 Changes in relative open probabilities of the fast gate**

Mutants marked with black bars have no effect on the fast gate, while white marked residues behave like WT barttin. Blue marked residues raise the minimal fast gate open probability. Residues marked with grey bars hardly show any fast gating. Asterisks indicate significant differences to WT barttin. All data are mean  $\pm$  s.e.; n  $\geq$  4 (\* p<0.05, \*\* p<0.01, \*\*\* p<0.001). The color-code of the letters compares the results with those found with hClC-Ka.

Compared with the mean current amplitudes and slow gate activation curves (Fig. 32 and 30), it gets obvious that all of these nine barttin mutants keep the fast gate in an almost closed state at negative potentials. Hardly any gating – activation or deactivation – is seen after a voltage step from 0 mV to -155 mV. But at this voltage the slow gate has its highest open probability, as shown in the activation curves in Fig.30+31. Only tiny instantaneous and steady state currents are observed. Upon depolarizing voltage steps to +125 mV, most often a fast activation is recorded. However, the slow gate open probability is even lower. So, the slow gate cannot be the reason for missing currents at negative potentials. We assume that the fast gate of V166E rClC-K1 is kept closed over almost the entire measured voltage range when

one of the mentioned barttins is present. This group of fast gate closing mutants includes three barttin mutants that were reported to be chaperone-function deficient (I12W, G15W and A20W barttin). This discrepancy of results – missing interaction with hCIC-Ka and interaction with V166E rCIC-K1 - may be either explained by the fact that the human and the rodent channel are regulated in different ways or by the different expression systems. However, these results may be also explained by similarities. There is no entire loss-of-chaperone function, but only a partial and the few channels that are in the plasma membrane are closed by these three chaperone-function deficient barttins.

Coexpressing two of the three other chaperone-function deficient barttin mutants with V166E rCIC-K1 also suggests the mentioned partial loss-of-chaperone function. Fast gating can be observed over the measured voltage range. Whereas S52W and Q55W barttin regulate the fast gate almost like WT barttin, G48W barttin has no influence on fast gating. Only for G48W barttin, the observed gating of V166E rCIC-K1 can be explained with missing interaction.

All barttin mutants that exhibit altered regulation of hCIC-Ka do not regulate the fast gate of the rodent channel in WT barttin like fashion. But in contrast to slow gate regulation, more hCIC-Ka activating mutants fail to regulate the fast gate of the rodent homolog in appropriate way (F11W, I46W, I50W, S52W and M53W barttin). As shown in the next two passages, there are more barttin mutants that slightly but significantly alter properties of only the fast gate. All of these barttins are subsequently summed in a table (Tab.16).

In summary, TM1 is crucial for fast gating. Binding to the rodent channel is never inhibited by a substitution of a amino acid of TM1 to tryptophan. But regulation of fast gating is conserved only for two mutations (L16W and L19W). Upon coexpression with I9W, G10W, F11W, V13W and L14W barttin channel activation over the measured voltage range is observed, in contrast to the rest of TM1 tryptophan substitutions. Many substitutions to tryptophan within TM1 lead to a closure of the channel, probably because the fast gate remains closed over almost the entire measured voltage range. For substitutions within TM1, hCIC-Ka activation could only be recorded with I9W, F11W, L16W and L19W barttin.

Fewer mutations within TM2 than within TM1 hinder fast gate regulation. Eight mutations do not change fast gate regulation compared to WT barttin. For T36W, G41W, M44W and G48W barttin, the activation curves of the fast gate could be fit with Boltzmann functions, but the fast gate of V166E rCIC-K1 is regulated as if no barttin is present. So, binding of these barttins to the rodent channel cannot be prompted with instance. Low expressing M40W and

V45W barttin raise the changes in fast gate open probability compared to channels without barttin. Same holds true for I46W, G47W, I50W, S52W, M53W, C54W and Q55W barttin, but the macroscopic currents only show little, but significant changes, when compared to those in presence of WT barttin. Of these mentioned substitutions in TM2, T36W, G41W, M44W, V45W, G48W and C54W barttin fail to activate hCIC-Ka.

### 3.2.6 Many mutations of barttin vary the voltage dependence of the fast, but not of the slow gate of V166E rCIC-K1

WT barttin not only modifies the minimal and maximal open probabilities of V166E rCIC-K1, but also shifts the activation curve of the fast gate. We fitted the fast and slow gate activation curves with Boltzmann functions (eq.2+4) and determined the voltage of half-maximal activation  $V_{0.5}$ . WT Barttin shifts the activation curve of the fast gate to a voltage close to the reversal potential ( $+67.7 \pm 7.4$  mV without and  $+7.4 \pm 0.9$  mV with barttin), while  $V_{0.5}$  of the slow gate remains unchanged (around -104 mV with and without barttin). Fig.35 sums the effects of mutant barttins on  $V_{0.5}$  of the fast and slow gate in bar charts. The color code is identical to the previous figures. For nine mutants  $V_{0.5}$  of the fast gate could not be determined (n.d.). Low current amplitudes and lack of gating avoided fitting procedure. These mutants were shown to prevent fast deactivation at negative potentials. Some of them allow fast gate activation at very positive potentials. Within TM2 of barttin, T36 and the center of the helix, especially M44, seem to be essential for the voltage dependence of fast gating.

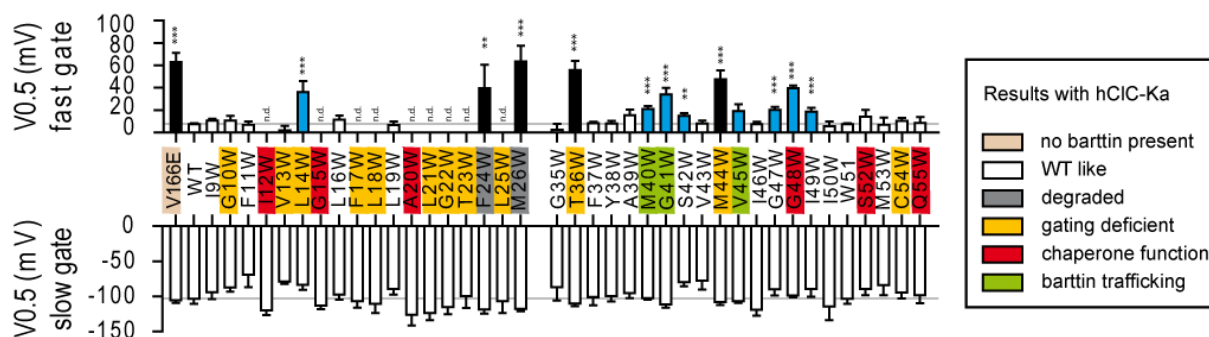


**Fig.35 Effect of barttin mutation on activation of the slow and the fast gate**

$V_{0.5}$  of the slow gate is never shifted. Mutants marked with black bars have no effect on the fast gate, while white marked residues behave like WT barttin. Blue marked residues shift the fast gate in none WT barttin-like fashion.  $V_{0.5}$  could not be determined for mutations marked with n.d. = not determinable. Asterisks indicate significant differences to WT barttin. All data are mean  $\pm$  s.e.;  $n \geq 4$  (\*  $p < 0.05$ , \*\*  $p < 0.01$ , \*\*\*  $p < 0.001$ ). The color-code of the letters compares the results with those found with hCIC-Ka.

The mutant barttins earlier claimed to exhibit only small changes in relative open probabilities of the fast gate (I46W, I50W, S52W, M53W, C54W and Q55W barttin) do not show significant differences in respect to the shift of the activation curve. Therefore, the role of these residues in fast gate regulation is a minor one. Same could hold true for I9W, G10W, F11W and V13W barttin as well.  $V_{0.5}$  of the fast gate is shifted to a level obtained with WT barttin. But the earlier unsuspecting mutants S42W and I49W barttin, now exhibit a slight, but significant rightward-shift of  $V_{0.5}$ . Of these twelve barttins mentioned above, only G10W, V13W and C54W barttin fail to activate hClC-Ka. All other non-activating barttin mutants do not regulate the fast gate of V166E rClC-K1 like WT barttin. The role of G47W barttin is not clear. This barttin exhibit altered slow and fast gating of V166E rClC-K1, but activates hClC-Ka.

### **3.2.7 Summary: Topology models of the effects of substitution on V166E rClC-K1 and hClC-Ka**

In two topology models (Fig.36), the results of mutant barttins on hClC-Ka (A) and gating regulation of V166E rClC-K1 (B) are summarized. White circles represent barttin mutants that behave like WT barttin and black circles represent degraded or misfolded barttin mutants in both models. The model on the left hand side comprises effects on hClC-Ka. Red circles represent barttin mutants with deficits in chaperone-function and green circles indicate trafficking deficiency. Orange circles group barttins that fail to activate hClC-Ka for unknown reason. We presume impaired gating properties; however we cannot distinguish between effects on slow or fast gate regulation of hClC-Ka.

In the model on the right hand side, displaying the effects on V166E rClC-K1, grey circles represent barttins that are non-functional. They do not show any effect on the channel. Dark blue circles represent residues that keep the fast gate almost closed over the entire voltage range and light blue circles indicate residues which evoke altered slow and fast gating. Yellow marked residues evoke marginal, but significant differences in fast gating, only. A39W barttin is the only mutant that solely alters slow gate regulation (red circle).



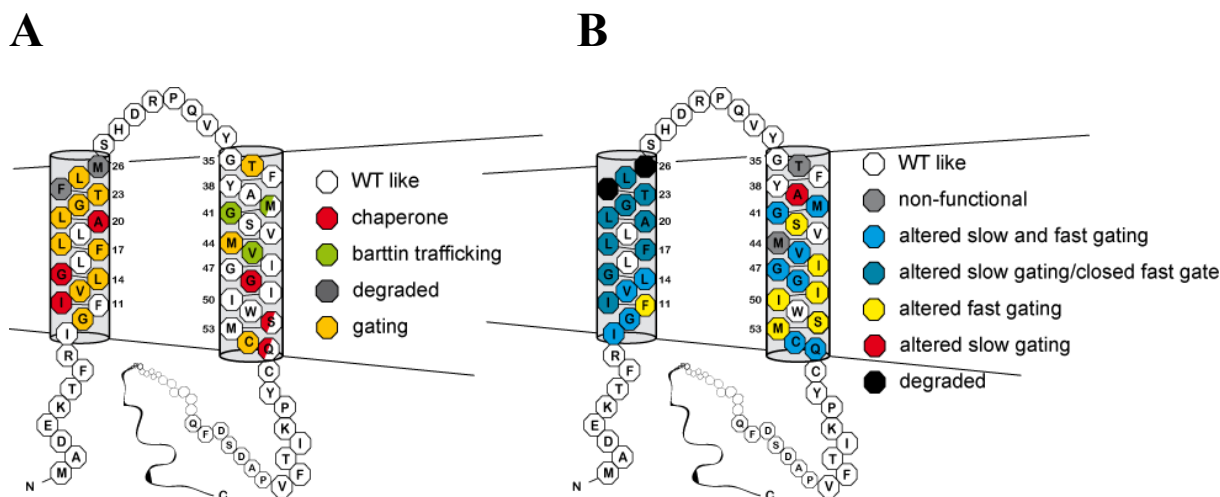


**Fig.36 Topology models of barttin and the effects of substituted residues on the hCIC-Ka (left) or V166E rCIC-K1 (right)**  
 Different effects caused by the substitution of an amino acid within the two transmembrane helices to tryptophan were observed. Color-coding the residues illustrate these effects as indicated.

Within TM1, two mutations left barttin function unaltered with hCIC-Ka and V166E rCIC-K1 (L16W and L19W). Two barttins are degraded or misfolded (F24W and M26W). The other barttin mutations within the first helix can be divided into two bigger groups. Mutants that activate V166E rCIC-K1 (I9W, G10W, F11W, V13W and L14W; only I9W and F11W activate hCIC-Ka) and mutants that keep the rodent and human channel closed over almost the entire voltage range (I12W, G15W, F17W, L18W, A20W, L21W, G22W, T23W and L25W).

Helix two is more resistant to tryptophan substitution. Tryptophan replacing G35, F37, Y38 or V43 leaves the function of barttin on both types of CIC channel unchanged. A39W barttin only fails to lock the slow gate of V166E rCIC-K1 into an open state, whereas the fast gate is regulated in WT barttin like fashion. It insignificantly decreases the current amplitude of hCIC-Ka, presumably caused by reduced expression. Gating of hCIC-Ka seems to be unaffected.

All results of co-expressed CIC-K1/barttin mutation T36W and M44W are comparable to those when no barttin is present. Residues marked in blue (M40W, G41W, V45W, G47W, G48W, C54W and Q55W) alter slow and fast gating, but at different degrees. While the macroscopic currents of G47W, C54W and Q55W barttin coexpressed with V166E rCIC-K1 look similar to WT barttin, macroscopic currents evoked by M40W, G41W, V45W and G48W barttin hardly show differences to the ones in absence of barttin.

The group labeled in light blue is quite inhomogeneous. Both gates of the channel are modified by the marked barttins, but the degree of functionality differs a lot, as shown in Tab.15.

	$\Delta p_{\text{open}}$ slow gate (%)	$\Delta p_{\text{open}}$ fast gate (%)	$V_{0.5}$ fast gate (mV)	$\tau$ fast gate (ms)
V166E rClC-K1	84.7	46.0	67.7	7.7
WT barttin	6.9	81.5	7.4	2.4
I9W barttin	31.7	61.4	10.7	3.7
<i>G10W barttin</i>	16.3	60.0	10.6	5.3
<i>V13W barttin</i>	19.1	66.6	1.7	4.1
<i>L14W barttin</i>	21.3	58.1	36.1	4.8
M40W barttin	45.1	57.8	21.1	3.3
<i>G41W barttin</i>	89.1	49.3	34.0	8.2
<i>V45W barttin</i>	38.8	60.6	19.0	2.8
G47W barttin	29.9	69.9	20.3	4.5
<i>G48W barttin</i>	52.7	48.1	39.5	6.6
<i>C54W barttin</i>	21.9	72.2	10.2	3.9
Q55W barttin	14.7	71.8	8.5	5.3

**Tab.15 Comparison of WT barttin and barttin mutants that alter slow and fast gate regulation**

Changes in relative open probabilities of the fast and slow gate are shown together with  $V_{0.5}$  of the fast gate the time constant of fast gate activation at +125 mV. Barttins written in italic letters cannot activate hClC-Ka while the others can. I9W barttin has a lower impact on slow gating than G10W, V13W or L14W barttin while fast gate regulation of I9W and the non-hClC-Ka-activating barttin mutants are comparable. Different regulation of hClC-Ka and V166E rClC-K1 is likely to be caused by different structure of the channel proteins at opposing positions. Same could hold true for G47W barttin as well.

Significant changes to the results found for WT barttin are highlighted in grey. While for example G10W, V13W or Q55W barttin almost appear to act as WT barttin, other barttins in this group appear to have lost almost the entire functionality, like for example, M40W, G41W or G48W barttin. Fast gate regulation evoked by I9W barttin is comparable to the ones observed with G10W or V13W barttin. But I9W barttin even has a lower impact on the slow gate than the two other mentioned barttins. However, I9W barttin activates hClC-Ka. Compared with the results for hClC-Ka activation, it cannot be stated whether the slow or the fast gate regulation is essential for the activation of the human channel homolog.

This becomes even more obvious when comparing these results with those barttins that change the regulation of only one gate (Tab.16). The slow gate regulation of A39W barttin is hindered and comparable to the one of I9W barttin. Both barttins activate hClC-Ka in contrast to G10W, V13W or L14W barttin that have stronger effect on the slow gate. So, proper fast gate and aggravated slow gate regulation is no hindrance for hClC-Ka activation.

	$\Delta p_{\text{open}}$ slow gate (%)	$\Delta p_{\text{open}}$ fast gate (%)	$V_{0.5}$ fast gate (mV)	$\tau$ fast gate (ms)
V166E rClC-K1	84.7	46.0	67.7	7.7
WT barttin	6.9	81.5	7.4	2.4
F11W barttin	15.0	68.7	7.1	2.9
S42W barttin	5.9	80.5	15.0	3.2
I46W barttin	11.8	75.5	7.3	2.3
I49W barttin	11.7	76.1	18.7	3.2
I50W barttin	9.9	69.8	5.6	6.4
S52W barttin	14.9	67.2	14.0	4.2
M53W barttin	13.5	72.2	7.0	4.5
A39W barttin	26.1	72.2	15.4	2.6

**Tab.16 Comparison of WT barttin and barttin mutants that alter regulation of only one gate**

Changes in relative open probabilities of the fast and slow gate are shown together with  $V_{0.5}$  of the fast gate the time constant of activation at +125 mV. Significant deviations to the values found with WT barttin are marked in grey. All of the here shown barttins activate hClC-Ka. A39W is the only mutation that solely changes slow gate regulation. The macroscopic currents of V166E rClC-K1 in presence of the other denoted barttins appear like the ones recorded in presence of WT barttin. However, fast gate properties are changed. Comparison of the values for  $\Delta p_{\text{open}}$  fast gate and  $V_{0.5}$  fast gate measured for A39W barttin with the other barttins in this table emphasize the mild effect on gating regulation.

S42W, I46W, I49W, I50W, S52W and M53W change only fast gate properties of V166E rClC-K1. For four of them (I46W, I49W, I50W, S52W), the expression is reduced. As shown in Tab. 16, the changes compared to the values found for WT barttin are very small. Thus, it is not surprising that these six mutants regulate hClC-Ka channels like WT barttin.

These tables show that the deviations especially in appropriate fast gating are moderate for some mutations. Neglecting the minor changes of yellow labeled residues in Fig. 36B, the two topology models would superimpose almost perfectly. Exceptions are I9W, A39W and G47W barttin that activate hClC-Ka, but exhibit altered gating of V166E rClC-K1.

## 4 Discussion

### 4.1 Effects of point mutations

In this study we investigated the interaction of ClC-K channels with their accessory subunit barttin that effects channel trafficking and gating. Using a systematic tryptophan scanning mutagenesis, we analyzed the impact of every single amino acid of the first and second transmembrane helix of barttin (TM1 and TM2) on channel function. By this methodology we presumed to find a small number of amino acids in the barttin protein that represent essential sites for binding to the alpha subunits of the channel protein. However, an unexpected large number of point mutations altered the function of barttin, as shown in Fig. 36. We found couple of amino acids to be crucial for the stability, trafficking or chaperone function of barttin, as well as several residues that may play a major role in channel activation/gating regulation. While almost the entire TM1 mainly contributes to fast gate regulation, several amino acids of TM2 are needed for slow gating.

Two residues at the extracellular ending of TM1 are crucial for the stability or structure of the protein. Upon substitutions **F24W** and **M26W**, barttin cannot be detected as full length protein. Degradation of all built proteins is demonstrated (Fig.18). As expected, coexpression of one of these barttins with hClC-Ka or V166E rClC-K1 did not modify channel properties.

Whole cell current recordings of V166E rClC-K1 and hClC-Ka in presence of **T36W** or **M44W** barttin lead to macroscopic currents similar to those in absence of barttin. Binding between barttin and the channel subunit seems to be impaired at first glance. However, confocal images and moreover biotinylation assay impressively assure the interaction with hClC-Ka. These two residues then must be crucial for gating/activation of ClC-Ka. Co-expressed with V166E rClC-K1, there is no electrophysiological result that allows a statement on interaction. All evaluations of the macroscopic currents are similar to those when no barttin is present. However, gating and not interaction with V166E rClC-K1 and hClC-Ka seems to be hindered upon substitution of T36 or M44 to tryptophan. It is likely that these barttins loosely bind to both channel orthologs, but gating regulation is interfered. Confocal imaging and biotinylation assays of hClC-Ka co-expressed with these barttin allow clearer statements on the interaction. Preliminary data concerning the interaction with V166E rClC-K1 is shown in Fig.48 as supplemental data. The interaction is assumed according to

confocal images. The chaperone function of barttin on V166E rClC-K1 seems to be conserved despite point mutations T36W or M44W within the structure of barttin. This indicates the necessity of these residues for channel gating.

**M40W, G41W and V45W** barttin are poorly expressed and travel hardly to the plasma membrane (Fig. 22). Co-expressed with hClC-Ka, interaction of M40W barttin is demonstrated by channel activation (Fig.12 and 13). Co-expressed with V166E rClC-K1, patch clamp recordings show that all three barttins do interact with the channel and modify gating. It remains unclear whether the results found for G41W barttin are caused by the mutation or by the low expression of this barttin. For M40W and V45W barttin, it was shown that selected cells for patch clamp recordings had barttin in excess at the plasma membrane. With these barttins, the time constant of channel activation at +125 mV is the same as for WT barttin (Fig.41, supplemental data). Therefore, the observed changes in gating modification are caused by the mutation of barttin and are not artificial due to low expression and/or trafficking distortion.

**I12W, G15W, A20W, G48W, S52W and Q55W** barttin evoked a significant reduction of channel protein in the plasma membrane, although trafficking of barttin itself is intact and barttin is expressed in such high levels that guarantee an excess of the subunit (Fig.20 and 22). Therefore, they are good candidates to form the binding interface between barttin and hClC-Ka. However, interaction is not completely inhibited upon substitution of one amino acid to tryptophan. When compared to G35W barttin that is rather low expressed, but favors hClC-Ka trafficking (rel. insertion level of 80%, Fig.22), the S52W mutation clearly hinders the chaperone function of barttin. Nevertheless, patch clamp recordings and confocal images prove the interaction of S52W barttin and ClC-Ka channels in the plasma membrane. Compromising, a partial loss-of-function is assumed for S52W, but as consequence as well for I12W, G15W, A20W, G48W and Q55W barttin. These barttins all bring a comparable or even bigger fraction of hClC-Ka protein into the plasma membrane compared to S52W barttin. Therefore we assume interaction of all of these barttins with hClC-Ka, while only S52W and Q55W barttin can open the human channel. For some unknown reason, the trafficking of ClC-Ka is impaired when co-expressed with one of these six barttins. Probably, the binding affinity is reduced upon substitution of one of those residues. While these barttins traffic more or less regularly to the plasma membrane, the amount of channels in the cytoplasm is higher. But still, a couple of barttin bound channels are inserted into the plasma

membrane. These results fit to already published data. Riazuddin et al. (2009) showed that a point mutation I12T barttin allows activation of hClC-Ka/Kb, but trafficking is impaired. Substitution of I12 to bulky tryptophan instead of threonine may not only impair chaperone function, but also channel activation. Same may hold true for the other small amino acids G15, A20 and G48. As part of the binding interface, these residues are supposed to face towards the channel protein. Upon substitution to tryptophan, binding is aggravated, but not inhibited. However, a fine mechanism for channel activation is heavily disordered.

It needs to be mentioned that in contrast to the patch clamp recordings, the experiments for surface membrane trafficking were performed with MDCKII cells which may have different regulation patterns.

If trafficking and gating of the rodent channel homolog is regulated in similar ways like the human channel, patch clamp recordings with V166E rClC-K1 additionally contradict missing interaction. I12W, G15W and A20W barttin avoid channel activation over almost the entire measured voltage range. If they could not bind to V166E rClC-K1, macroscopic currents similar to those when no barttin is present are expected. However, each of these three mutations closes the channel.

The three other chaperone-function deficient barttins also interact with the rodent channel homolog. For S52W and Q55W barttin,  $V_{0.5}$  of the fast gate and, in case of S52W barttin, as well  $\Delta p_{open}$  of the slow gate (Tab.15 and 16) is similar to the regulation of WT barttin. This only can be when barttin is in excess, and macroscopic currents are not a mixture of currents of barttin bound and unbound channels. For G48W barttin, the excessive binding of barttin to the channel protein in the plasma membrane cannot be assumed, although this barttin is sufficiently expressed and inserted into the surface membrane. But still, gating of the channel is influenced by G48W barttin, assuring that these two proteins bind to each other.

The mutation G48W, as well as the other five mentioned mutations, obviously decreases the binding affinity to at least hClC-Ka. The changes in gating of V166E rClC-K1 may be again explained by a circumstance that several residues are needed for gating regulation. Binding still can occur, because probably several amino acids participate in binding to the channel, but proper gating of the channel needs the correct interplay of these residues. One single point mutation within TM1 or TM2 is not enough to prevent binding, but to impair gating.

Concluding for these six barttin residues, we assume them to be part of the binding interface and they also participate in gating regulation. I12W, G15W and A20W barttin keep both channels closed, while S52W and Q55W barttin almost behave like WT barttin. The role of G48 on gating remains unsolved.

Many mutated barttins are still fully functional in regards of chaperone function, but fail to activate hClC-Ka. These residues are marked in orange in fig.36A. Most of them reside in TM1 and only a few in TM2. Due to different effects on V166E rClC-K1, these residues are divided into different groups - mutants that show no effect on V166E rClC-K1 (Fig. 36B, grey), mutants that close hClC-Ka and the fast gate of the rodent channel (dark blue), mutants with altered fast OR slow gating (yellow or red) and mutants with altered fast AND slow gating (light blue). The light blue group is the least homogeneous group. Some residues exhibit different function on hClC-Ka and V166E rClC-K1. These differences are probably due to different structures of the two orthologs, or, as shown in a recent study, post-translational modification of barttin plays a major role in hClC-Ka activation and V166E rClC-K1 gating regulation.

Palmitoylation of barttin was shown to be important for channel regulation, especially for hClC-Ka activation (Steinke et al., unpublished data). C54 and C56 are the only cysteines that are palmitoylated within the primary structure of barttin. A double mutant C54S/C56S fails to activate hClC-Ka. Reduction in palmitoylation level is observed for the single mutants and is correlated with lower current amplitudes of hClC-Ka. The palmitoylation of barttin at C54 and C56 is also reduced when G47 is substituted to arginine (Steinke et al., unpublished data). This dependence might contribute to the disease-causing effect of G47R barttin that reduces hClC-Ka/Kb currents (Janssen et al. 2009). It is possible that barttin with G47 substituted to tryptophan (G47W) is not properly palmitoylated as well. Current traces and open probabilities of V166E rClC-K1 coexpressed with G47R and G47W barttin appear similar and hClC-Ka is activated, but lower mean current amplitudes are evoked because of fewer active channels. C54W barttin abolishes hClC-Ka activation and this mutation does not fully open the slow gate of V166E rClC-K1 at positive potentials. This is likely to be caused by a reduction in palmitoylation level. Since acylation of tryptophan is impossible, only one palmitoylation site remains. In this study, bulky tryptophan at position 54 may hinder palmitoylation of C56, too.

So far, barttin palmitoylation has not been explored when Q55, the residue in between the two palmitoylation sites, was mutated. When Q55 is substituted by bulky tryptophan, it is possible that palmitoylation of C54 and/or C56 is impaired, because recognition of the substrate by palmitate transferases might be hindered.

**G47W, C54W and Q55W** most probable impair palmitoylation of barttin which is needed for hClC-Ka-activation and proper V166E rClC-K1 gating modulations thus explaining lower current amplitudes of hClC-Ka and altered gating of V166E rClC-K1.

Upon co-expression of **F17W**, **L18W**, **L21W**, **G22W**, **T23W** or **L25W** barttin with hCIC-Ka, no channel activation could be recorded. These mutants are different from other mutations that fail to activate hCIC-Ka, since the current amplitude remains small not only with the human, but also with the rodent channel homolog. Complexes are not retained in intracellular compartments as shown by biotinylation assays and confocal images. We assume a reduced open probability of human and rodent channel homolog when co-expressed with one of these barttin mutants.

Despite the small current amplitudes, activation curves with V166E rCIC-K1 could be determined providing unshifted slow gate activation curves.  $V_{0.5}$  of the fast gate could not be determined. Activation could only be seen at very positive potentials, indicating a rightward-shift of the fast gate activation curve. The slow gate is not kept open over the measured voltage range. The fact that at negative potentials hardly any activation of the channel is recorded, although the activation curves indicate an opened slow gate, leads to the assumption that the fast gate open probability is low and voltage independent at negative potentials. An explanation might be a rightwardly shifted activation curve or a dramatically reduced absolute open probability. Noise measurements or single channel recordings would reveal deeper insights in the absolute open probabilities as well as the asymmetric use of anions could reveal additional information, too.

I12W, G15W and A20W barttin exert similar effects on gating as the above described. Although they were already shown to be important for channel binding and trafficking, they play a role in gating regulation, too. If binding of these three barttins to V166E rCIC-K1 could not occur, currents similar to barttin-less channels are expected.

If the closure of the fast gate was additionally mediated via parts of TM2, analog results would have been observed upon substitution of a residue of TM2 to tryptophan. This is not the case. Due to the similar effects on gating regulation, we assume direct binding of amino acids I12, G15, F17, L18, A20, L21, G22, T23 and L25 of TM1 to CIC-K which is crucial for the voltage dependence of the fast gate.

In Fig. 36B, several residues **marked in light blue** alter fast and slow gate properties. These results are also listed in Tab. 15. The changes in function observed for G47W, C54W and Q55W barttin were already discussed as palmitoylation level dependent. M40W and V45W barttin were already discussed to be necessary mainly for slow gating. G41W barttin was shown to be low expressed and G48W barttin was shown to exhibit a partial loss-of-chaperone function. Both mutations, G41W and G48W, could result in barttin-less channels in



the membrane and macroscopic currents that are a mixture of currents of barttin bound and unbound channels.

Only four barttins remain unexplained in this group of light blue labeled barttins. Due to careful selection of patch clamped cells, a mixture of currents is not very likely for **I9W**, **G10W**, **V13W** and **L14W** barttin. More convincing,  $V_{0.5}$  of the fast gate activation of V166E rClC-K1 (Fig.35) contradicts a mixture of currents for three of these barttins. Besides, the expression level of all four is high enough to guarantee an excess of barttin (see. Fig.15 and 21) and biotinylation assay reveals appropriate membrane insertion of these barttins and hClC-Ka (Fig.20). We therefore conclude that I9, G10, V13 but as well M40 and V45 exert an effect on gating. While the fast gate properties are almost similar to those observed in presence of WT barttin, the slow gate is not kept open at positive potentials. L14W barttin cause effects on gating of V166E rClC-K1 that could be the bridge to the effects observed for the mutants marked in dark blue as shown by the rightward-shift in fast gate activation (Fig.35). By listing these mutant barttins from the one that shows the biggest loss-of-function on slow gate regulation to the one which appears to reach almost the entire functionality of WT barttin (compare with Tab. 15), it gets obvious that the human and the rodent channel must be gated in different ways. In a row starting with M40W – V45W – I9W – L14W – V13W – G10W barttin, the latter three (and V45W) barttin do not activate hClC-Ka, although they nearly work like WT barttin on V166E rClC-K1. Different structures of the channels and therefore other regulatory mechanisms may be an explanation. But the different results found for hClC-Ka and V166E rClC-K1 can also be explained otherwise as described in following. Different post-translational modification may play a major role for the mentioned mutations within TM1. As shown in the work of Janssen et al. (2009), the disease-causing mutations R8L and G10S barttin evoke current traces and activation curves with V166E rClC-K1 similar to G47W/R or other palmitoylation aggravating barttin mutants (C54S or C56S, Steinke et al., unpublished data). And these macroscopic currents are similar to those measured with I9W, G10W, V13W and L14W barttin (Fig.30, Tab.15). However, Steinke et al. (unpublished data) found out that at least G10S is properly palmitoylated. Therefore, we assume this modification to take place for G10W barttin as well.

If changes in gating are not caused by a reduction in palmitoylation level, the changes in gating behavior may be due to endogenous processes of the expression system. Co-expressed in *Xenopus* oocytes, mean current amplitudes of hClC-Kb in presence of G10S barttin are comparable to the ones evoked by WT barttin (Estévez et al. 2001), in contrast to the found results with the expression in human cell lines (Janssen et al. 2009). This discrepancy between

HEK293T cells and oocytes indicates that this residue G10 is somehow implicated in another mechanism crucial for channel regulation which may also play a role for the differences between the regulation of hCIC-Ka and V166E rCIC-K1. One may speculate that in only one of the two expression systems, a binding to another component or a protein modification is mediated via G10 and/or neighboring residues occurs. This indicates that G10 is facing away from the channel protein and contradicts a direct effect of G10 on gating. As mentioned before, binding probably occurs via amino acids I12 and G15, amongst others. In contrast to G10W, V13W and L14W barttin, I9W barttin still allows hCIC-Ka activation because with this mutation, bulky tryptophan is too far away to sterically impair proper binding of I12 and G15.

No matter if there is an additional binding partner or not, we conclude that the N-terminal region of TM1 is needed for the human channel activation. Binding is never inhibited upon mutations I9W, G10W, V13W or L14W barttin, but I9W barttin shows the biggest deficits in V166E rCIC-K1 regulation although hCIC-Ka is activated. We assume different regulation due to different structure or modification of the channels.

Every third amino acid of an  $\alpha$ -helix is supposed to face to the same side. Helix-helix interaction therefore may take place via every third amino acid of a helix. But here, almost every residue in TM1 seems to be essential for channel regulation. This implies that TM1 may have several docking stations within the CIC-K channel protein.

**F11W, S42W, I46W, I49W, I50W, S52W and M53W** barttin are labeled in yellow in Fig.36B. These mutations evoke altered fast gating of V166E rCIC-K1. Differences to WT and WT-like barttin mutations (L16W, L19W, G35W, F37W, Y38W and V43W) in concerns of V166E rCIC-K1 regulation were only found for fast gate modulation. F11W, I46W, I50W, S52W and M53W barttin show significant changes in fast gate open probability, but changes still are bigger than 67 % (for WT barttin  $\Delta p_{\text{open}} \approx 81\%$ ). Regarding the time constants of fast gate activation at hyperpolarization (Fig.41, supplemental data), only I50W, S52W and M53W slow down the gating kinetics. S42W and I49W barttin only shift  $V_{0.5}$  of the fast gate to more positive potentials compared to WT barttin. This shift in  $V_{0.5}$  is of significant difference, but not bigger than the one observed for other mutant barttins like L16W or A39W.

All of those barttins activate hCIC-Ka, indicating that these mutations do not influence the pore of the human channel ortholog. The rodent channel, however, needs the intracellular

orientated half of TM2 and F11 for fast gate regulation, but because of the small changes, the role of these residues for gating is a minor.

**A39W** barttin is the only mutant that changes solely the regulation of the slow gate of the rodent channel (Fig.32+33 compared with Fig.34+35). The fast gate of V166E rClC-K1 is regulated in WT barttin fashion and hClC-Ka is activated. We therefore assume that proper slow gate activation is not the determining step in hClC-Ka activation. In addition to the results found for mutants that only alter the fast gate regulation, we can postulate that whether a inappropriate fast or slow gate regulation leads to impaired hClC-Ka activation, but the coordinated interplay of fast and slow gate is needed.

A39W, M40W and V45W barttin change mainly the slow gate regulation of V166E rClC-K1. This and the previous passage clarified the need of TM2 for fast and slow gating of V166E rClC-K1, but the effect on fast gating remains rather small.

## **4.2 Hypothesis of binding**

As mentioned in the introduction, the N-terminus, the transmembrane core and a short stretch after the transmembrane helices (I72X barttin, Janssen et al. 2009) of barttin is expected to regulate gating. Substitution of an amino acid of the transmembrane core to tryptophan often leads to altered gating. Tajima et al. (2007) showed that barttin binds to the B- and the J-helices of rClC-K2. These aspects and following thoughts lead to a hypothesis how barttin may bind to ClC-K channels.

The so-called gating glutamate is commonly accepted as the fast gate. In the crystal structure of *EcClC* (Fig.37), the B-helix of the channel is in close relationship of the gating glutamate E148. This residue is located at the beginning of the F-helix (Dutzler et al. 2003). A point mutation K231R ClC-1, corresponding to R147 in *EcClC*, leads to altered slow and fast gating (Fahlke et al. 1997, Gramkow et al., unpublished data). In ClC-5, corresponding residue (K210) is necessary for the selectivity of the pore (De Stefano et al. 2011). A recent study (Gradogna and Pusch 2013) has shown this residue in ClC-K channel (K165) to be sensitive to the extracellular pH.

In *Ec*CIC structure, the side chain of R147 is facing towards the B-helical residues D54 (1.8 Å) and V57 (4.2 Å). The B-helix is a proposed barttin binding site (Tajima et al. 2007). F53 (3.4 Å) and again V57 (4.4 Å) may coordinate L139, a residue in the loop between the E- and the F-helix. Another B-helical residue is likely to influence the positioning of the F-helix. The distance V46 to I158 is only 3.6 Å.

The B-helical residue D54 was shown to be essential for gating of CIC channels. In CIC-1, mutation of this residue to glycine (D136G) results in profound changes in the voltage dependence of gating (Fahlke et al. 1995). CIC-1 chloride channels usually show fast and slow gating as well. At hyperpolarizing potentials WT channels deactivate, but D136G hCIC-1 activates without exhibition of fast gating processes. This underlines the importance of this aspartate residue for fast gate regulation. However, substitution of aspartate by asparagine (D54N) in *Ec*CIC does not affect transport function (Accardi et al. 2005).

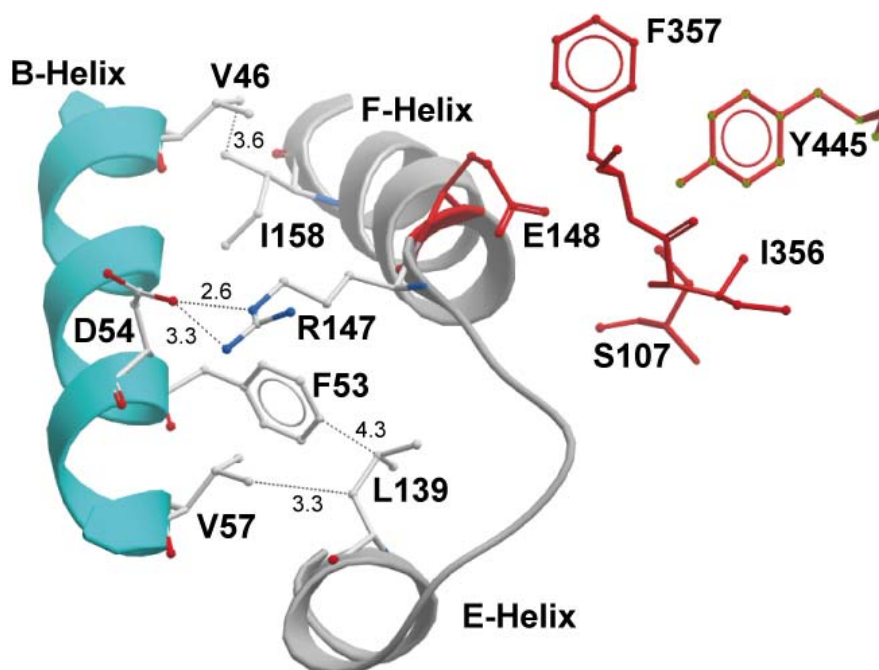


**Fig.37 Pore-coordinating amino acids in *Ec*CIC and their proximity to the B-helix**

The outer (E148 via R147) chloride binding site is in close proximity to the B-helix that is assumed to bind barttin. Regulation of the selectivity filter via V46, F53, D54 and/or V57 is expected.

It was shown that many residues of TM1 of barttin keep the fast gate almost closed upon substitution to tryptophan. These results suggest that TM1 of barttin binds to the B-helix of the channel for fast gate regulation, because this domain is in close proximity to the proposed

fast gate. Exchange of the B-helix probably introduces an additional fast gate (Fig.46, supplemental data), however the effect of barttin on the **chimera** ClC-2 with the B-Helix of ClC-K1 (Fig.47, supplemental data) could not be characterized in detail yet, and hence the here proposed regulation of fast gating by barttin.

In following passage, a binding mechanism is proposed. TM1 of barttin is rich in leucines (I9, I12, L14, L16, L18, L19, L21 and L25). They could act as a leucine zipper. These residues are likely to form hydrophobic bonds with a partner protein (Kobe and Deisenhofer 1995A+B, Bornberg-Bauer et al. 1998), in this case ClC-K chloride channels. If overlapping heptad repeats of leucines or isoleucines are needed to form a leucine zipper, they are given as indicated in small letters in Tab.17 (9-16, 12-19, 14-21 and 18-25). Methionines, valines or phenylalanine may participate in such a binding domain as well (Gurezka and Langosch 2001), thus enlarging this motif (11-18, 17-24, 19-26). The primary structure of TM1 of barttin is given in capital letters. Turquoise marks illustrate the high amount of unpolar amino acids. Besides one threonine and three small glycines, TM1 of barttin consists only of unpolar amino acids.

IGFIVLGLFLLALGTFLM  
g.bc.e.gabc.e..abc

**Tab.17 TM1 of barttin and its unpolar residues**

Besides four amino acids, TM1 mainly consists of unpolar residues (turquoise marks). Amino acids of a possible leucine zipper (LZ) are indicated in small letters. Overlapping heptad repeats of leucines, valins, isoleucines or phenylalanines are proposed to contribute to the formation of a LZ.

Upon mutation of one of those residues of a possible leucine zipper, binding of barttin to the channel can still occur because many residues participate in binding, but the regulation of gating probably prerequisites exact interplay of many of these residues. Adaption of barttin to the channel protein seems to be very complex.

On behalf of the  $\alpha$ -subunit and within one of the proposed barttin binding sites (Tajima et al. 2007), a leucine zipper may be indentified, as well, which is a prerequisite for dimerization of two helical structures. In Tab.18, this leucine zipper is indicated in small letters beyond the alignment of the B-helices of *EcClC*, ClC-Ka and ClC-K1. Different primary structure of the aligned B-helices of ClC-Ka and ClC-K1 are marked in grey and the proposed regulatory amino acids are marked in black. Outward facing residues within the structure of *EcClC* are marked in yellow. Beneath this alignment of the B-helix, barttin is aligned manually in regards of several aspects.

B-Helix	intracellular	extracellular
Ec ClC (35)	ILFMAAVVGTLVGLAAVAEDKGVAWLQ	NQRM
ClC-Ka (49)	DWYFLMTLGVLMALVSYAMNFATGCVVRAHQ	
ClC-K1 (49)	DWHFLVALGVLMALISYAMNFATGRVVRAHK	
	gab.d.fga.cd...a.c.e..ab	
	↓   ↓↓   ↓   ↓↓   ↓↓ IGFIVLGLFLLAIGTFLM	
Barttin (9)	g.bcde.gabc.e..abc	

**Tab.18 Alignment of B-helices of *Ec*ClC, ClC-Ka and ClC-K1 and residues proposed to build a leucine zipper**

Yellow marked indicate outward facing residues within the structure of *Ec*ClC. Grey marked illustrate different residues within ClC-Ka and ClC-K1. Black marks correspond to residues that may participate in gating regulation. In analogy to Tab.17, residues that may contribute to barttin binding via a leucine zipper are indicated with small letters. TM1 of barttin is aligned to the leucine zipper of the channel with respect of more assumptions (see text) with possible binding partners marked with arrows. Turquoise marks illustrate unipolar residues.

The extracellular loop behind TM1 of barttin starts after M26. Regarding the crystal structure and the sequence of *Ec*ClC, the first extracellular amino acids after the B-helix may be the polar sequence NQR. TM1 of barttin and the B-helix of ClC-K channels are assumed to be oriented in parallel fashion because almost all point mutations evoke tremendous, but comparable effects on gating of ClC-K1/Ka. Therefore it is likely that the extracellular exit sites of the two binding partners reside, too. An additional assumption leads to the annealing of barttin to the B-helix in Tab. 18.

Different regulation and missing activation of hClC-Ka co-expressed with G10W, V13W or L14W barttin is probably a result of deviating sequences of ClC-K channels and these three residues could oppose the B-helix (ClC-K) at positions 59, 62 and 63. In ClC-Ka, valine V63 could oppose V13 of barttins primary structure, while in ClC-K1 an isoleucine I63 may be coordinated. Substitution of V13 to tryptophan may cause different effects on the channel due to the different lengths of the side chains of V/I63. Substitutions G10W or L14 may sterically impair the binding of V13.

Closing speculations about the role of TM2 of barttin follow in this passage. Within TM2, three residues (A39, M40 and V45) were found to be important especially for slow gating. This regulation may take place via the J-helix of the channel, the second potential barttin binding site (Tajima et al. 2007).

In *Ec*CIC, Jayaram et al. (2008) assume that two gates of the Cl<sup>-</sup>-pathway lay within the pore (E148 = Glu<sub>ex</sub> and Y445 = Tyr<sub>c</sub> together with S107 = Ser<sub>c</sub>). Fast and slow gate were stated to be independent (Accardi and Pusch, 2000), so these two gates of the chloride pathway are probably not the fast and the slow gate, although it is commonly accepted that E148 is the fast gate (Fahlke et al. 1997, Dutzler et al. 2003, Zuñiga et al. 2004, de Santiago et al. 2005) and that the C-terminus of the channel which is next to the Tyr<sub>c</sub>-bearing R-helix moves during slow gating (Bykova et al. 2006). Tyr<sub>c</sub> is a pore coordinating residue that may contribute as well to fast protopore gating together with E148. Further down the R-helix, another residue, threonine T452, was reported to participate in gating regulation (Wang et al. 2010, Chen et al. 2003, Accardi and Pusch 2003). If barttin binds to the J-helix, additional positioning of the R-helix may be facilitated, leading to positional effects on the C-terminus and slow gate regulation. This positioning may take place via Q277 and R451, a J- and a R-helical residue which are 3.4 Å apart (not shown in Fig.38).

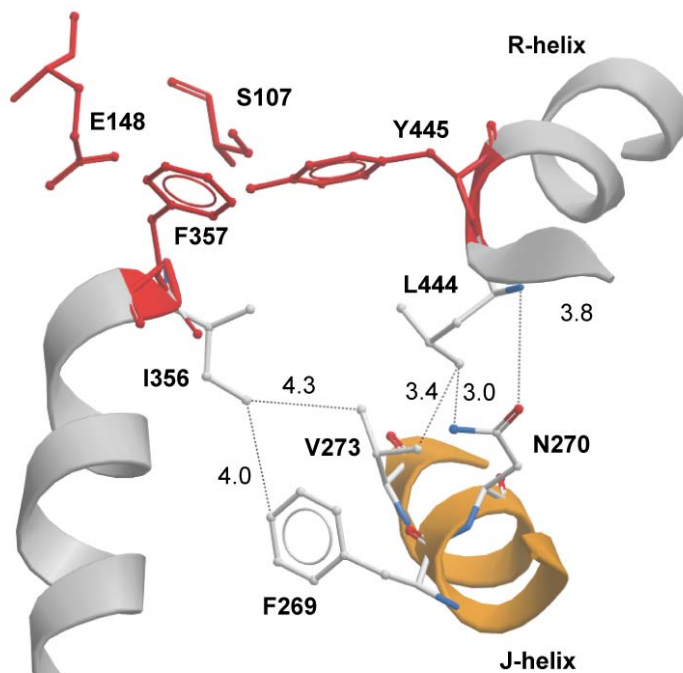


**Fig.38 Pore-coordinating amino acids in *Ec*CIC and their proximity to the J-helix as well as the R-helix**

The inner (Y445 via L444) and central (F357 via I356) chloride binding site is in close proximity to the J-helix that is assumed to bind barttin. Regulation of the selectivity filter via F269, N270 and/or V273 is expected.

The J-helix is in close proximity to the R-helix and another pore-coordinating residue (F357). Two residues of the J-helix, F269 and N270, are in close proximity to I356, respective L444, direct neighbors of pore coordinating F357 or Y445 (Fig.38). A third J-helical residue, V273,

is 4.3 Å away from I356 and only 3.4 Å away from L444. The J-helix may also play a role for the coordination of the central chloride binding site.

Higher homology of the J-helix and only A39W and M40W barttin within TM2 that evoke different regulation of the two channels indicate a binding of TM2 to the J-helix, but still, it is not solved if one or more barttins bind to the channel protein. So, the orientation of barttin and the J-helix remain unclear.

T36, A39, M40, G41, M44, V45 and G48 barttin probably bind to both observed ClC-K channel, but lost their capability to regulate gating. Possible mechanisms necessary for regulation could be phosphorylation of T36 (PKC), alkylation of M40 and M44, or H-bonds via glycines (Dong et al. 2012) G41 and G48 fitting in helix interstices.

J-helix	extracellular	intracellular
Ec ClC	(253)	WLYLILGIIIFGI FGP I FNKWWLGMQDLLHR
ClC-Ka	(283)	FFFVALGGICGVLSCAYLFCORTFLSFIKT
ClC-K1	(283)	FFFVALGICGVLSCAYLFCORTFLSFIKT

**Tab.19 Alignment of J-helices of EcClC, ClC-Ka and ClC-K1**

Yellow marked residues in the primary structure of EcClC are facing away of the core of the protopore and are therefore good candidates for barttin binding. Black marked residues are in close proximity to pore coordinating residues (compare with Fig.38). Grey marks illustrate different amino acids in ClC-Ka and ClC-K1.

It remains unclear how barttin binds to the channel, and because of the unsolved binding stoichiometry further hypothesis of binding become even more speculative than the here proposed regulatory mechanisms within the channel structure. If one barttin is enough, which is not very likely, and TM1 is oriented almost parallel to the B-helix of the channel, and if both proposed barttin binding sites, the B- and the J-helix, are indeed bound by barttin, then the extracellular loop of barttin need to span over the channel protein because of the antiparallel orientation of the B- and the J-helices. Then, TM2 would cross the J-helix. This intra-protopore binding is illustrated in Fig. 39 A. In Fig. 39 B, a possibility of inter-dimer binding would be that the channels form a cluster with barttin as the glue. To occupy all binding domains of ClC-K, an excess of barttin must be guaranteed to satisfy the binding sites at the edges of the cluster. This could be the reason for the loss-of-function of the concatamer barttin/V166E rClC-K1.

No matter if there is a 1:1 or higher stoichiometry, additional domains of the channel protein are likely to be under the control of barttin. ClC-K channels are complex glycosylated mainly



in presence of barttin. Glycosylation site is the loop between the helices L and M (Estévez and Jentsch 2002).

Furthermore, the loop between the D- and the E-helix and a di-leucine motif within the CBS-2 domain were reported for CIC-2 and CIC-3 to be important for membrane targeting, respective sorting of the channel (Zhao et al. 2007, Cornejo et al. 2009). Adaptor proteins are known to regulate membrane trafficking and sorting of CIC-1 and CIC-2 (Stauber et al. 2010, Peña-Münzenmayer et al. 2005) and interestingly for a family member of one of these adaptor proteins (AP-1), the binding via a leucine zipper was published (Erlanson et al. 1996, Chytil et al. 1998). For CIC-K channels, these motifs may only be accessible in presence of barttin, as the membrane trafficking of the channel is dependent on the presence of the  $\beta$ -subunit and the basolateral orientation of the channel is dependent on the C-terminal of barttin (Janssen et al. 2009).

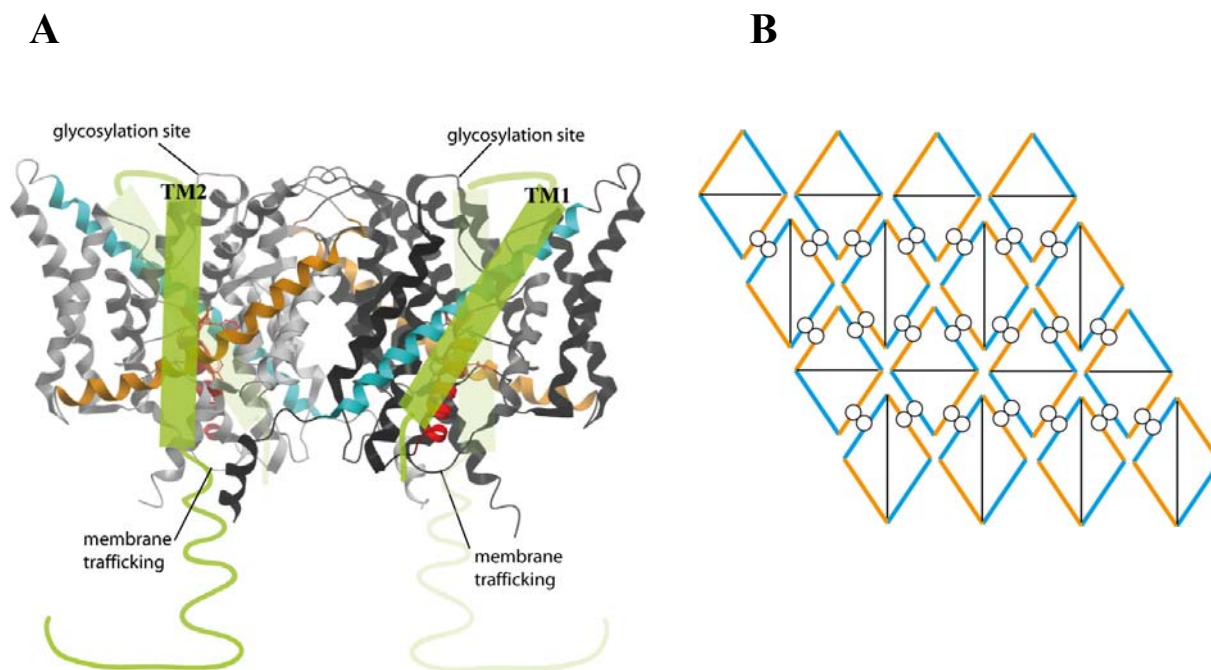


**Fig.39 two hypothetical binding possibilities of barttin to CIC-K channels**

**A)** intraprotopore binding of barttin (front: dark green; back: light green) to the B- (blue) and J-helix (orange) of CIC-K with a 1:1 stoichiometry. Within one protopore, the short N-terminus of barttin resides in the intracellular compartment, TM1 crosses the membrane along the B-helix and the extracellular loop spans over the channel protein where TM2 crosses the J-helix and leaves the C-terminus in the intracellular compartment.

**B)** Scheme of clustered CIC-K channels with barttin bound between two channels. Two triangles with the barttin binding sites marked in blue (B-helix) and orange (J-helix) form the channel dimer. The triangle is completed by a black line corresponding to the protopore interface. One barttin molecule (two circles represent TM1 and TM2) could bind between two protopores of different channels and occupy both binding domains of the channel. An excess of barttin is needed to occupy the binding site at the border of the cluster.

### 4.3 Conclusions

The major findings of the here performed tryptophan scan are outlined in a topology model of barttin (Fig.40). Yellow circles highlight residues that cannot activate hCIC-Ka and keep the fast gate of V166E rCIC-K1 almost closed over the measured voltage range. Residues marked in grey lost their gating capability. Blue represents barttin mutations that evoked altered function on the rodent and human channel (half of the circle marked in blue shows hCIC-Ka activation) which is most likely explained by different structure of the binding interface on behalf of the channel protein.

In regards of a better overview, the two barttin residues necessary for structure are no longer highlighted in color in Fig.40. As described, the mutations F24W and M26W interfere the building or the maintenance of barttin. Only misfolded or degraded barttin could be detected in SDS-PAGE gels.

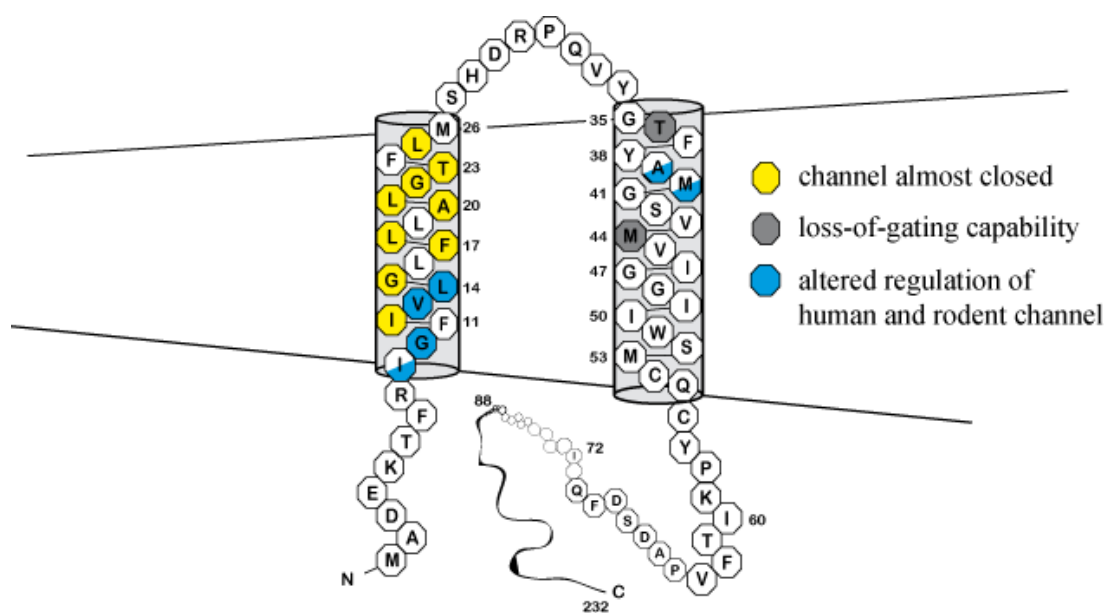


**Fig.40 Topology model of barttin with color-coded effects of tryptophan substitution**

The two proposed transmembrane helices of barttin are shown in grey cylinders. Regulatory residues within the secondary structure are marked yellow, grey or blue. Residues marked in grey regulate gating as if no barttin is present although the channel is brought to the membrane. Yellow marks represent residues that keep hCIC-Ka and the fast gate of V166E rCIC-K1 almost closed. Blue marked residues show different regulation of hCIC-Ka and V166E rCIC-K1, probably due to different channel structure. Circles marked half with blue indicate residues that activate hCIC-Ka.

T36W, G41W and M44W barttin co-expressed with V166E rCIC-K1 evoke relative slow gate open probabilities similar to those when no barttin is present and G48W barttin has only a minor impact on slow gating (Fig. 33), but all four mutations still allow binding of barttin to

V166E rCIC-K1. However, barttin excess at the plasma membrane could not be shown for G41W and G48W barttin. It was shown that T36W and M44W barttin bind to hCIC-Ka as well. These two mutations lead to a loss-of-gating capability of barttin on both channel orthologs.

We found several functional determinants within barttins structure. Many residues of TM1 (I12, G15, F17, L18, A20, L21, G22, T23, L25) are crucial mainly for fast gate opening of V166E rCIC-K1 and hCIC-Ka activation (4.4.3). The fast gate remains closed over almost the entire voltage range.

For I9W, G10W, V13W, L14W, A39W and M40W barttin, different regulation mechanisms on hCIC-Ka and V166E rCIC-K1 are observed. I9W, A39W and M40W barttin can activate hCIC-Ka, but gating of V166E rCIC-K1 is dramatically altered. G10W, V13W and L14W barttin cannot activate hCIC-Ka, although gating of V166E rCIC-K1 is not that severely impaired. It could not be determined whether accurate slow or fast gating is the essential regulatory mechanism needed for hCIC-Ka-activation. Moreover coordinated interplay of the fast and the slow gate is needed. The different regulation of these residues is probably caused by different binding interface on the behalf of the channel.

#### **4.4 Outlook**

In this study, the binding interface could not be determined with instance. It appears as if many residues within barttins structure are needed to bind to CIC-K channel protein. So, a single point mutation did not prevent binding. But several functional residues have been found. However, the binding of two of the here investigated barttin mutants to the human channel remains unclear. Pull-down assays, high-resolution clear native gel electrophoresis and/or crosslinking strategies should be performed to clarify and characterize the eventual binding of G41W and G48W barttin to hCIC-Ka.

The binding of two other barttins to V166E rCIC-K1 remained unclear. Biotinylation assays with cells co-expressing T36W or M44W barttin with V166E rCIC-K1 should be performed, although confocal images already suggest their interaction.

The proposed binding interface of leucine-zipper-dimerization needs to be proven. Thermodynamic mutant cycles of TM1 and the B-helix of ClC-K chloride channels may provide additional information about interacting residues. The substitution of an unpolar by a charged residue within the B-helix of the channel may lead to changes in gating behavior or barttin binding that may be rescued by analog substitution of barttin within TM1.

To answer the question of stoichiometry, LUX-FRET or TIRF microscopy could be the solution. In addition, the already measured concatamer barttin/V166E rClC-K1 could be linked with consecutive barttins. By whole cell patch clamp recordings, it should become obvious if a third, fourth or second barttin has no additional effect on gating of V166E rClC-K1.

The N-terminal link of YFP to the concatamer barttin/V166E rClC-K1 leads to loss-of-function, indicating the need of the N-terminal of barttin for gating regulation. Mass spectroscopy may confirm speculations on the modification of barttin in this or other regions. Deletion of the N-terminal and/or mutation of single amino acids could lead to new ideas of how this short sequence may regulate gating. It also needs to be shown that the concatamers are built in full length, but all attempts to pull-down or to immuno-detect the concatamer after western blotting were performed without success, so far.

Single channel recordings of the chimera should be done to clarify the effect of the helix substitution on gating. The binding of WT barttin to the chimera ClC-2/B-helix of ClC-K1 needs to be proven and characterized biochemically, too. Deeper insights in the signal transduction of barttin binding are expected.

Further regulatory effects of barttin may allow better understanding of how barttin binds to the channel. As mentioned, the loop between the D- and the E-helix of ClC-2 chloride channels is necessary for membrane recycling (Cornejo et al. 2009), and the basolateral orientation of ClC-2 is mediated by the C-terminal of the channel (Peña-Münzenmayer et al. 2005). Both tasks, membrane insertion and sorting, are fulfilled by barttin. Regulatory effects of barttin on corresponding regions in ClC-K need to be investigated.

Besides the chaperone function, the glycosylation of the channel protein is barttin dependent. The effect of this modification is unknown at present. The glycosylated amino acid (in the loop between helices L and M, Estévez and Jentsch, 2002) may be under the influence of and therefore in spatial orientation to barttin as well. Another amino acid in ClC-Ka that may be influenced by barttin is K527 (K519 in ClC-0), a residue reported to be essential for channel activation (Wang et al. 2010).

A far away aim of this study is the generation of therapeutics for bartter syndrome type IV patients or the generation of new diuretics. Therefore, the binding of barttin and its regulatory effects on ClC-K channels need to be understood first. To regulate other close relatives of ClC-K, like ClC-1 or ClC-2, with modified barttins would furthermore enable us to eventually cure myotonia congenita or epilepsy.

## 5 References

- Accardi, Alessio, Séverine Lobet, Carole Williams, Christopher Miller, and Raimund Dutzler, 'Synergism Between Halide Binding and Proton Transport in a CLC-type Exchanger', *Journal of Molecular Biology*, 362 (2006), 691–699 <doi:10.1016/j.jmb.2006.07.081>
- Accardi, Alessio, and Alessandra Picollo, 'CLC Channels and Transporters: Proteins with Borderline Personalities', *Biochimica et Biophysica Acta (BBA) - Biomembranes*, 1798 (2010), 1457–1464 <doi:10.1016/j.bbamem.2010.02.022>
- Accardi, Alessio, and Michael Pusch, 'Conformational Changes in the Pore of CLC-0', *The Journal of General Physiology*, 122 (2003), 277–294 <doi:10.1085/jgp.200308834>
- , 'Fast and Slow Gating Relaxations in the Muscle Chloride Channel Clc-1', *The Journal of General Physiology*, 116 (2000), 433–444 <doi:10.1085/jgp.116.3.433>
- Accardi, Alessio, Michael Walden, Wang Nguitragool, Hariharan Jayaram, Carole Williams, and Christopher Miller, 'Separate Ion Pathways in a Cl<sup>-</sup>/H<sup>+</sup> Exchanger', *The Journal of General Physiology*, 126 (2005), 563–570 <doi:10.1085/jgp.200509417>
- Adachi, S, S Uchida, H Ito, M Hata, M Hiroe, F Marumo, and others, 'Two isoforms of a chloride channel predominantly expressed in thick ascending limb of Henle's loop and collecting ducts of rat kidney', *The Journal of biological chemistry*, 269 (1994), 17677–17683
- Alekov, Alexi K., and Christoph Fahlke, 'Channel-like Slippage Modes in the Human Anion/proton Exchanger ClC-4', *The Journal of General Physiology*, 133 (2009), 485–496 <doi:10.1085/jgp.200810155>
- Bartter, Frederic C., Pacita Pronove, John R. Gill Jr., and Ross C. MacCardle, 'Hyperplasia of the Juxtaglomerular Complex with Hyperaldosteronism and Hypokalemic Alkalosis: A New Syndrome', *The American Journal of Medicine*, 33 (1962), 811–828 <doi:10.1016/0002-9343(62)90214-0>
- Bateman, Alex, 'The Structure of a Domain Common to Archaeobacteria and the Homocystinuria Disease Protein', *Trends in Biochemical Sciences*, 22 (1997), 12–13 <doi:10.1016/S0968-0004(96)30046-7>
- Bennetts, Brett, Grigori Y. Rychkov, Hooi-Ling Ng, Craig J. Morton, David Stapleton, Michael W. Parker, and others, 'Cytoplasmic ATP-sensing Domains Regulate Gating of Skeletal Muscle ClC-1 Chloride Channels', *Journal of Biological Chemistry*, 280 (2005), 32452–32458 <doi:10.1074/jbc.M502890200>
- Birkenhäger, Ralf, Edgar Otto, Maria J. Schürmann, Martin Vollmer, Eva-Maria Ruf, Irina Maier-Lutz, and others, 'Mutation of BSND Causes Bartter Syndrome with Sensorineural Deafness and Kidney Failure', *Nature Genetics*, 29 (2001), 310–314 <doi:10.1038/ng752>
- Bonifacino, Juan S., and Linton M. Traub, 'Signals for Sorting of Transmembrane Proteins to Endosomes and Lysosomes \*', *Annual Review of Biochemistry*, 72 (2003), 395–447 <doi:10.1146/annurev.biochem.72.121801.161800>
- Bornberg-Bauer, Erich, Eric Rivals, and Martin Vingron, 'Computational Approaches to Identify Leucine Zippers', *Nucleic Acids Research*, 26 (1998), 2740–2746 <doi:10.1093/nar/26.11.2740>
- Bösl, M R, V Stein, C Hübner, A A Zdebik, S E Jordt, A K Mukhopadhyay, and others, 'Male Germ Cells and Photoreceptors, Both Dependent on Close Cell-cell Interactions, Degenerate Upon ClC-2 Cl(-) Channel Disruption', *The EMBO journal*, 20 (2001), 1289–1299 <doi:10.1093/emboj/20.6.1289>
- Braulke, Thomas, and Juan S. Bonifacino, 'Sorting of Lysosomal Proteins', *Biochimica et Biophysica Acta (BBA) - Molecular Cell Research*, 1793 (2009), 605–614 <doi:10.1016/j.bbamcr.2008.10.016>

- Brown, Edward M., and R. John MacLeod, 'Extracellular Calcium Sensing and Extracellular Calcium Signaling', *Physiological Reviews*, 81 (2001), 239–297
- Bykova, Ekaterina A., Xiao-Dong Zhang, Tsung-Yu Chen, and Jie Zheng, 'Large Movement in the C Terminus of CLC-0 Chloride Channel During Slow Gating', *Nature Structural & Molecular Biology*, 13 (2006), 1115–1119 <doi:10.1038/nsmb1176>
- Cao, Lin, Xiao-Dong Zhang, Xiaobo Liu, Tsung-Yu Chen, and Min Zhao, 'Chloride Channels and Transporters in Human Corneal Epithelium', *Experimental Eye Research*, 90 (2010), 771–779 <doi:10.1016/j.exer.2010.03.013>
- Catalán, Marcelo, María Isabel Niemeyer, L.Pablo Cid, and Francisco V. Sepúlveda, 'Basolateral CLC-2 Chloride Channels in Surface Colon Epithelium: Regulation by a Direct Effect of Intracellular Chloride', *Gastroenterology*, 126 (2004), 1104–1114 <doi:10.1053/j.gastro.2004.01.010>
- Chen, Mei-Fang, and Tsung-Yu Chen, 'Side-chain Charge Effects and Conductance Determinants in the Pore of CLC-0 Chloride Channels', *The Journal of General Physiology*, 122 (2003), 133–145 <doi:10.1085/jgp.200308844>
- Chen, Tim T., Tara L. Klassen, Alica M. Goldman, Carla Marini, Renzo Guerrini, and Jeffrey L. Noebels, 'Novel Brain Expression of CLC-1 Chloride Channels and Enrichment of CLCN1 Variants in Epilepsy', *Neurology*, 80 (2013), 1078–1085 <doi:10.1212/WNL.0b013e31828868e7>
- Chen, Tsung-Yu, Mei-Fang Chen, and Chia-Wei Lin, 'Electrostatic Control and Chloride Regulation of the Fast Gating of CLC-0 Chloride Channels', *The Journal of General Physiology*, 122 (2003), 641–651 <doi:10.1085/jgp.200308846>
- Chytil, Milan, Blake R. Peterson, Daniel A. Erlanson, and Gregory L. Verdine, 'The Orientation of the AP-1 Heterodimer on DNA Strongly Affects Transcriptional Potency', *Proceedings of the National Academy of Sciences*, 95 (1998), 14076–14081 <doi:10.1073/pnas.95.24.14076>
- Cohen, Jordi, and Klaus Schulten, 'Mechanism of Anionic Conduction Across CLC', *Biophysical Journal*, 86 (2004), 836–845 <doi:10.1016/S0006-3495(04)74159-4>
- Cornejo, Isabel, María Isabel Niemeyer, Leandro Zúñiga, Yamil R. Yusef, Francisco V. Sepúlveda, and L. Pablo Cid, 'Rapid Recycling of CLC-2 Chloride Channels Between Plasma Membrane and Endosomes: Role of a Tyrosine Endocytosis Motif in Surface Retrieval', *Journal of Cellular Physiology*, 221 (2009), 650–657 <doi:10.1002/jcp.21900>
- Dong, Hao, Mukesh Sharma, Huan-Xiang Zhou, and Timothy A. Cross, 'Glycines: Role in  $\alpha$ -Helical Membrane Protein Structures and a Potential Indicator of Native Conformation', *Biochemistry*, 51 (2012), 4779–4789 <doi:10.1021/bi300090x>
- Dutzler, Raimund, 'A Structural Perspective on CLC Channel and Transporter Function', *FEBS Letters*, 581 (2007), 2839–2844 <doi:10.1016/j.febslet.2007.04.016>
- , 'Structural Basis for Ion Conduction and Gating in CLC Chloride Channels', *FEBS Letters*, 564 (2004), 229–233 <doi:10.1016/S0014-5793(04)00210-8>
- , 'The CLC Family of Chloride Channels and Transporters', *Current Opinion in Structural Biology*, 16 (2006), 439–446 <doi:10.1016/j.sbi.2006.06.002>
- , 'The Structural Basis of CLC Chloride Channel Function', *Trends in Neurosciences*, 27 (2004), 315–320 <doi:10.1016/j.tins.2004.04.001>
- Dutzler, Raimund, Ernest B. Campbell, Martine Cadene, Brian T. Chait, and Roderick MacKinnon, 'X-ray Structure of a CLC Chloride Channel at 3.0 [Å] Reveals the Molecular Basis of Anion Selectivity', *Nature*, 415 (2002), 287–294 <doi:10.1038/415287a>
- Dutzler, Raimund, Ernest B. Campbell, and Roderick MacKinnon, 'Gating the Selectivity Filter in CLC Chloride Channels', *Science*, 300 (2003), 108–112 <doi:10.1126/science.1082708>
- Elvington, Shelley M, Corey W Liu, and Merritt C Maduke, 'Substrate-driven Conformational Changes in CLC-ec1 Observed by Fluorine NMR', *The EMBO Journal*, 28 (2009), 3090–3102 <doi:10.1038/emboj.2009.259>

- Embark, Hamdy M., Christoph Böhmer, Monica Palmada, Jeyaganesh Rajamanickam, Amanda W. Wyatt, Sabine Wallisch, and others, 'Regulation of CLC-Ka/barttin by the Ubiquitin Ligase Nedd4-2 and the Serum- and Glucocorticoid-dependent Kinases', *Kidney International*, 66 (2004), 1918–1925 <doi:10.1111/j.1523-1755.2004.00966.x>
- Engh, Anita M., José D. Faraldo-Gómez, and Merritt Maduke, 'The Mechanism of Fast-Gate Opening in CLC-0', *The Journal of General Physiology*, 130 (2007), 335–349 <doi:10.1085/jgp.200709759>
- , 'The Role of a Conserved Lysine in Chloride- and Voltage-dependent CLC-0 Fast Gating', *The Journal of General Physiology*, 130 (2007), 351–363 <doi:10.1085/jgp.200709760>
- Erlanson, D A, M Chytil, and G L Verdine, 'The leucine zipper domain controls the orientation of AP-1 in the NFAT.AP-1.DNA complex', *Chemistry & biology*, 3 (1996), 981–991
- Estévez, Raúl, Thomas Boettger, Valentin Stein, Ralf Birkenhäger, Edgar Otto, Friedhelm Hildebrandt, and others, 'Barttin Is a Cl<sup>-</sup> Channel B-subunit Crucial for Renal Cl<sup>-</sup> Reabsorption and Inner Ear K<sup>+</sup> Secretion', *Nature*, 414 (2001), 558–561 <doi:10.1038/35107099>
- Estévez, Raúl, and Thomas J Jentsch, 'CLC Chloride Channels: Correlating Structure with Function', *Current Opinion in Structural Biology*, 12 (2002), 531–539 <doi:10.1016/S0959-440X(02)00358-5>
- Estévez, Raúl, Michael Pusch, Carles Ferrer-Costa, Modesto Orozco, and Thomas J. Jentsch, 'Functional and Structural Conservation of CBS Domains from CLC Chloride Channels', *The Journal of Physiology*, 557 (2004), 363–378 <doi:10.1113/jphysiol.2003.058453>
- Fahlke, C, H T Yu, C L Beck, T H Rhodes, and A L George Jr, 'Pore-forming Segments in Voltage-gated Chloride Channels', *Nature*, 390 (1997), 529–532 <doi:10.1038/37391>
- Fahlke, Christoph, and Martin Fischer, 'Physiology and Pathophysiology of CLC-K/barttin Channels', *Frontiers in Physiology*, 1 (2010), 155 <doi:10.3389/fphys.2010.00155>
- Fahlke, Christoph, Reinhardt Riidel, Nenad Mitrovic, Ming Zhou, and Alfred L. George Jr, 'An Aspartic Acid Residue Important for Voltage-dependent Gating of Human Muscle Chloride Channels', *Neuron*, 15 (1995), 463–472 <doi:10.1016/0896-6273(95)90050-0>
- Farmer, Laurel M., Brandy N. Le, and Deborah J. Nelson, 'CLC-3 Chloride Channels Moderate LTP at Schaffer collateral-CA1 Synapses', *The Journal of Physiology*, 2012 <doi:10.1113/jphysiol.2012.243485>
- Feng, Liang, Ernest B. Campbell, Yichun Hsiung, and Roderick MacKinnon, 'Structure of a Eukaryotic CLC Transporter Defines an Intermediate State in the Transport Cycle', *Science*, 330 (2010), 635–641 <doi:10.1126/science.1195230>
- Fischer, Martin, Audrey G H Janssen, and Christoph Fahlke, 'Barttin Activates CLC-K Channel Function by Modulating Gating', *Journal of the American Society of Nephrology: JASN*, 21 (2010), 1281–1289 <doi:10.1681/ASN.2009121274>
- Flores, Sandra Y., Christophe Debonneville, and Olivier Staub, 'The Role of Nedd4/Nedd4-like Dependant Ubiquitylation in Epithelial Transport Processes', *Pflügers Archiv*, 446 (2003), 334–338 <doi:10.1007/s00424-003-1027-x>
- Flores, Sandra Y., Dominique Loffing-Cueni, Elena Kamynina, Dorothee Daidié, Carole Gerbex, Sting Chabanel, and others, 'Aldosterone-Induced Serum and Glucocorticoid-Induced Kinase 1 Expression Is Accompanied by Nedd4-2 Phosphorylation and Increased Na<sup>+</sup> Transport in Cortical Collecting Duct Cells', *Journal of the American Society of Nephrology*, 16 (2005), 2279–2287 <doi:10.1681/ASN.2004100828>
- Földy, Csaba, Sang-Hun Lee, Robert J. Morgan, and Ivan Soltesz, 'Regulation of Fast-spiking Basket Cell Synapses by the Chloride Channel CLC-2', *Nature Neuroscience*, 13 (2010), 1047–1049 <doi:10.1038/nn.2609>
- Fong, Peying, Annett Rehfeldt, and Thomas J. Jentsch, 'Determinants of Slow Gating in CLC-0, the Voltage-gated Chloride Channel of *Torpedo marmorata*', *American Journal of Physiology - Cell Physiology*, 274 (1998), C966–C973



- Friedman, P. A., and F. A. Gesek, 'Calcium Transport in Renal Epithelial Cells', *American Journal of Physiology - Renal Physiology*, 264 (1993), F181–F198
- Friedrich, Thomas, Tilman Breiderhoff, and Thomas J. Jentsch, 'Mutational Analysis Demonstrates That ClC-4 and ClC-5 Directly Mediate Plasma Membrane Currents', *Journal of Biological Chemistry*, 274 (1999), 896–902 <doi:10.1074/jbc.274.2.896>
- Fujita, Nobuyuki, Hirotada Mori, Takashi Yura, and Akira Ishihama, 'Systematic Sequencing of the Escherichia Coli Genome: Analysis of the 2.4–4.1 Min (110,917–193,643 Bp) Region', *Nucleic Acids Research*, 22 (1994), 1637–1639 <doi:10.1093/nar/22.9.1637>
- G, BUYSE, TROUET D, VOETS T, MISSIAEN L, DROOGMANS G, NILIUS B, and others, 'Evidence for the Intracellular Location of Chloride Channel (ClC)-type Proteins: Co-localization of ClC-6a and ClC-6c with the Sarco/endoplasmic-reticulum Ca<sup>2+</sup> Pump SERCA2b', 1998 <<http://www.biochemj.org/bj/330/1015/bj3301015.htm>> [accessed 13 December 2012]
- García-Nieto, Víctor, Carlos Flores, Maria I. Luis-Yanes, Eduardo Gallego, Jesús Villar, and Félix Claverie-Martín, 'Mutation G47R in the BSND Gene Causes Bartter Syndrome with Deafness in Two Spanish Families', *Pediatric Nephrology*, 21 (2006), 643–648 <doi:10.1007/s00467-006-0062-1>
- Garcia-Olivares, Jennie, Alexi Alekov, Mohammad Reza Boroumand, Birgit Begemann, Patricia Hidalgo, and Christoph Fahlke, 'Gating of Human ClC-2 Chloride Channels and Regulation by Carboxy-terminal Domains', *The Journal of Physiology*, 586 (2008), 5325–5336 <doi:10.1113/jphysiol.2008.158097>
- George, Alfred L., Michael A. Crackower, Judith A. Abdalla, Arthur J. Hudson, and George C. Ebers, 'Molecular Basis of Thomsen's Disease (autosomal Dominant Myotonia Congenita)', *Nature Genetics*, 3 (1993), 305–310 <doi:10.1038/ng0493-305>
- Gradogna, Antonella, Elena Babini, Alessandra Picollo, and Michael Pusch, 'A Regulatory Calcium-binding Site at the Subunit Interface of CLC-K Kidney Chloride Channels', *The Journal of General Physiology*, 136 (2010), 311–323 <doi:10.1085/jgp.201010455>
- Gradogna, Antonella, Cristina Fenollar-Ferrer, Lucy R. Forrest, and Michael Pusch, 'Dissecting a Regulatory Calcium-binding Site of CLC-K Kidney Chloride Channels', *The Journal of General Physiology*, 2012 <doi:10.1085/jgp.201210878>
- Gradogna, Antonella, and Michael Pusch, 'Alkaline pH Block of CLC-K Kidney Chloride Channels Mediated by a Pore Lysine Residue', *Biophysical Journal*, 105 (2013), 80–90 <doi:10.1016/j.bpj.2013.05.044>
- Graham, F. L., J. Smiley, W. C. Russell, and R. Nairn, 'Characteristics of a Human Cell Line Transformed by DNA from Human Adenovirus Type 5', *Journal of General Virology*, 36 (1977), 59–72 <doi:10.1099/0022-1317-36-1-59>
- Graham, F.L., and A.J. van der Eb, 'A New Technique for the Assay of Infectivity of Human Adenovirus 5 DNA', *Virology*, 52 (1973), 456–467 <doi:10.1016/0042-6822(73)90341-3>
- Graves, Austin R., Patricia K. Curran, Carolyn L. Smith, and Joseph A. Mindell, 'The Cl<sup>-</sup>/H<sup>+</sup> Antiporter ClC-7 Is the Primary Chloride Permeation Pathway in Lysosomes', *Nature*, 453 (2008), 788–792 <doi:10.1038/nature06907>
- Greger, R, and E Schlatter, 'Presence of Luminal K<sup>+</sup>, a Prerequisite for Active NaCl Transport in the Cortical Thick Ascending Limb of Henle's Loop of Rabbit Kidney', *Pflügers Archiv: European journal of physiology*, 392 (1981), 92–94
- , 'Properties of the lumen membrane of the cortical thick ascending limb of Henle's loop of rabbit kidney', *Pflügers Archiv: European journal of physiology*, 396 (1983), 315–324
- Greger, R, E Schlatter, and F Lang, 'Evidence for electroneutral sodium chloride cotransport in the cortical thick ascending limb of Henle's loop of rabbit kidney', *Pflügers Archiv: European journal of physiology*, 396 (1983), 308–314
- Gross, J B, M Imai, and J P Kokko, 'A Functional Comparison of the Cortical Collecting Tubule and the Distal Convolute Tubule.', *Journal of Clinical Investigation*, 55 (1975), 1284–1294

- Günther, Willy, Anke Lüchow, Françoise Cluzeaud, Alain Vandewalle, and Thomas J. Jentsch, 'CLC-5, the Chloride Channel Mutated in Dent's Disease, Colocalizes with the Proton Pump in Endocytotically Active Kidney Cells', *Proceedings of the National Academy of Sciences*, 95 (1998), 8075–8080
- Gurezka, Rolf, and Dieter Langosch, 'In Vitro Selection of Membrane-spanning Leucine Zipper Protein-Protein Interaction Motifs Using POSSYCCAT', *Journal of Biological Chemistry*, 276 (2001), 45580–45587 <doi:10.1074/jbc.M105362200>
- Handlogten, Mary E., Chunfa Huang, Naoki Shiraiishi, Hisataka Awata, and R. Tyler Miller, 'The Ca<sup>2+</sup>-sensing Receptor Activates Cytosolic Phospholipase A2 via a Gq $\alpha$ -dependent ERK-independent Pathway', *Journal of Biological Chemistry*, 276 (2001), 13941–13948 <doi:10.1074/jbc.M007306200>
- Hayama, Atsushi, Tatemitsu Rai, Sei Sasaki, and Shinichi Uchida, 'Molecular Mechanisms of Bartter Syndrome Caused by Mutations in the BSND Gene', *Histochemistry and cell biology*, 119 (2003), 485–493 <doi:10.1007/s00418-003-0535-2>
- Hebeisen, Simon, Alexander Biela, Bernd Giese, Gerhard Müller-Newen, Patricia Hidalgo, and Christoph Fahlke, 'The Role of the Carboxyl Terminus in CLC Chloride Channel Function', *Journal of Biological Chemistry*, 279 (2004), 13140–13147 <doi:10.1074/jbc.M312649200>
- Hebeisen, Simon, and Christoph Fahlke, 'Carboxy-Terminal Truncations Modify the Outer Pore Vestibule of Muscle Chloride Channels', *Biophysical Journal*, 89 (2005), 1710–1720 <doi:10.1529/biophysj.104.056093>
- Hebert, Steven C, 'Bartter Syndrome', *Current opinion in nephrology and hypertension*, 12 (2003), 527–532 <doi:10.1097/01.mnh.0000088732.87142.43>
- Hechenberger, Mirko, Blanche Schwappach, Wolf N. Fischer, Wolf B. Frommer, Thomas J. Jentsch, and Klaus Steinmeyer, 'A Family of Putative Chloride Channels from Arabidopsis and Functional Complementation of a Yeast Strain with a CLC Gene Disruption', *Journal of Biological Chemistry*, 271 (1996), 33632–33638 <doi:10.1074/jbc.271.52.33632>
- Huang, Meng-Er, Jean-Claude Chuat, and Francis Galibert, 'A Voltage-gated Chloride Channel in the Yeast *Saccharomyces Cerevisiae*', *Journal of Molecular Biology*, 242 (1994), 595–598 <doi:10.1006/jmbi.1994.1607>
- Ignoul, Sofie, and Jan Eggermont, 'CBS Domains: Structure, Function, and Pathology in Human Proteins', *American Journal of Physiology - Cell Physiology*, 289 (2005), C1369–C1378 <doi:10.1152/ajpcell.00282.2005>
- Imai, M, and J P Kokko, 'Mechanism of Sodium and Chloride Transport in the Thin Ascending Limb of Henle.', *Journal of Clinical Investigation*, 58 (1976), 1054–1060
- Janssen, Audrey G. H, Ute Scholl, Constanze Domeyer, Doreen Nothmann, Ariane Leinenweber, and Christoph Fahlke, 'Disease-Causing Dysfunctions of Barttin in Bartter Syndrome Type IV', *Journal of the American Society of Nephrology*, 20 (2009), 145–153 <doi:10.1681/ASN.2008010102>
- Jayaram, Hariharan, Alessio Accardi, Fang Wu, Carole Williams, and Christopher Miller, 'Ion Permeation Through a Cl<sup>-</sup>-selective Channel Designed from a CLC Cl<sup>-</sup>/H<sup>+</sup> Exchanger', *Proceedings of the National Academy of Sciences*, 105 (2008), 11194–11199 <doi:10.1073/pnas.0804503105>
- Jeck, Nikola, Martin Konrad, Melanie Peters, Stefanie Weber, Klaus E. Bonzel, and Hannsjörg W. Seyberth, 'Mutations in the Chloride Channel Gene, CLCNKB, Leading to a Mixed Bartter-Gitelman Phenotype', *Pediatric Research*, 48 (2000), 754–758 <doi:10.1203/00006450-200012000-00009>
- Jeck, Nikola, Stephan C. Reinalter, Thomas Henne, Wolfgang Marg, Rudolf Mallmann, Katharina Pasel, and others, 'Hypokalemic Salt-Losing Tubulopathy With Chronic Renal Failure and Sensorineural Deafness', *Pediatrics*, 108 (2001), e5–e5 <doi:10.1542/peds.108.1.e5>

- Jentsch, Thomas J., Klaus Steinmeyer, and Gisela Schwarz, 'Primary Structure of Torpedo Marmorata Chloride Channel Isolated by Expression Cloning in *Xenopus* Oocytes', *Nature*, 348 (1990), 510–514 <doi:10.1038/348510a0>
- Jung, Jeesun, Bin Sun, Deukwoo Kwon, Daniel L. Koller, and Tatiana M. Foroud, 'Allelic-Based Gene-Gene Interaction Associated With Quantitative Traits', *Genetic epidemiology*, 33 (2009), 332–343 <doi:10.1002/gepi.20385>
- Kamynina, Elena, and Olivier Staub, 'Concerted Action of ENaC, Nedd4–2, and Sgk1 in Transepithelial Na<sup>+</sup> Transport', *American Journal of Physiology - Renal Physiology*, 283 (2002), F377–F387 <doi:10.1152/ajprenal.00143.2002>
- Kelly, Bernard T., Airlie J. McCoy, Kira Späte, Sharon E. Miller, Philip R. Evans, Stefan Höning, and others, 'A Structural Explanation for the Binding of Endocytic Dileucine Motifs by the AP2 Complex', *Nature*, 456 (2008), 976–979 <doi:10.1038/nature07422>
- Kieferle, S., P. Fong, M. Bens, A. Vandewalle, and T. J. Jentsch, 'Two Highly Homologous Members of the ClC Chloride Channel Family in Both Rat and Human Kidney', *Proceedings of the National Academy of Sciences*, 91 (1994), 6943–6947
- Kifor, Olga, R. John MacLeod, Ruben Diaz, Mei Bai, Toru Yamaguchi, Tham Yao, and others, 'Regulation of MAP Kinase by Calcium-sensing Receptor in Bovine Parathyroid and CaR-transfected HEK293 Cells', *American Journal of Physiology - Renal Physiology*, 280 (2001), F291–F302
- Kitanaka, Sachiko, Utako Sato, Kenichi Maruyama, and Takashi Igarashi, 'A Compound Heterozygous Mutation in the BSND Gene Detected in Bartter Syndrome Type IV', *Pediatric Nephrology*, 21 (2006), 190–193 <doi:10.1007/s00467-005-2091-6>
- Kleefuß-Lie, Ailing, Waltraut Friedl, Sven Cichon, Karsten Haug, Maike Warnstedt, Alexi Alekov, and others, 'CLCN2 Variants in Idiopathic Generalized Epilepsy', *Nature Genetics*, 41 (2009), 954–955 <doi:10.1038/ng0909-954>
- Kobayashi, K, S Uchida, S Mizutani, S Sasaki, and F Marumo, 'Developmental Expression of CLC-K1 in the Postnatal Rat Kidney', *Histochemistry and cell biology*, 116 (2001), 49–56
- , 'Intrarenal and Cellular Localization of CLC-K2 Protein in the Mouse Kidney', *Journal of the American Society of Nephrology: JASN*, 12 (2001), 1327–1334
- Kobayashi, Katsuki, Shinichi Uchida, Hiro-oki Okamura, Fumiaki Marumo, and Sei Sasaki, 'Human CLC-KB Gene Promoter Drives the EGFP Expression in the Specific Distal Nephron Segments and Inner Ear', *Journal of the American Society of Nephrology*, 13 (2002), 1992–1998 <doi:10.1097/01.ASN.0000023434.47132.3D>
- Kobe, Bostjan, and Johann Deisenhofer, 'A Structural Basis of the Interactions Between Leucine-rich Repeats and Protein Ligands', *Nature*, 374 (1995), 183–186 <doi:10.1038/374183a0>
- , 'Proteins with Leucine-rich Repeats', *Current Opinion in Structural Biology*, 5 (1995), 409–416 <doi:10.1016/0959-440X(95)80105-7>
- Koch, M C, K Steinmeyer, C Lorenz, K Ricker, F Wolf, M Otto, and others, 'The skeletal muscle chloride channel in dominant and recessive human myotonia', *Science (New York, N.Y.)*, 257 (1992), 797–800
- Kornak, Uwe, Dagmar Kasper, Michael R Bösl, Edelgard Kaiser, Michaela Schweizer, Ansgar Schulz, and others, 'Loss of the ClC-7 Chloride Channel Leads to Osteopetrosis in Mice and Man', *Cell*, 104 (2001), 205–215 <doi:10.1016/S0092-8674(01)00206-9>
- Krämer, Bernhard K, Tobias Bergler, Benjamin Stoelcker, and Siegfried Waldegger, 'Mechanisms of Disease: The Kidney-specific Chloride Channels ClCKA and ClCKB, the Barttin Subunit, and Their Clinical Relevance', *Nature clinical practice. Nephrology*, 4 (2008), 38–46 <doi:10.1038/ncpneph0689>
- Landau, D, H Shalev, M Ohaly, and R Carmi, 'Infantile Variant of Bartter Syndrome and Sensorineural Deafness: a New Autosomal Recessive Disorder', *American journal of medical genetics*, 59 (1995), 454–459 <doi:10.1002/ajmg.1320590411>

- Lange, Philipp F., Lena Wartosch, Thomas J. Jentsch, and Jens C. Fuhrmann, 'ClC-7 Requires Ostm1 as a B-subunit to Support Bone Resorption and Lysosomal Function', *Nature*, 440 (2006), 220–223 <doi:10.1038/nature04535>
- Leisle, Lilia, Carmen F. Ludwig, Florian A. Wagner, Thomas J. Jentsch, and Tobias Stauber, 'ClC-7 Is a Slowly Voltage-gated 2Cl<sup>-</sup>/1H<sup>+</sup>-exchanger and Requires Ostm1 for Transport Activity', *The EMBO Journal*, 30 (2011), 2140–2152 <doi:10.1038/emboj.2011.137>
- Lin, Yu-Wen, Chia-Wei Lin, and Tsung-Yu Chen, 'Elimination of the Slow Gating of Clc-0 Chloride Channel by a Point Mutation', *The Journal of General Physiology*, 114 (1999), 1–12 <doi:10.1085/jgp.114.1.1>
- Lobet, Séverine, and Raimund Dutzler, 'Ion-binding Properties of the ClC Chloride Selectivity Filter', *The EMBO Journal*, 25 (2006), 24–33 <doi:10.1038/sj.emboj.7600909>
- Lourdel, Stéphane, Teddy Grand, Johanna Burgos, Wendy González, Francisco V. Sepúlveda, and Jacques Teulon, 'ClC-5 Mutations Associated with Dent's Disease: a Major Role of the Dimer Interface', *Pflügers Archiv - European Journal of Physiology*, 463 (2012), 247–256 <doi:10.1007/s00424-011-1052-0>
- Ludwig, Uwe, Michael Pusch, and Thomas J. Jentsch, 'Two Physically Distinct Pores in the Dimeric ClC-0 Chloride Channel', *Nature*, 383 (1996), 340–343 <doi:10.1038/383340a0>
- Markovic, Sandra, and Raimund Dutzler, 'The Structure of the Cytoplasmic Domain of the Chloride Channel ClC-Ka Reveals a Conserved Interaction Interface', *Structure*, 15 (2007), 715–725 <doi:10.1016/j.str.2007.04.013>
- Martinez, Gilbert Q., and Merritt Maduke, 'A Cytoplasmic Domain Mutation in ClC-Kb Affects Long-Distance Communication Across the Membrane', *PLoS ONE*, 3 (2008), e2746 <doi:10.1371/journal.pone.0002746>
- Matsumura, Yoshihiro, Shinichi Uchida, Yoshiaki Kondo, Hiroaki Miyazaki, Shigeru B. H. Ko, Atsushi Hayama, and others, 'Overt Nephrogenic Diabetes Insipidus in Mice Lacking the CLC-K1 Chloride Channel', *Nature Genetics*, 21 (1999), 95–98 <doi:10.1038/5036>
- Maulet, Y, R C Lambert, S Mykita, J Mouton, M Partisani, Y Bailly, and others, 'Expression and Targeting to the Plasma Membrane of xClC-K, a Chloride Channel Specifically Expressed in Distinct Tubule Segments of Xenopus Laevis Kidney.', *Biochemical Journal*, 340 (1999), 737–743
- Meyer, Sebastian, and Raimund Dutzler, 'Crystal Structure of the Cytoplasmic Domain of the Chloride Channel ClC-0', *Structure*, 14 (2006), 299–307 <doi:10.1016/j.str.2005.10.008>
- Meyer, Sebastian, Sara Savaresi, Ian C. Forster, and Raimund Dutzler, 'Nucleotide Recognition by the Cytoplasmic Domain of the Human Chloride Transporter ClC-5', *Nature Structural & Molecular Biology*, 14 (2007), 60–67 <doi:10.1038/nsmb1188>
- Middleton, Richard E., Deborah J. Pheasant, and Christopher Miller, 'Homodimeric Architecture of a ClC-type Chloride Ion Channel', *Nature*, 383 (1996), 337–340 <doi:10.1038/383337a0>
- Miller, C., 'Open-State Substructure of Single Chloride Channels from Torpedo Electropax', *Philosophical Transactions of the Royal Society of London. B, Biological Sciences*, 299 (1982), 401–411 <doi:10.1098/rstb.1982.0140>
- Miyamura, Nobuhiro, Kazuya Matsumoto, Tetsuya Taguchi, Hiroshi Tokunaga, Takeshi Nishikawa, Kenro Nishida, and others, 'Atypical Bartter Syndrome with Sensorineural Deafness with G47R Mutation of the  $\beta$ -Subunit for ClC-Ka and ClC-Kb Chloride Channels, Barttin', *Journal of Clinical Endocrinology & Metabolism*, 88 (2003), 781–786 <doi:10.1210/jc.2002-021398>
- Mohammad-Panah, Raha, Rene Harrison, Sonja Dhani, Cameron Ackerley, Ling-Jun Huan, Yanchun Wang, and others, 'The Chloride Channel ClC-4 Contributes to Endosomal Acidification and Trafficking', *Journal of Biological Chemistry*, 278 (2003), 29267–29277 <doi:10.1074/jbc.M304357200>

- Morgan, T, M Tadokoro, D Martin, and R W Berliner, 'Effect of Furosemide on Na<sup>+</sup> and K<sup>+</sup> Transport Studied by Microperfusion of the Rat Nephron', *The American journal of physiology*, 218 (1970), 292–297
- Naderi, Amir Said Alizadeh, and Robert F Reilly Jr, 'Hereditary Etiologies of Hypomagnesemia', *Nature clinical practice. Nephrology*, 4 (2008), 80–89 <doi:10.1038/ncpneph0680>
- Neagoe, Ioana, Tobias Stauber, Pawel Fidzinski, Eun-Yeong Bergsdorf, and Thomas J. Jentsch, 'The Late Endosomal CIC-6 Mediates Proton/Chloride Countertransport in Heterologous Plasma Membrane Expression', *Journal of Biological Chemistry*, 285 (2010), 21689–21697 <doi:10.1074/jbc.M110.125971>
- Pearce, Simon H.S., Catherine Williamson, Olga Kifor, Mei Bai, Malcolm G. Coulthard, Michael Davies, and others, 'A Familial Syndrome of Hypocalcemia with Hypercalciuria Due to Mutations in the Calcium-Sensing Receptor', *New England Journal of Medicine*, 335 (1996), 1115–1122 <doi:10.1056/NEJM199610103351505>
- Peña-Münzenmayer, Gaspar, Marcelo Catalán, Isabel Cornejo, Carlos D. Figueroa, James E. Melvin, María I. Niemeyer, and others, 'Basolateral Localization of Native CIC-2 Chloride Channels in Absorptive Intestinal Epithelial Cells and Basolateral Sorting Encoded by a CBS-2 Domain Di-leucine Motif', *Journal of Cell Science*, 118 (2005), 4243–4252 <doi:10.1242/jcs.02525>
- Piccolo, Alessandra, Mattia Malvezzi, Jon C. D. Houtman, and Alessio Accardi, 'Basis of Substrate Binding and Conservation of Selectivity in the CLC Family of Channels and Transporters', *Nature Structural & Molecular Biology*, 16 (2009), 1294–1301 <doi:10.1038/nsmb.1704>
- Piccolo, Alessandra, Yanyan Xu, Niklaus Johner, Simon Bernèche, and Alessio Accardi, 'Synergistic Substrate Binding Determines the Stoichiometry of Transport of a Prokaryotic H<sup>+</sup>/Cl<sup>-</sup> Exchanger', *Nature Structural & Molecular Biology*, 19 (2012), 525–531 <doi:10.1038/nsmb.2277>
- Pressey, Sarah N.R., Kieran J. O'Donnell, Tobias Stauber, Jens C. Fuhrmann, Jaana Tyynelä, Thomas J. Jentsch, and others, 'Distinct Neuropathologic Phenotypes After Disrupting the Chloride Transport Proteins CIC-6 or CIC-7/Ostm1', *Journal of Neuropathology and Experimental Neurology*, 69 (2010), 1228–1246 <doi:10.1097/NEN.0b013e3181ffe742>
- Pusch, Michael, Uwe Ludwig, and Thomas J. Jentsch, 'Temperature Dependence of Fast and Slow Gating Relaxations of CIC-0 Chloride Channels', *The Journal of General Physiology*, 109 (1997), 105–116 <doi:10.1085/jgp.109.1.105>
- Qu, Chunyan, Fenghe Liang, Wei Hu, Zhijun Shen, Samuel S. Spicer, and Bradley A. Schulte, 'Expression of CLC-K Chloride Channels in the Rat Cochlea', *Hearing Research*, 213 (2006), 79–87 <doi:10.1016/j.heares.2005.12.012>
- Rai, Tatemitsu, Shinichi Uchida, Sei Sasaki, and Fumiaki Marumo, 'Isolation and Characterization of Kidney-Specific CLC-K2 Chloride Channel Gene Promoter', *Biochemical and Biophysical Research Communications*, 261 (1999), 432–438 <doi:10.1006/bbrc.1999.1038>
- Riazuddin, Saima, Saima Anwar, Martin Fischer, Zubair M. Ahmed, Shahid Y. Khan, Audrey G.H. Janssen, and others, 'Molecular Basis of DFNB73: Mutations of BSND Can Cause Nonsyndromic Deafness or Bartter Syndrome', *The American Journal of Human Genetics*, 85 (2009), 273–280 <doi:10.1016/j.ajhg.2009.07.003>
- Riccardi, Daniela, and Edward M. Brown, 'Physiology and Pathophysiology of the Calcium-sensing Receptor in the Kidney', *American Journal of Physiology - Renal Physiology*, 298 (2010), F485–F499 <doi:10.1152/ajprenal.00608.2009>
- Rinke, Ilka, Judith Artmann, and Valentin Stein, 'CIC-2 Voltage-Gated Channels Constitute Part of the Background Conductance and Assist Chloride Extrusion', *The Journal of Neuroscience*, 30 (2010), 4776–4786 <doi:10.1523/JNEUROSCI.6299-09.2010>
- Saint-Martin, Cécile, Grégory Gauvain, Georgeta Teodorescu, Isabelle Gourfinkel-An, Estelle Fedirko, Yvonne G. Weber, and others, 'Two Novel CLCN2 Mutations Accelerating Chloride

- Channel Deactivation Are Associated with Idiopathic Generalized Epilepsy', *Human Mutation*, 30 (2009), 397–405 <doi:10.1002/humu.20876>
- Sakmann, B, and E Neher, 'Patch Clamp Techniques for Studying Ionic Channels in Excitable Membranes', *Annual Review of Physiology*, 46 (1984), 455–472 <doi:10.1146/annurev.ph.46.030184.002323>
- Sambrook, Joseph, and David W Russell, 'The Inoue Method for Preparation and Transformation of Competent E. Coli: "Ultra-competent" Cells', *CSH protocols*, 2006 (2006) <doi:10.1101/pdb.prot3944>
- Santiago, Jose Antonio de, Keith Nehrke, and Jorge Arreola, 'Quantitative Analysis of the Voltage-dependent Gating of Mouse Parotid ClC-2 Chloride Channel', *The Journal of General Physiology*, 126 (2005), 591–603 <doi:10.1085/jgp.200509310>
- Saviane, Chiara, Franco Conti, and Michael Pusch, 'The Muscle Chloride Channel ClC-1 Has a Double-Barreled Appearance That Is Differentially Affected in Dominant and Recessive Myotonia', *The Journal of General Physiology*, 113 (1999), 457–468 <doi:10.1085/jgp.113.3.457>
- Schlatter, E, R Greger, and C Weidtko, 'Effect of "high ceiling" diuretics on active salt transport in the cortical thick ascending limb of Henle's loop of rabbit kidney. Correlation of chemical structure and inhibitory potency', *Pflügers Archiv: European journal of physiology*, 396 (1983), 210–217
- Schmidt, Christoph, Klaus H?cherl, Frank Schweda, and Michael Bucher, 'Proinflammatory Cytokines Cause Down-regulation of Renal Chloride Entry Pathways During Sepsis\*', *Critical Care Medicine*, 35 (2007), 2110–2119 <doi:10.1097/01.ccm.0000281447.22966.8b>
- Scholl, Ute, Simon Hebeisen, Audrey G. H. Janssen, Gerhard Müller-Newen, Alexi Alekov, and Christoph Fahlke, 'Barttin Modulates Trafficking and Function of ClC-K Channels', *Proceedings of the National Academy of Sciences*, 103 (2006), 11411–11416 <doi:10.1073/pnas.0601631103>
- Scott, John W., Simon A. Hawley, Kevin A. Green, Miliea Anis, Greg Stewart, Gillian A. Scullion, and others, 'CBS Domains Form Energy-sensing Modules Whose Binding of Adenosine Ligands Is Disrupted by Disease Mutations', *Journal of Clinical Investigation*, 113 (2004), 274–284 <doi:10.1172/JCI19874>
- Stefano, Silvia De, Michael Pusch, and Giovanni Zifarelli, 'Extracellular Determinants of Anion Discrimination of the Cl<sup>-</sup>/H<sup>+</sup> Antiporter Protein ClC-5', *Journal of Biological Chemistry*, 286 (2011), 44134–44144 <doi:10.1074/jbc.M111.272815>
- Steinmeyer, Klaus, Rainer Klocke, Christoph Ortland, Monika Gronemeier, Harald Jockusch, Stefan GrÜnder, and others, 'Inactivation of Muscle Chloride Channel by Transposon Insertion in Myotonic Mice', , *Published online: 28 November 1991; | doi:10.1038/354304a0*, 354 (1991), 304–308 <doi:10.1038/354304a0>
- Steinmeyer, Klaus, Christoph Ortland, and Thomas J. Jentsch, 'Primary Structure and Functional Expression of a Developmentally Regulated Skeletal Muscle Chloride Channel', , *Published online: 28 November 1991; | doi:10.1038/354301a0*, 354 (1991), 301–304 <doi:10.1038/354301a0>
- Stobrawa, Sandra M., Tilman Breiderhoff, Shigeo Takamori, Dominique Engel, Michaela Schweizer, Anselm A. Zdebik, and others, 'Disruption of ClC-3, a Chloride Channel Expressed on Synaptic Vesicles, Leads to a Loss of the Hippocampus', *Neuron*, 29 (2001), 185–196 <doi:10.1016/S0896-6273(01)00189-1>
- Stöltzing, Gabriel, Georgeta Teodorescu, Birgit Begemann, Julian Schubert, Rima Nabbout, Mohammad Reza Toliat, and others, 'Regulation of ClC-2 Gating by Intracellular ATP', *Pflügers Archiv - European Journal of Physiology*, 1–15 <doi:10.1007/s00424-013-1286-0>
- Tajima, Masato, Atsushi Hayama, Tatemitsu Rai, Sei Sasaki, and Shinichi Uchida, 'Barttin Binds to the Outer Lateral Surface of the ClC-K2 Chloride Channel', *Biochemical and Biophysical Research Communications*, 362 (2007), 858–864 <doi:10.1016/j.bbrc.2007.08.097>

- Townley, R., and L. Shapiro, 'Crystal structures of the adenylate sensor from fission yeast AMP-activated protein kinase', *Science*, 315 (2007), 1726–1729 <doi:10.1126/science.1137503>
- Uchida, S, 'In Vivo Role of CLC Chloride Channels in the Kidney', *American journal of physiology. Renal physiology*, 279 (2000), F802–808
- , 'Physiological Role of CLC-K1 Chloride Channel in the Kidney', *Nephrology, dialysis, transplantation: official publication of the European Dialysis and Transplant Association - European Renal Association*, 15 Suppl 6 (2000), 14–15
- Uchida, S, and F Marumo, 'Severely Impaired Urine-concentrating Ability in Mice Lacking the CLC-K1 Chloride Channel', *Experimental nephrology*, 8 (2000), 361–365
- Uchida, S, S Sasaki, K Nitta, K Uchida, S Horita, H Nihei, and others, 'Localization and Functional Characterization of Rat Kidney-specific Chloride Channel, ClC-K1', *The Journal of clinical investigation*, 95 (1995), 104–113 <doi:10.1172/JCI117626>
- Uchida, S., S. Sasaki, T. Furukawa, M. Hiraoka, T. Imai, Y. Hirata, and others, 'Molecular Cloning of a Chloride Channel That Is Regulated by Dehydration and Expressed Predominantly in Kidney Medulla.', *Journal of Biological Chemistry*, 268 (1993), 3821
- Vandewalle, A., F. Cluzeaud, M. Bens, S. Kieferle, K. Steinmeyer, and T. J. Jentsch, 'Localization and Induction by Dehydration of ClC-K Chloride Channels in the Rat Kidney', *American Journal of Physiology - Renal Physiology*, 272 (1997), F678–F688
- Vanoye, Carlos G., and Alfred L. George, 'Functional Characterization of Recombinant Human ClC-4 Chloride Channels in Cultured Mammalian Cells', *The Journal of Physiology*, 539 (2002), 373–383 <doi:10.1113/jphysiol.2001.013115>
- Waldegger, Siegfried, Nikola Jeck, Petra Barth, Melanie Peters, Helga Vitzthum, Konrad Wolf, and others, 'Barttin Increases Surface Expression and Changes Current Properties of ClC-K Channels', *Pflügers Archiv*, 444 (2002), 411–418 <doi:10.1007/s00424-002-0819-8>
- Waldegger, Siegfried, and Thomas J. Jentsch, 'Functional and Structural Analysis of ClC-K Chloride Channels Involved in Renal Disease', *Journal of Biological Chemistry*, 275 (2000), 24527–24533 <doi:10.1074/jbc.M001987200>
- Walden, Michael, Alessio Accardi, Fang Wu, Chen Xu, Carole Williams, and Christopher Miller, 'Uncoupling and Turnover in a Cl<sup>-</sup>/H<sup>+</sup> Exchange Transporter', *The Journal of General Physiology*, 129 (2007), 317–329 <doi:10.1085/jgp.200709756>
- Wang, Xiao-Qing, Tao Yu, Jian-Ping Sang, Xian-Wu Zou, Tsung-Yu Chen, Diana Bolser, and others, 'A Three-State Multi-Ion Kinetic Model for Conduction Properties of ClC-0 Chloride Channel', *Biophysical Journal*, 99 (2010), 464–471 <doi:10.1016/j.bpj.2010.04.047>
- Wang, Xue Qing, Ludmila V. Deriy, Sarah Foss, Ping Huang, Fred S. Lamb, Marcia A. Kaetzel, and others, 'CLC-3 Channels Modulate Excitatory Synaptic Transmission in Hippocampal Neurons', *Neuron*, 52 (2006), 321–333 <doi:10.1016/j.neuron.2006.08.035>
- Weinberger, Sebastian, Daniel Wojciechowski, Damien Sternberg, Frank Lehmann-Horn, Karin Jurkat-Rott, Toni Becher, and others, 'Disease-causing Mutations C277R and C277Y Modify Gating of Human ClC-1 Chloride Channels in Myotonia Congenita', *The Journal of Physiology*, 590 (2012), 3449–3464 <doi:10.1113/jphysiol.2012.232785>
- Zhao, Zhifang, Xinhua Li, Junfang Hao, John H. Winston, and Steven A. Weinman, 'The ClC-3 Chloride Transport Protein Traffics Through the Plasma Membrane via Interaction of an N-terminal Dileucine Cluster with Clathrin', *Journal of Biological Chemistry*, 282 (2007), 29022–29031 <doi:10.1074/jbc.M703506200>
- Zúñiga, Leandro, María Isabel Niemeyer, Diego Varela, Marcelo Catalán, L. Pablo Cid, and Francisco V. Sepúlveda, 'The Voltage-dependent ClC-2 Chloride Channel Has a Dual Gating Mechanism', *The Journal of Physiology*, 555 (2004), 671–682 <doi:10.1113/jphysiol.2003.060046>

## 6 Supplemental data

### 6.1 Time course of activation - many mutations slow down the fast gate kinetic

The kinetics of activation of the fast gate of V166E rClC-K1 is changed by barttin. At +125 mV, WT barttin accelerates the time constant  $\tau$  of activation of the fast gate from  $+7.7 \pm 1.5$  mV up to  $+2.6 \pm 0.2$  ms. Values for  $\tau$  are given in bar charts in Fig.41 for all measured barttin mutants. Blue bars illustrate barttin mutants that show significant differences to values with and without WT barttin. Black bars correspond to time constants similar to those measured when no barttin is present. White bars show no difference to values found in presence of WT barttin. Color-coding the letters helps for comparison with results obtained on hClC-Ka.

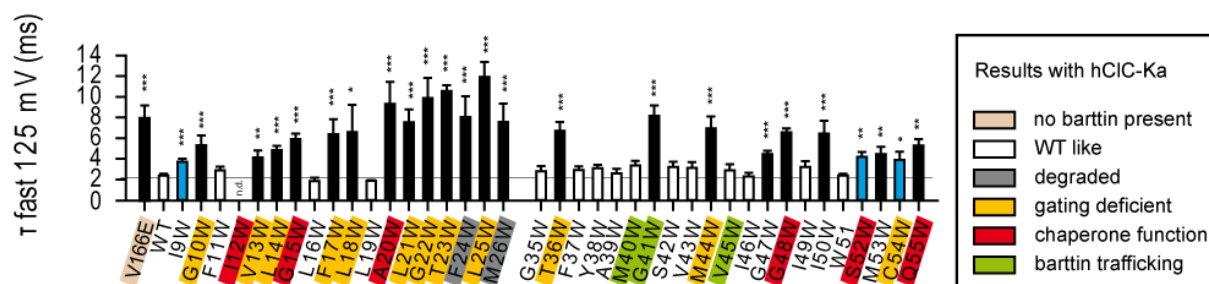


**Fig.41 Time constants of activation at 125 mV of all scanned barttin mutants**

Mutants marked with black bars evoked time constants similar to barttin-less channels, while white marked residues accelerate the fast gate in WT barttin like manner. Blue marked residues evoke time constants of activation in between the ones found for V166E rClC-K1 bound to WT- or no barttin.

Except two, all mutants marked as functional deficient on hClC-Ka change fast gate kinetics. Surprisingly, low expressing M40W and V45W barttin are still able to accelerate the fast gate activation to values found with WT barttin, although they were additionally reported as trafficking and chaperone-function deficient. If only a portion of channels are bound by barttin, this would result in a mixture of currents, and as a consequence, a time constant that is in between the values found in presence and absence of barttin. Thus it is clear that these two barttins are in excess to the channel protein and nearly all channels are bound by barttin.

The mutants that keep the fast gate close at hyperpolarizing condition all display time constants at +125 mV similar to the one found when no barttin is present. Same holds true for



T36W, G41W, M44W and G48W barttin – barttin mutants that do not affect open probability of the fast gate – but as well for hClC-Ka-activating and fast gate modifying G47W, I50W, M53W and Q55W barttin. I9W, S52W and C54W barttin slow down the fast gate to  $\tau$  values significant different to the ones observed in presence or absence of WT barttin. I50W, S52W and M53W barttin evoke only altered fast gating as shown already by the analysis of the changes in relative open probabilities.

## **6.2 Concatenated barttin/V166E rClC-K1 suggests a stoichiometry of barttin:protopore higher than 1:1**

Three barttin mutants express badly and hardly travel to the membrane. Macroscopic currents recorded with V166E rClC-K1 co-expressed with these barttins appear to be a mixture of barttin bound and unbound channels. We constructed concatenated proteins with WT, M40W, G41W or V45W barttin and V166E rClC-K1 in order to guarantee a 1:1 stoichiometry between barttin and the single protopore.

Barttin was covalently fused to the N-terminus of V166E rClC-K1. Fig.42 shows representative whole cell patch clamp recordings of WT barttin coexpressed with V166E rClC-K1 (A, n=13) compared to the concatamer WT barttin/V166E-rClC-K1 (B, n=12) and the concatamer WT barttin/V166E rClC-K1 coexpressed with WT barttin (C, n=6) as indicated by topology models. When the concatamer was additionally labeled with YFP (D, n=7) at the N-terminal of barttin, channel function was altered. The currents diverge drastically from cells expressing concatamers containing WT barttin without YFP-label or from cells co-expressing WT barttin together with V166E rClC-K1. Most probable, the N-terminal of barttin has regulatory function on V166E rClC-K1, but due to the big fluorescence protein at the short N-terminal, this regulation can no longer take place. Please note that for tryptophan scanning analysis the fluorophore was generally added to the long C-terminus of barttin that had been shown to leave all barttin functions unchanged (Scholl et al. 2006).

Figs.42 E-G show representative current recordings of concatamers with mutant barttin. Fusion of M40W (n=5) or G41W barttin (n=4), as well as V45W (n=8) barttin to V166E rCIC-K1 leads to impaired barttin function. Further analysis of relative open probabilities, V0.5 and kinetics reveal better insights in the regulatory capacity of the concatenated barttins.

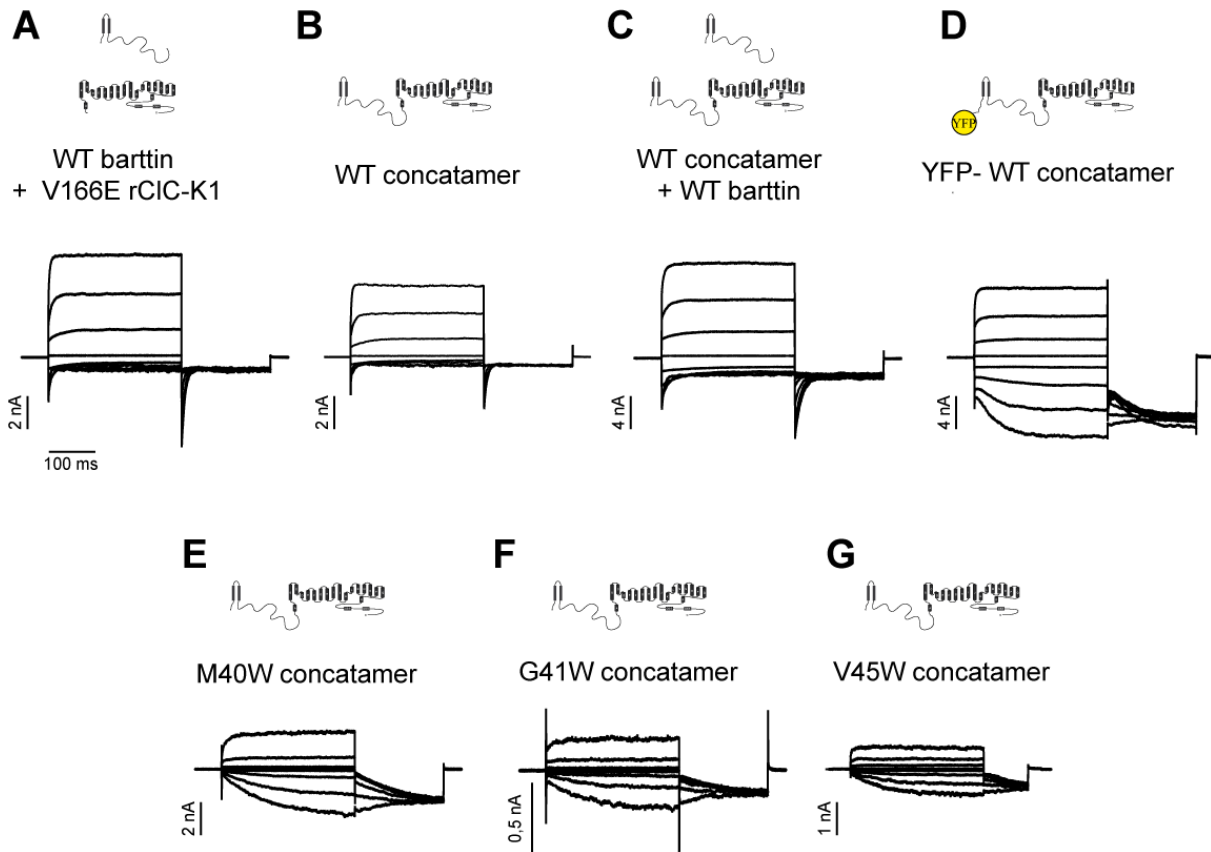


**Fig. 42** Representative whole cell current recordings of HEK293T cells expressing (A) WT barttin and V166E rCIC-K1, or concatenated (B) WT barttin/V166E rCIC-K1, (C) WT barttin/V166E rCIC-K1 together with additional WT barttin, (D) YFP-WT barttin/V166E rCIC-K1, (E) M40W barttin/V166E rCIC-K1, (F) G41W barttin/V166E rCIC-K1 and (G) V45W barttin/V166E rCIC-K1

The current traces of A, B and C look similar. N-terminally YFP-labeled concatamers exhibit impaired function. The concatamers built with mutant barttins all seem to have lost the functionality of barttin on the channel. The currents appear like the ones when no barttin is present. Further evaluations will show different results.

In Fig.43, I-V-plots emphasize the observations of the macroscopic currents. Normalizing steady state current amplitudes at -155 mV and comparing the I-V-plots of cells co-expressing WT barttin and V166E rClC-K1, they superimpose with the I-V-plot of cells expressing concatamers built with WT barttin. Additional barttin has no further effect.

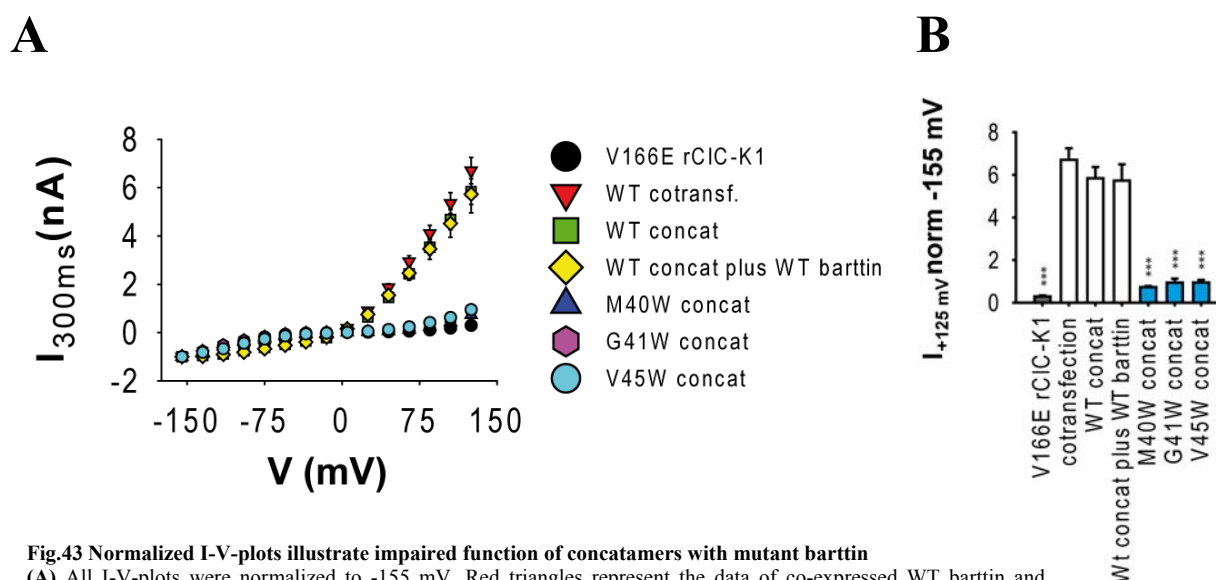


**Fig.43 Normalized I-V-plots illustrate impaired function of concatamers with mutant barttin**

(A) All I-V-plots were normalized to -155 mV. Red triangles represent the data of co-expressed WT barttin and V166E rClC-K1. This data superimpose with the data found for WT barttin concatenated to V166E rClC-K1. Black circles depict the I-V correlation of V166E rClC-K1 expressed in HEK293T cells. The data of concatamers built with mutant barttins (M40W, G41W, V45W barttin) superimpose almost entirely. (B) Comparison of relative current amplitudes at +125 mV. Asterisks indicate significant differences to cells coexpressing WT barttin and V166E rClC-K1. A second students' t-test versus values found for cells expressing only the channel protein results in color codes of the bars. Blue bars correspond to constructs exhibiting significant differences to the channel with or without WT barttin. White bars correspond to values found for the channel in presence of WT barttin. The mutant concatamers show a significant increase in relative mean current amplitude, indicating a weak, but existing interaction of these barttins with the channel.

The normalized I-V-plots illustrate that concatamers with mutant barttins appear to act as if no barttin is present. However, unpaired students' t-test versus results found for channels without barttin reveals small, but significant differences (Fig.43 B, blue bars) in current amplitudes at +125 mV for concatamers built with M40W, G41W and V45W barttin. This indicates an interaction of these concatenated barttins with the channel protein.

To validate this interaction, we next investigated the slow gate regulation. Activation curves are given in Fig.44A. Like before (see 3.2.4), changes in relative open probabilities were calculated and shown in Fig. 44B.

Again, two students' t-test were performed; once against the values found for cells co-expressing WT barttin and V166E rClC-K1 (indicated with asterisks) and once against values found for cells only expressing V166E rClC-K1 (grey bars = no difference, blue bars = different to V166E rClC-K1 with and without barttin, white bars = different to V166E rClC-K1 in absence of barttin). WT barttin concatenated to V166E rClC-K1 does not entirely lock the slow gate in an open state (A, green squares compared to red triangles). The difference in changes of rel.  $p_{open}$  are small, but significant (B). Additional WT barttin restores this insufficiency (yellow diamonds). This indicates a higher stoichiometry than 1:1.

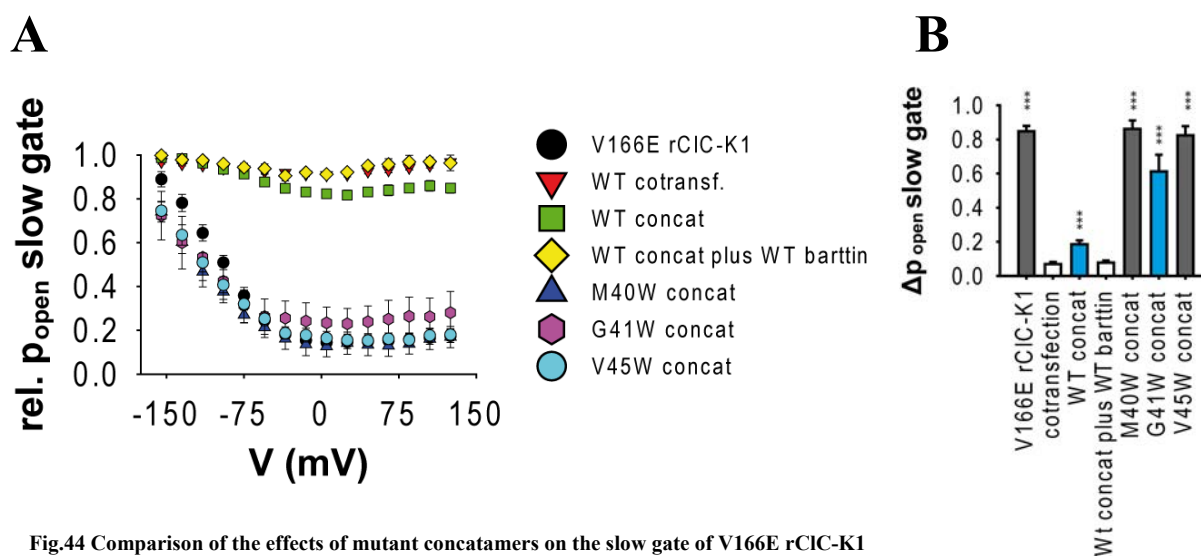


**Fig.44 Comparison of the effects of mutant concatamers on the slow gate of V166E rClC-K1**

(A) Activation curves of the slow gate of concatamers and V166E rClC-K1 in presence (red triangles) or absence (black circles) of WT barttin. The concatamers built with WT barttin fails to lock the slow gate into an open state over the measured voltage range (green squares). Additional WT barttin (yellow diamonds) restores this dysfunction. Mutant concatamers (blue pyramids, purple hexagons and light blue circles) act as if no barttin is present. In analogy to the evaluations in chapter 3.2.4, the activation curves are fit with Boltzmann functions and in (B), changes in relative open probabilities of the slow gate are compared. Two students' t-tests were performed. Asterisks indicate differences to values found for cells co-expressing WT barttin with V166E rClC-K1. Black bars show no difference to cells expressing the channel only. Blue bars represent constructs which have an effect on the channel, but this effect is not like the one of WT barttin. White bars represent full functional constructs. The concatamers built with WT barttin and G41W barttin have an impact on the slow gate which is not like WT barttin.

Concatamers with mutant barttin fail to open the slow gate at positive potentials. When co-expressing V166E rClC-K1 with M40W or V45W barttin, changes in slow gating were observed (see Fig.33). These results could not be confirmed by the concatamers. Changes in the open probability of the slow gate are not different from those measured when only the channel protein is present. However, the concatamer G41W barttin-V166E rClC-K1 increases the relative open probability of the slow gate at +125 mV. This elevation is of significant difference compared to channels without barttin again indicating the interaction of both binding partners.

Fast gate activation curves were treated as before (see 3.2.5). Changes in fast gate open probabilities were calculated and given in Fig.45. Again, two students' t-test were performed. Significant differences to cells co-expressing WT barttin and V166E rCIC-K1 are marked with asterisks. Significant differences to the channel alone are illustrated by blue and white bars, as before. Grey bars illustrate no significant difference to the channel alone.

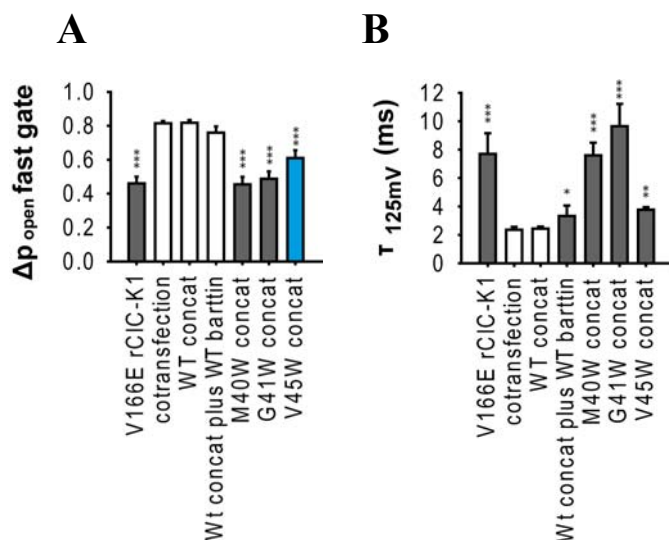


**Fig.45 (A) Changes in relative open probability of the fast gate and (B) time constants of activation at +125 mV of concatamers in comparison to cell expressing the channel only or co-expressing WT barttin**

Concatenated WT barttin does not show any differences in fast gate regulation regarding relative open probability or kinetics, compared to cells co-expressing V166E rCIC-K1 and WT barttin. In contrast, the results of concatenated mutant barttins do not confirm earlier results. In concatenated constructs, only V45W barttin seems to interact with the channel. Additional barttin expressed with the concatamer built with WT barttin slows down the fast gate for unknown reasons.

Experiments with co-expressing cells revealed that M40W and V45W barttin increase the changes in relative fast gate open probability (compared with Fig.34). Regarding the concatenated proteins, this holds true only for V45W barttin-V166E rCIC-K1. And only this concatamer shows the tendencies for fast gate acceleration observed upon co-expression experiments, although tau does not reach the value found for WT barttin, like in earlier results (Fig. 45 B compared with Fig. 41). Another aspect of the fast gate evaluation is that kinetics of the concatamer WT barttin-V166E rCIC-K1 is comparable to the results of coexpressed V166E rCIC-K1 and WT barttin, but concatenated WT barttin-V166E rCIC-K1 with additional barttin evoked slower time constants. This is in harsh contrast to the formerly observed restoration of function by additional barttin (compare with Fig. 44).

The macroscopic currents of V166E rClC-K1 that was N-terminally labeled with WT barttin are quite similar to those of cells co-expressing the channel and its subunit. The shown representative recording of the concatamer WT barttin/V166E rClC-K1 depicts a slow deactivation of the channel at positive potentials. Evaluations of concatamers reveal that the slow gate is not regulated like in co-expression experiments. A 1:1 stoichiometry is probably not enough to facilitate all barttin functions. Hence, 5 of 12 cells did not show any difference to the co-expression experiments.

In addition, the results of the concatamers built with mutant barttin indicate that one barttin is not enough to facilitate all tasks. The results observed upon co-expressing M40W, G41W or V45W barttin with V166E rClC-K1 could not be confirmed by the corresponding concatamers, indicating a higher stoichiometry. Nevertheless, binding of these barttins even within the concatenated structure is assumed.

N-terminal labeling of the concatamer barttin-V166E rClC-K1 with YFP leads to a loss-of-function. The slow gate is no longer set to an open state over the measured voltage range. Obviously, YFP fusion to the N-terminus of barttin impairs barttin function. Loss-of-function of the YFP labeled concatamers emphasizes the necessity of the N-terminus of barttin for gating regulation.

### 6.3 Chimeric channels reveal the B-helix to be essential for fast gating

CIC-2 is the closest relative of CIC-K channels within the CIC-family. We used this channel to examine the binding of barttin to the B- and J-helices of CIC-K channels. In Fig. 46, two whole cell current recordings are shown. In A, current traces of CIC-2 show biphasic activation at negative potentials corresponding to the fast and the slow gate activation. CIC-2 is an inward rectifier. The fast and the slow gate of CIC-2 were already reported to open under hyperpolarizing conditions (Garcia-Olivares et al. 2008). In B, current traces of a chimeric channel are given. For this construct, we used the backbone of CIC-2 and substituted the B-helix by the B-helix of rCIC-K1. This substitution seems to introduce an additional fast gate that activates at positive potentials.

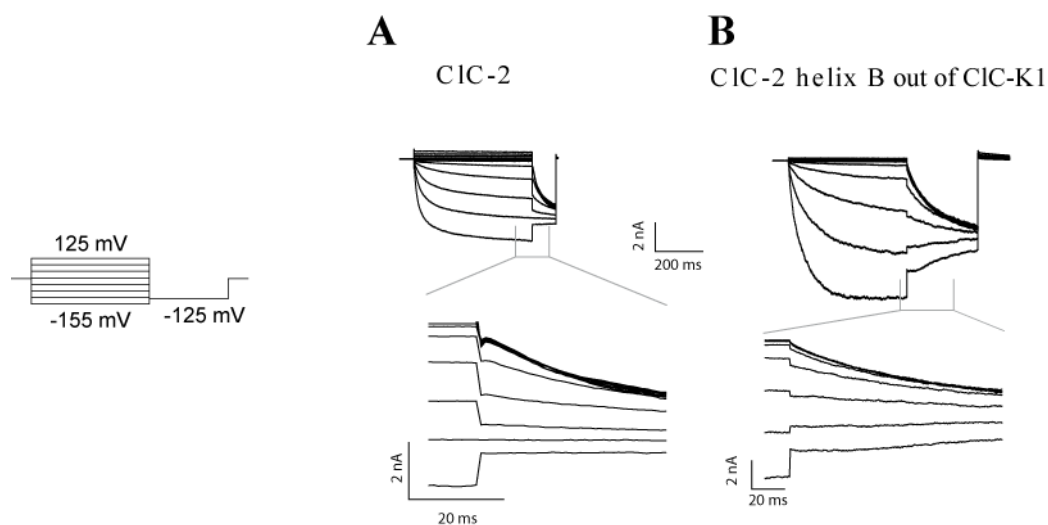


**Fig.46 Representative whole cell current recordings of HEK293T cells expressing A) hCIC-2 or B) hCIC-2 with B-helix of rCIC-K1**

Standard voltage protocols were run with a holding potential of 0 mV. Application of a test pulse to -125 mV reveals the opening state of the channels fast and slow gate due to the prepulses. (A) CIC-2 shows biphasic behavior. Magnification of the test pulse currents show a fast deactivation followed by slow activation coming from positive potentials. The fast gate is opened at positive potentials, in contrast to (B). Substitution of the B-helix leads to an inversion of the fast gate that is now opened at very negative potentials.

This experiment was planned to prove the binding of barttin to the B-helix. Co-expression of barttin reduces the mean current amplitude (Fig.47A+B) although more channels are built in presence of barttin (Fig.47C) and trafficking of barttin and chimeric channel seems to be not altered as shown by confocal images (Fig.47B). There may be some changes in the gating behavior of the chimer when barttin is present, but low current amplitude and moreover the unknown gating events of the chimer avoid further analysis of the gating events.

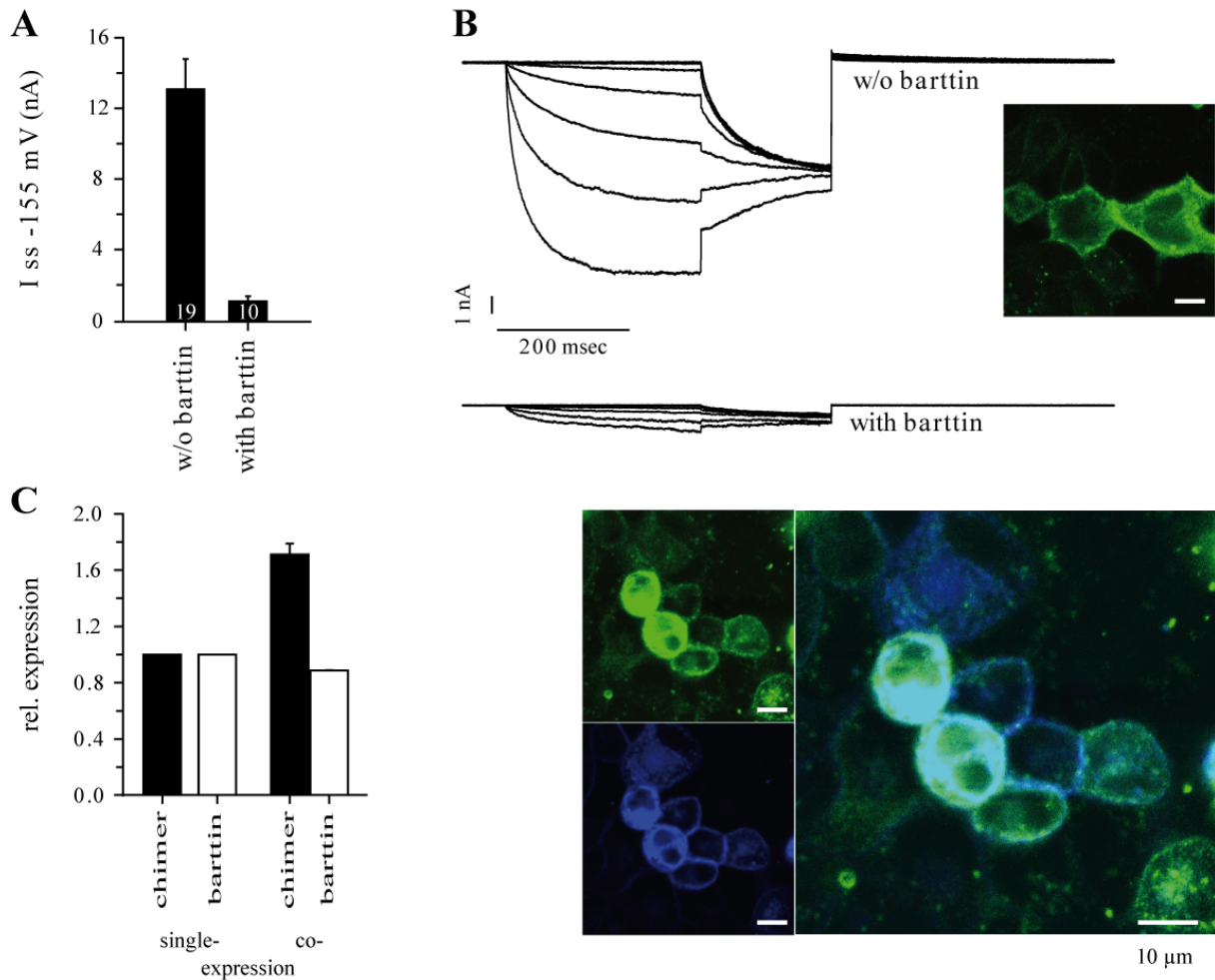


**Fig.47 (A) Mean current amplitudes and (B) representative whole cell current recordings of HEK293T cell expressing chimeric CIC-2 in presence and absence of barttin are compared with the expression level (C) and subcellular distribution (confocal images in B)**

The B-helix of CIC-2 was replaced by the B-helix of rCIC-K1, a proposed binding site of barttin. Barttin reduces the mean current amplitude of the chimeric CIC-2, despite higher expression of the chimer in presence of barttin and despite appropriate membrane insertion of the channel (green) and barttin (blue).

Further constructs were built and measured. Another helix of rCIC-K2 is reported to bind barttin, but substitution of the J-helix avoids macroscopic currents of chimeric channel with the backbone of hCIC-2 or rCIC-K1. Same holds true for chimeric channels in which the B- and the J-helices were swapped.



## 6.4 Point mutations T36W or M44W do not impair binding of barttin to V166E rCIC-K1

Macroscopic currents HEK293T cells co-expressing V166E rCIC-K1 together with T36W or M44W barttin are alike the ones as if no barttin is present. Further analyses are needed to clarify the question if these barttins cannot bind to the channel protein, or if the missing gating alterations are caused by the introduced tryptophan. Confocal microscopy gives first insights.

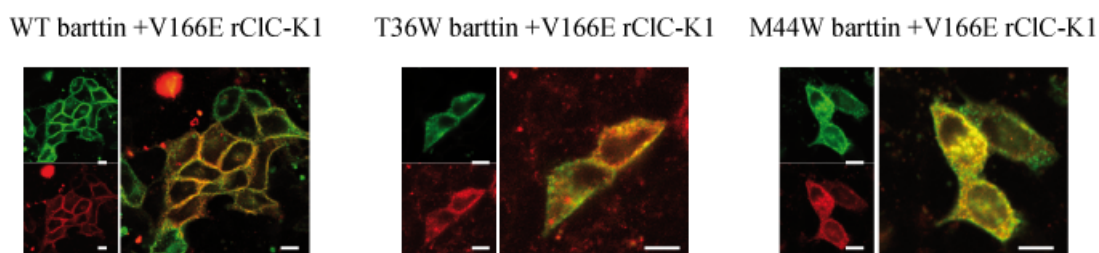


**Fig.48 Confocal images of MDCKII cell co-expressing V166E rCIC-K1 YFP (red) together with WT, T36W or M44W barttin mCFP (green)**

Without barttin, the channel remains mainly in the intracellular (Janssen et al. 2006). In the presence of barttin, CIC-K channels are taken to the membrane. This chaperone function is conserved upon barttin mutations T36W and M44W. Like with WT barttin, T36W and M44W barttin facilitate enhance membrane trafficking of the channel protein. Scale bar = 10  $\mu\text{m}$ .

As shown by Scholl et al. (2006), when expressed without barttin, rCIC-K1 mainly retains in intracellular compartments. In presence of barttin, the channel is taken to the membrane analog to hCIC-Ka. In Fig.48, the chaperone function of barttin seems to be conserved for T36W and M44W barttin. Both binding partners, barttin and V166E rCIC-K1, are predominantly expressed in the plasma membrane which lead to the assumption that both barttin mutants still can bind to the channel protein and the changes in gating behavior are indeed caused by the introduced point mutation.

Additional quantification of the membrane insertion of the channel protein by biotinylation assays should be performed to validate this assumption.

## 7 Acknowledgements

I would like to thank Prof. Dr. Christoph Fahlke for his trust in giving me the opportunity to work in his lab. His leadership, his scientific and educational skills and his brilliant mind creates an enlightening environment. I am also thankful for the possibility to attend two scientific congresses.

I would like to thank Prof. Dr. Gerardy-Schahn and Prof. Dr. Ngezahayo for being my co-referees and their time to read this manuscript.

Special thanks go to Dr. Martin Fischer, the best suited successor for the position of the head of neurophysiology. The accuracy of the way he works helped almost as much as his advice in concerns of experiments or writing this thesis. I also thank Gabriel Stölting for the discussions on CIC channels and the even fewer chess games in between. Credits go to Yvonne Schill and Alexander Wirth for opening views beyond the horizon of CIC channels and their innumerable hints regarding biochemistry.

Of course, I need to thank Birgit Begemann, Petra Kilian and Toni Becher for superb and ambitious technical support and Christin Dähling for keeping the lab running.

Thank all the colleagues of the Institute of Neurophysiology for having a great time. We should have an annual barbeque and everybody must join...Peter, David, Nicole, Jasmin, Matthias, Alexi, Erick, Raul, Dennis, Jan-Phillip, Bettina, Yunping, Silke, Chen, Dalia, Patty, André, Sonal, Malte, Dascha, Uschi, Beate, Natascha, Viktoriya, Evgeni and all the bachelors, masters and MDs.

Thanks to my mother for making everything possible, thanks to my sister for keeping the spirit alive, thanks to my father, hope you can hear it, thanks to my granny for always believing in me and keeping me on righteous tracks and thanks to Katharina for being there to ease my mind.

## 8 Curriculum Vitae

### Personal Information

Daniel Wojciechowski

Born 21.04.1977 in Augsburg, Germany

### Educational and Professional Background

- |                      |  |
|----------------------|--|
| 01.04.2009 – present | Scientific employee at the Centre of Physiology<br>Institute for Neurophysiology<br>Medical School Hannover  |
| 2011 – present       | PhD studies at the Naturwissenschaftliche Fakultät<br>Gottfried Wilhelm Leibniz Universität Hannover<br>Conducted at the<br>Institute for Neurophysiology<br>Medical School Hannover<br>Supervisor: Prof. Dr. Christoph Fahlke |
| 2000-2008            | Student of biology at the<br>Johannes-Gutenberg-Universität Mainz<br>Degree: Diplom-Biologe  |
| 1996-1999            | Maria-Theresia-Gymnasium Augsburg<br>Degree: Abitur  |

## 9 List of publications

Weinberger, Sebastian, Daniel Wojciechowski, Damien Sternberg, Frank Lehmann-Horn, Karin Jurkat-Rott, Toni Becher, and others, 'Disease-causing Mutations C277R and C277Y Modify Gating of Human ClC-1 Chloride Channels in Myotonia Congenita', *The Journal of Physiology*, 590 (2012), 3449–3464 <doi:10.1113/jphysiol.2012.232785>